NASA TECHNICAL NOTE

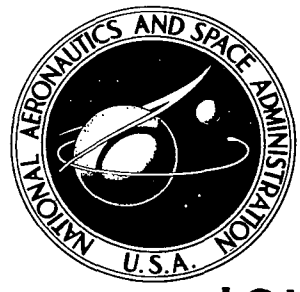

NASA TN D-6178

NASA TN D-6178

ACOUSTIC AND AERODYNAMIC PERFORMANCE OF A 6-FOOT-DIAMETER FAN FOR TURBOFAN ENGINES

III - Performance With Noise Suppressors

by Edward J. Rice, Charles E. Feiler, and Loren W. Acker

Lewis Research Center
Cleveland, Ohio 44135

NATIONAL AERONAUTICS AND SPACE ADMINISTRATION • WASHINGTON, D. C. • FEBRUARY 1971

1. Report No.	2. Government Accession No.	3. Recipient's Catalog No.
NASA TN D-6178		

4. Title and Subtitle
ACOUSTIC AND AERODYNAMIC PERFORMANCE OF A 6-FOOT-DIAMETER FAN FOR TURBOFAN ENGINES III - PERFORMANCE WITH NOISE SUPPRESSORS

5. Report Date: February 1971

6. Performing Organization Code

7. Author(s): Edward J. Rice, Charles E. Feiler, and Loren W. Acker

8. Performing Organization Report No.: E-5878

9. Performing Organization Name and Address
Lewis Research Center
National Aeronautics and Space Administration
Cleveland, Ohio 44135

10. Work Unit No.: 126-61

11. Contract or Grant No.

12. Sponsoring Agency Name and Address
National Aeronautics and Space Administration
Washington, D.C. 20546

13. Type of Report and Period Covered: Technical Note

14. Sponsoring Agency Code

15. Supplementary Notes

16. Abstract

Inlet and exhaust noise suppressors for a 6-ft- (1.83-m-) diameter fan for a high-bypass-ratio turbofan engine were tested. The perforated-plate-on-honeycomb suppressors provided a much broader band noise attenuation than was predicted. Perceived noise level attenuations obtained due to the suppressors were 13 and 12 PNdB for simulated approach and takeoff conditions, respectively. The theory used for the design of the suppressors is discussed. In general, the theory predicts the frequency for peak attenuation but underpredicts the peak attenuation amplitude. For frequencies above and below peak, the observed attenuations are more than predicted. Degradations of aerodynamic performance caused by the noise suppressors were smaller than the experimental errors, which were estimated to be 2 percent.

17. Key Words (Suggested by Author(s))
Acoustic attenuation; Acoustics; Acoustic impedance; Aircraft noise; Noise reduction; Sound transmission; Turbofan engines

18. Distribution Statement
Unclassified - unlimited

19. Security Classif. (of this report)	20. Security Classif. (of this page)	21. No. of Pages	22. Price*
Unclassified	Unclassified	61	$3.00

*For sale by the National Technical Information Service, Springfield, Virginia 22151

ACOUSTIC AND AERODYNAMIC PERFORMANCE OF A 6-FOOT-DIAMETER FAN FOR TURBOFAN ENGINES
III - PERFORMANCE WITH NOISE SUPPRESSORS

by Edward J. Rice, Charles E. Feiler, and Loren W. Acker
Lewis Research Center

SUMMARY

Inlet and exhaust noise suppressors for a 6-foot- (1.83-m-) diameter fan for a high-bypass-ratio turbofan engine were tested. The perforated-plate-on-honeycomb suppressors provided a much broader band noise attenuation than was predicted. Perceived noise level attenuations obtained due to the suppressors were 13 and 12 PNdB for simulated approach and takeoff conditions, respectively.

The theory used for the design of the suppressors is discussed. In general, the theory predicts the frequency for peak attenuation but underpredicts the peak attenuation amplitude. For frequencies above and below peak, the observed attenuations are more than predicted.

Degradations of aerodynamic performance caused by the noise suppressors were smaller than the experimental errors, which were estimated to be 2 percent.

INTRODUCTION

Current four-engine aircraft using ducted fans of the 707/DC-8 class produce about 120 perceived noise decibels (PNdB) at standard measuring points during both takeoff and landing. The NASA Quiet Engine Program was initiated to demonstrate the feasibility of reducing this noise 15 PNdB by engine design changes and perhaps another 10 PNdB by the use of absorptive duct liners. In support of these goals, a facility described in reference 1 has been built for determining the performance and noise characteristics of full-scale fans. Performance and noise data without acoustic treatment are reported in reference 2 for the first 6-foot- (1.83-m-) diameter fan tested.

This report describes the noise reduction attained by the use of acoustic liners in

the inlet and exhaust ducts of the fan. The use of acoustic treatment to suppress engine noise has recently received considerable attention. Numerous experimental and analytical studies have been performed to develop liner design methods (e.g., refs. 3 and 4).

The liners used in this study were of a perforated-plate-on-honeycomb construction. The basis for their design is discussed and a comparison of experimental and theoretical results is presented. Estimates are made of the flyover noise characteristics (without core engine noise) of an airplane having this fan and treatment on four engines.

SYMBOLS

b	backing depth of liner resonators, ft (m)
c	speed of sound, ft/sec (m/sec)
D	circular-duct diameter or annular-duct height, ft (m)
d	perforated-plate hole diameter, ft (m)
dB_{max}	maximum possible sound power attenuation for a given η and L/D, dB
f	frequency, Hz
L	length of acoustic treatment, ft (m)
M	average steady flow Mach number
P	acoustic pressure, lbf/ft^2 (N/m^2)
S/A	ratio of acoustic treatment area to duct cross-section area
t	perforated-plate sheet thickness, ft (m)
V_n	normal gas velocity at a lined wall, ft/sec (m/sec)
V_o	orifice gas velocity in Helmholtz resonator, ft/sec (m/sec)
δ	orifice-end correction (see eq. (7)), ft (m)
η	frequency parameter, Df/c
θ	specific acoustic resistance (see eqs. (2) and (3))
θ_{NL}	nonlinear specific acoustic resistance (see eq. (4))
λ	sound wavelength, ft (m)
ν	gas kinematic viscosity, ft^2/sec (m^2/sec)
ρ	gas density, lbm/ft^3 (kg/m^3)
σ	open-area ratio (orifice area to wall area)

χ specific acoustic reactance (see eq. (2))

ω angular frequency

APPARATUS AND PROCEDURE

Fan Description

A cutaway view of the fan is shown in figure 1. The single-stage fan has a large rotor-stator spacing (3.6 rotor chords) and is without inlet guide vanes. The fan is driven by electric motors through the shaft shown emerging from the fan inlet.

The detailed design of the fan is presented in reference 1. The following fan parameters are given here for convenience. Aerodynamic parameters are corrected to standard sea-level atmosphere of 518.7° R (288.2 K) and 2116.2 pounds per square foot (1.013×10^5 N/m^2):

Rotor tip diameter, in. (m)	71.81 (1.8240)
Stator tip diameter, in. (m)	67.94 (1.7257)
Rotor tip speed at 3533 rpm (cruise design corrected value), ft/sec (m/sec)	1107 (337.4)
Design stagnation pressure ratio	1.5
Design weight flow (corrected value), lbm/sec (kg/sec)	873 (396)
Rotor hub-tip ratio (inflow face)	0.50
Stator hub-tip ratio	0.59
Rotor to stator spacing (trailing to leading edges), in. (cm)	20 (50.8)
Number of blades:	
Rotor	53
Stator	112
Chord length, in. (cm):	
Rotor	5.5 (13.97)
Stator	2.69 (6.83)

Noise Suppressor Construction

The inlet and exhaust noise suppressors can be seen in figure 1. The inlet suppressor consists of a lined outer cowl and three splitter rings with acoustic lining on both sides. The exhaust suppressor has only the lined outer cowl and centerbody.

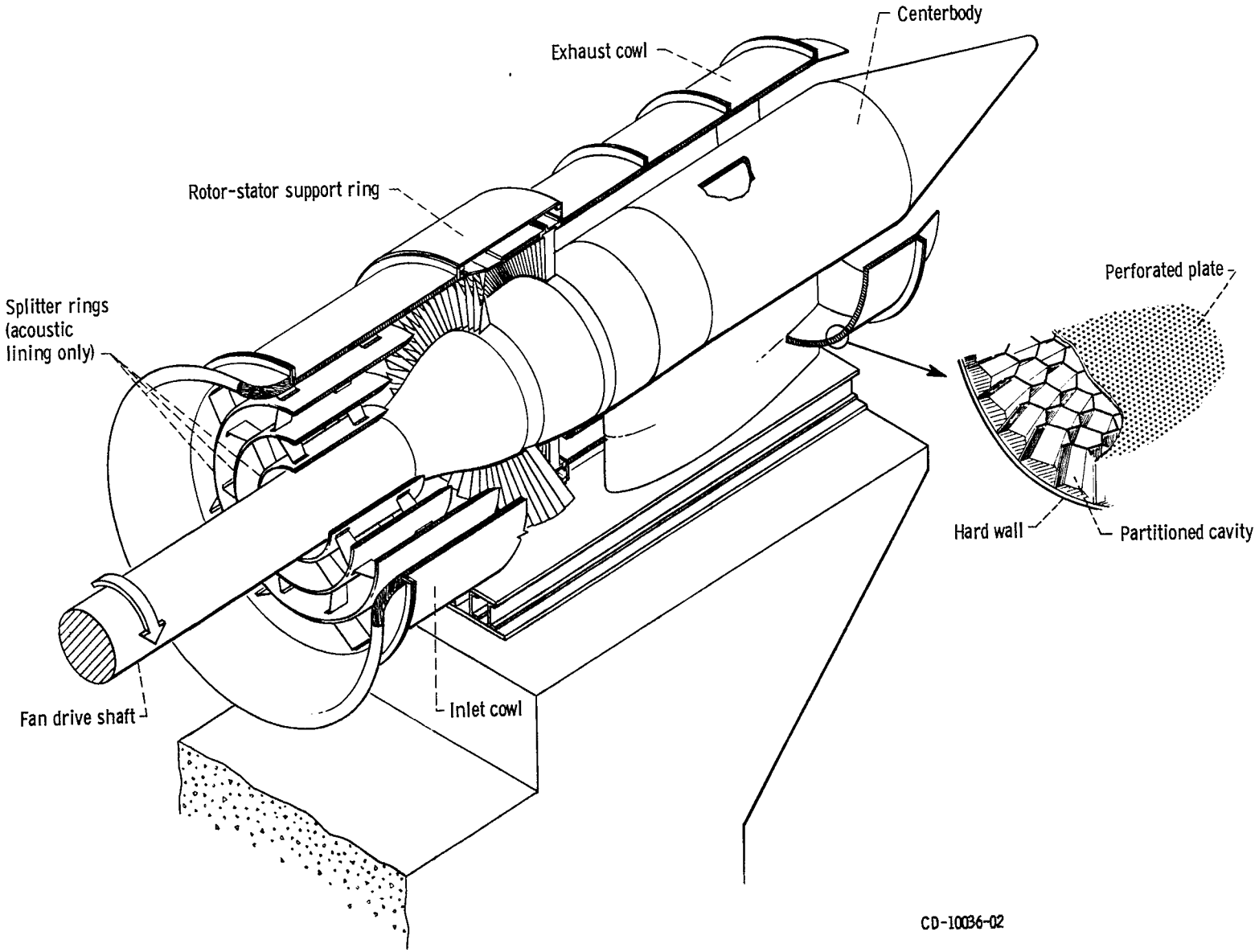

Figure 1. - Cutaway view of fan and suppressor assembly.

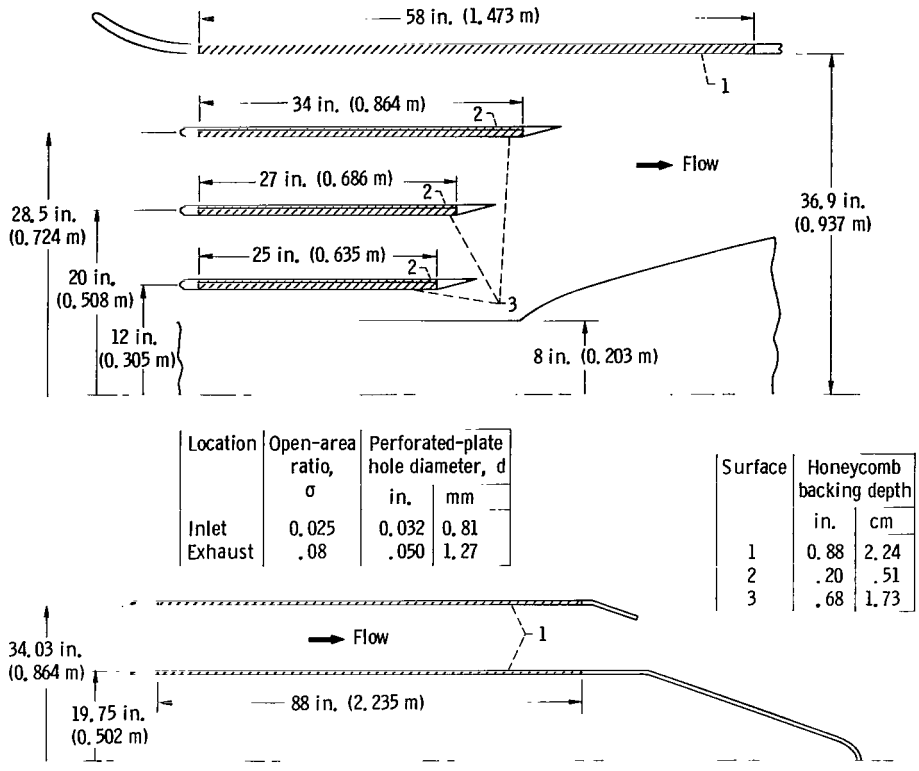

Figure 2. - Suppressor dimensions and materials. All perforated-plate sheet, 0.02-inch- (0.51-mm-) thick aluminum; all honeycomb, 3/8 inch (0.95 cm) hexagonal.

The suppressor dimensions and the materials used in the acoustic liners are shown in figure 2. The liner is constructed with a perforated aluminum sheet bonded to a honeycomb backing. All facing materials are 0.020-inch- (0.51-mm-) thick perforated aluminum sheet metal. The three surface treatments indicated on the inlet differ only in the thickness of the honeycomb backing material.

A cross section of an inlet splitter ring is shown in figure 3, where the two different honeycomb thicknesses are apparent. This construction was used to broaden the frequency range of noise suppression. Each passage in the inlet was thus bounded by two surfaces tuned to two different frequencies.

The construction of the noise suppressors followed the technique outlined in reference 3 (p. 63). A modified epoxy adhesive film, supported by a synthetic fabric carrier, is inserted between the honeycomb core and the septum of the splitter ring. The bond is then made by oven curing the above assembly. An adhesive film without a fabric carrier is then applied to the honeycomb. Heat is applied to the adhesive and it coagulates into a bead along the honeycomb edges. The perforated sheet-metal facing plate is then applied to the honeycomb and bonded by oven curing.

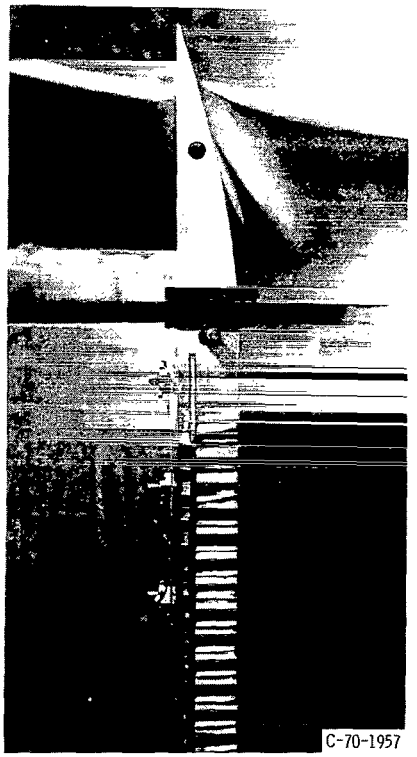

Figure 3. - Cross section of inlet splitter ring.

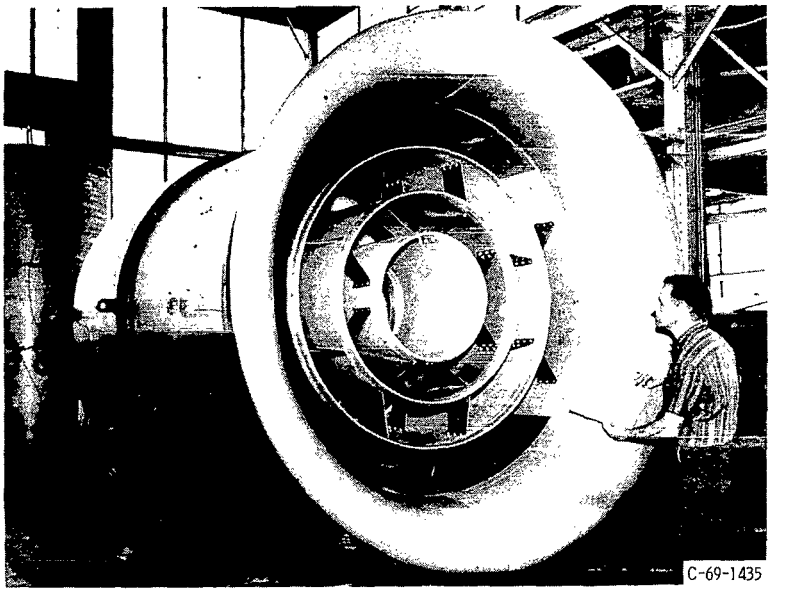

Figure 4. - Inlet duct with splitter rings.

The assembled inlet noise suppressor is shown in figure 4. The fan drive shaft enters through the center, reducing the size of this passage.

Data for four configurations are reported herein. These result from combinations of two inlet lengths and two exhaust nozzle areas. The length of the inlet is the distance from the bellmouth flange to the front edge of the rotor-stator support ring (see fig. 1). The leading edge of the rotor at the root lies 5.2 inches (0.132 m) behind this support-ring front edge. The short inlet is 60.5 inches (1.537 m) and the long inlet is 101.5 inches (2.578 m). The standard nozzle area is 1895 square inches (1.223 m^2), which is 97 percent of the design value. The 10-percent-oversized nozzle has an area of 2150 square inches (1.387 m^2) and is 110 percent of the design value.

Noise Suppressor Design

The noise suppressor design philosophy is contained in the answers to three questions. First, how much and in what configuration can the noise-absorbing material be

applied to the fan ducts without excessive losses due to flow blockage? Second, what lining material impedance will result in the maximum noise attenuation within the imposed geometry restrictions? Finally, what wall construction will provide the optimum wall impedance at the frequency of the maximum noise?

For an estimate of the necessary noise suppressor treatment, the theory of reference 5 is used. This theory describes the propagation of an initially plane pressure wave in a cylindrical duct without mean flow. Figure 5 (ref. 5) relates maximum possible sound power attenuation to the duct length-to-diameter ratio L/D and frequency parameter η where

$$\eta = \frac{D}{\lambda} \tag{1}$$

Although figure 5 was derived from the circular-duct theory, an estimate for the attenuation in annular ducts can be made by using one-half the ordinate. This factor results from the consideration of duct-lined area to cross-sectional area ratio. Equation (8) (p. 17) shows the sound power attenuation to be proportional to this ratio (an approxi-

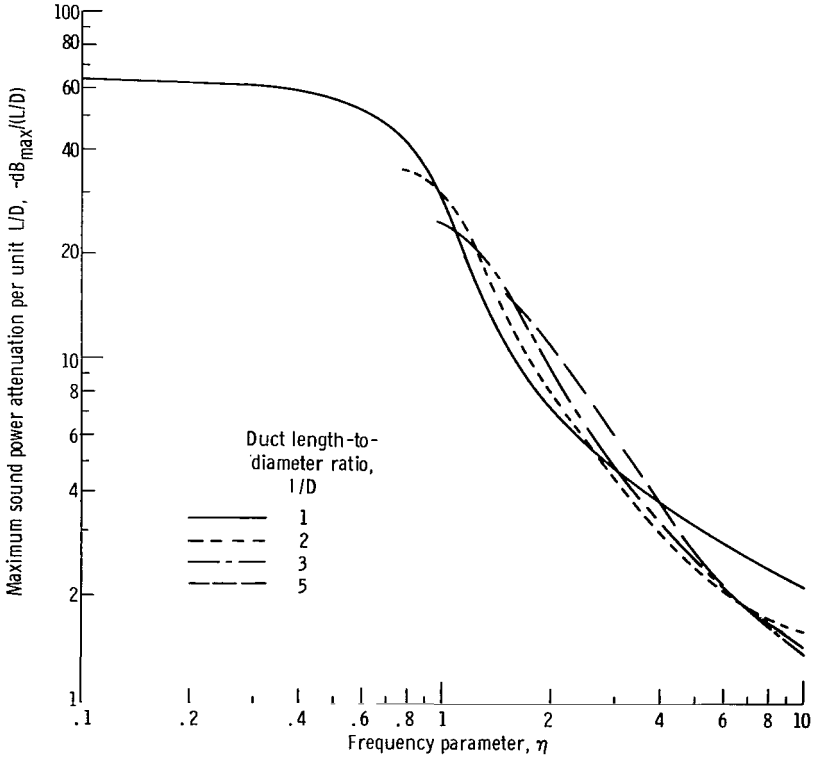

Figure 5. - Dependence of maximum possible sound power attenuation on frequency parameter (η) for various duct length-to-diameter ratios.

mation). This ratio is twice as large for a circular duct as for an annular duct when D is interpreted as the distance between lined surfaces in the annulus.

The curves of figure 5 can be used to give a quick estimate of the performance of a proposed liner configuration. For the following estimates a frequency of 3500 hertz (λ = 3.84 in., 9.75 cm) is assumed. First, consider just lining the 6-foot- (1.83-m-) diameter inlet for a length of 6 feet (1.83 m). The duct has an L/D of 1 and an η of 18.75. By extrapolating in figure 5 and applying the factor of 1/2 to the ordinate, an attenuation of less than -1 decibel is obtained. Clearly, splitter rings or lined struts must be used to increase the effective L/D and decrease η. Next, consider three splitter rings of 3-foot (0.91-m) length in the fan inlet. Now D $\approx$ 8 inches (20.3 cm), L/D $\approx$ 4, and $\eta \approx 2.1$. From figure 5 the maximum possible sound power attenuation is -19 decibels (the ordinate in fig. 5 multiplied by 1/2 as previously discussed). If this attenuation could be achieved at 3500 hertz by the proper wall construction, it would be sufficient for the purposes of this experiment. More noise attenuation could be obtained by increasing the number of splitter rings, but three was considered as a reasonable compromise between noise attenuation and flow losses.

The spacings of the three inlet splitter rings are shown in figure 2. Due to the enlargement of the hub near the rotor, the inner rings had to be made shorter than the outer rings. The spacing between splitters was thus adjusted by using figure 5 to provide approximately the same maximum sound power attenuation ($-dB_{max}$) for all passages.

Once the overall geometry of the suppressor is decided, the optimum wall impedance can be determined from figure 6. These curves, obtained from reference 5, show the relation between L/D, η, and wall impedance required to produce the attenuations of figure 5. Continuing the previous example with L/D $\approx$ 4 and $\eta \approx 2.1$, the wall specific resistance should be 2.4 and reactance should be -1.25.

The optimum wall impedance can then be corrected for a finite steady flow by dividing it by 1 + M according to reference 6. The Mach number is considered positive for the exhaust duct and negative for the inlet, where the sound propagation opposes the steady gas flow.

Thus for the same L/D and η the inlet must have a larger resistance and more negative reactance than the exhaust duct. In reference 6 it was shown that the curves in figure 5 were not altered by a steady, uniform gas flow.

Finally, when the required wall impedance is known at a particular frequency, the wall construction must be specified to produce the desired impedance. The following relations are given to relate acoustic impedance to wall construction for a perforated plate mounted over a backing cavity. The equations, or in some cases the data from which the equations were determined, are available in the literature and are reviewed in reference 7.

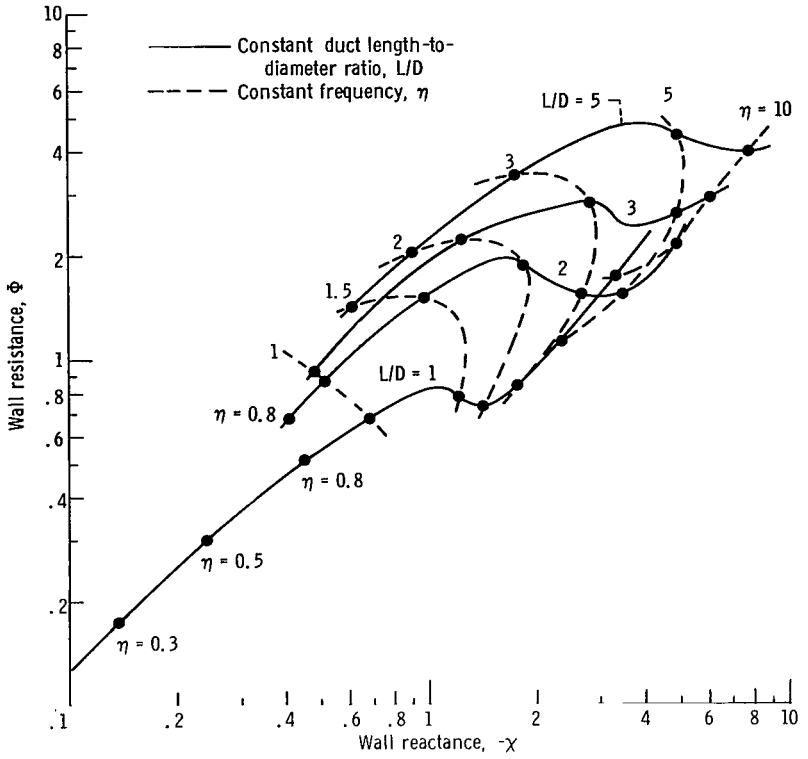

Figure 6. - Locus of maximum sound power attenuation in wall impedance plane.

The specific acoustic impedance is defined as

$$\frac{P}{\rho c V_n} = \theta + i\chi \tag{2}$$

The resistance is given by

$$\theta = \frac{\sqrt{8\nu\omega}}{\sigma c}\left(1 + \frac{t}{d}\right) + \theta_{NL} \tag{3}$$

where

$$\theta_{NL} = \frac{|V_o|}{\sigma c}(1 + 6.67\ M) \tag{4}$$

The first term in equation (3) is the linear resistance of a Helmholtz resonator array due to viscous dissipation in the oscillatory boundary layers at the walls and in the ori-

fice. In the absence of steady grazing flow and for very small sound levels, this is the entire acoustic resistance of the wall.

The second term in equation (4) is an empirical expression to account for the increase in acoustic resistance of the wall due to grazing flow. The peak orifice velocity accounts for the nonlinear acoustic resistance due to finite pressure amplitude, and is related to the pressure amplitude by

$$|V_o| = \frac{|P|}{\rho c \sigma \sqrt{\theta^2 + \chi^2}} \tag{5}$$

The specific acoustic reactance of the wall can be expressed as

$$\chi = \frac{\omega(t + \delta)}{\sigma c} - \cot\left(\frac{\omega b}{c}\right) \tag{6}$$

where δ is the orifice end correction and is given by

$$\delta = \frac{0.85\, d\left(1 - 0.7\sqrt{\sigma}\right)}{1 + 305\, M^3} \tag{7}$$

When the liner geometry, flow conditions, and noise spectrum are given, equations (3) to (5) must be solved by iteration for θ. The reactance is obtained directly from equations (6) and (7).

The converse of the problem of calculating acoustic impedance is of most interest for liner design. Given the optimum specific acoustic impedance at a certain frequency, the steady flow velocity, and the noise spectrum, what are the required values of σ, t, d, and b? The wall geometry can be determined from equations (3) to (7) when the following two conditions are given: First, the peak overall sound pressure level is used in equation (5). This approximation accounts for the nonlinear effect of the noise spectrum upon the resistance at the frequency in question. In reference 7 this approach was used with some success to correlate the results of a two-frequency resistance experiment. The second condition is that the facing sheet thickness and hole diameter must be specified. The facing sheet thickness would probably be specified by material strength considerations. The hole diameter should be at least as large and preferably larger than the thickness if the holes are to be punched. The hole diameter d is a very weak parameter when high flow velocity and sound pressure level exist in the suppressor. The linear resistance (first term in eq. (3)), in which hole diameter appears, is usually much smaller than the nonlinear resistance. The hole diameter appears in the reac-

tance through the orifice end correction, which approaches zero as flow velocity is increased (see eq. (7)).

When thickness t and hole diameter d are specified, the open-area ratio σ can be obtained by combining equations (3) to (5). The backing distance b is then obtained by combining equations (6) and (7).

Instrumentation

The instrumentation to measure the aerodynamic performance of the fan was reported in detail in reference 1. Some important aspects of the noise measuring apparatus and the test site are mentioned here for convenience.

The fan center is located 19 feet (5.79 m) above the ground. The 1/2-inch (1.27-cm) condenser microphones are at the same elevation as the fan center.

The microphone locations are shown in figure 7. The microphones are located at 10^{o} increments from 10^{o} to 160^{o} with 0^{o} being the fan axis at the inlet. The 70^{o} to 160^{o}

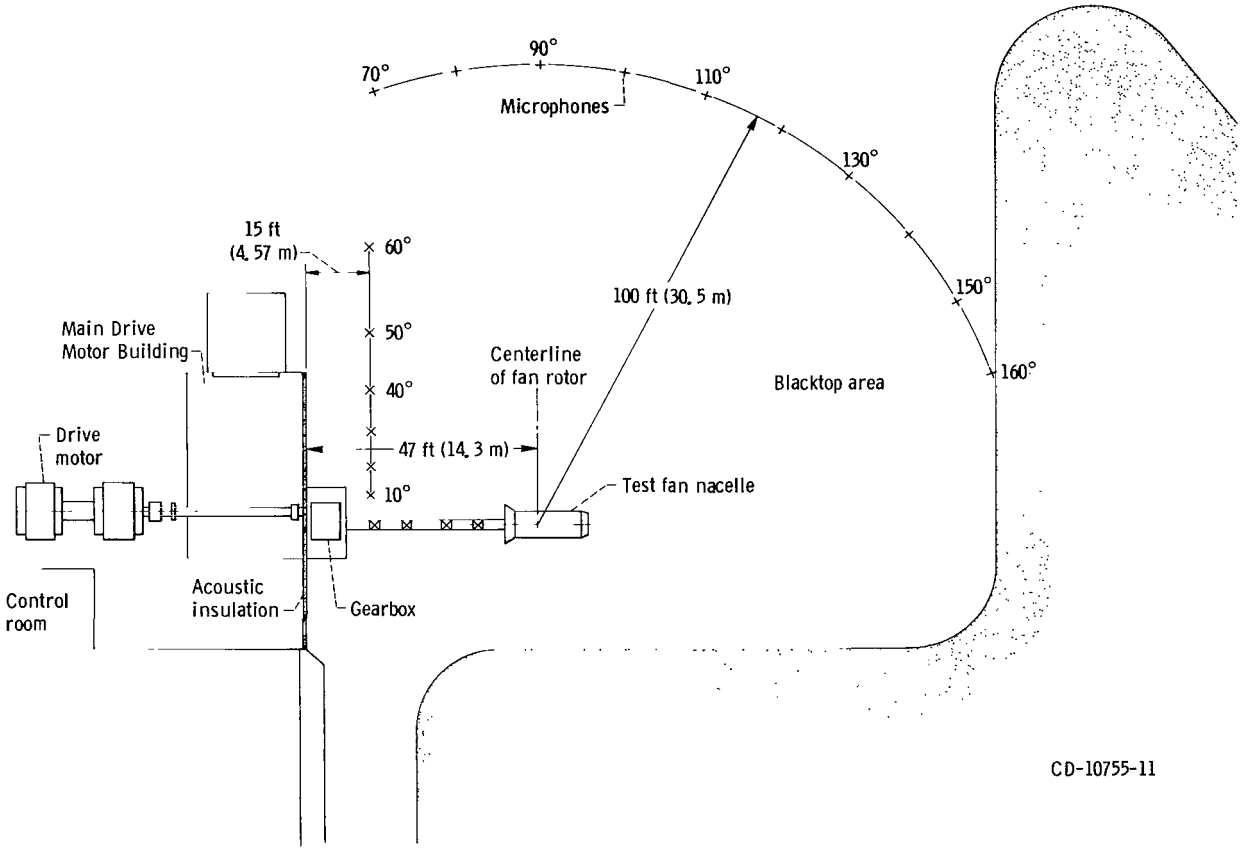

Figure 7. - Overall plan of test facility with microphone locations.

microphones are located on a 100-foot (30.48-m) radius measured from the center of the fan rotor. The 10^{o} to 60^{o} microphones are on a line which is perpendicular to the fan axis and are located 31.5 feet (9.6 m) in front of the fan.

The area between the fan and the microphones is asphalt surfaced. The face of the drive motor building is lined with 6-inch- (15.24-cm-) thick polyurethane ether open-cell foam.

Test Procedure and Data Reduction

The techniques for acquisition and reduction of acoustic data are presented in reference 1. Some aspects of the procedure are given here for convenience.

The tests were run from low speed to high speed and then back down to low speed. One set of data was obtained at each speed on the way up and two sets on the way down. Each of the three data samples is from 1 to 3 minutes duration. Each microphone output was recorded on magnetic tape. Acoustic data were not taken if the wind speed exceeded 13 knots (6.7 m/sec) or if there was any precipitation.

Cable loss corrections were applied to the data. The largest correction was 3 decibles at 10 000 hertz. The data were corrected to a 100-foot (30.48-m) radius for those microphones which were not at 100 feet (30.48 m), that is, those located at 10^{o} to 60^{o}, using the inverse squared distance rule. A 1/3-octave band analysis from 50 to 10 000 hertz was performed on all the data. The sound pressure levels were corrected to standard-day conditions (70 percent relative humidity; 59^{o} F, 288.2 K) using the methods of reference 8.

No site calibration corrections were applied to the acoustic data. In reference 1 a test of the site showed that the nearby building with foam lining did not affect the data above 500 hertz. However, at least a ground reflection effect, which has not been accounted for, remains.

RESULTS AND DISCUSSION

Acoustic Data

The acoustic data in the form of sound pressure level frequency spectra (in dB referenced to 2×10^{-4} microbar) are presented in the appendix in figures 12 to 75. The sound pressure levels have been corrected to a 100-foot (30.48-m) radius and to standard-day conditions, as described in the previous section. Each figure presents the results of four fan speeds at a particular microphone location.

All the data presented herein are for acoustically treated inlet and exhaust ducts. To obtain the noise suppressor performance at a particular speed and polar angle, these data must be compared to the corresponding hard-wall data of reference 2. The performance of the noise suppressors on the basis of overall acoustic power is discussed in the next two sections.

Data for four configurations (10 to 13) are referred to in figures 12 to 75. As seen in the figure titles, these configurations differ in inlet length and nozzle area. These configurations have been discussed in the apparatus section of this report.

Acoustic Power Comparisons - Hard and Soft Ducts

Several acoustic power spectra are presented in figures 8 and 9. The inlet and exhaust powers are determined by summation of the power in the front and rear hemispheres. The 90 and 60 percent speeds are representative of takeoff and landing engine speeds. On each figure data for long and short inlets are shown with and without acoustic treatment. Figures 8(a) to (d) are for the standard nozzle, while figure 9 also contains the data for the 10-percent-oversized nozzle.

The power spectra for the inlet at 60 percent speed are shown in figure 8(a). About a 1-decibel difference between the long and short hard-cowl data can be seen over the entire frequency spectrum. Similar shifts of up to 3 decibels can be seen in later figures. These apparent shifts in the data have not as yet been explained. They may come from an insufficient averaging time in the sound pressure level averaging circuits (about 1.5 sec), or possibly from some systematic error. Small differences in acoustic power spectra, such as in figure 8(a), may not be significant. However, several significant points about the power spectra should be noted. A large sound power attenuation (18 dB at the blade passage frequency) was obtained with the short treated inlet over a wide frequency range. Only at the blade passage frequency did the long treated inlet provide a significant additional attenuation. An increased attenuation was observed between 2500 and 6300 hertz, but it was small and possibly not significant. Doubling the amount of acoustic treatment without further reduction of sound power level strongly suggests that a noise floor has been reached. This implies that the noise measured in the far field in front of the fan is not dominated by direct radiation out of the inlet. The source of this noise floor has not been determined. It may be caused by radiation out of the fan shell, a flanking ground path, or even electric drive motor noise.

Figure 8(b) shows the rear hemisphere power spectra at 60 percent speed. Again a significant noise attenuation was obtained over a wide frequency range with the short inlet suppressor. The long inlet suppressor should not cause a further reduction in the rear-end noise. In this case a slight increase in noise was observed which may not be significant.

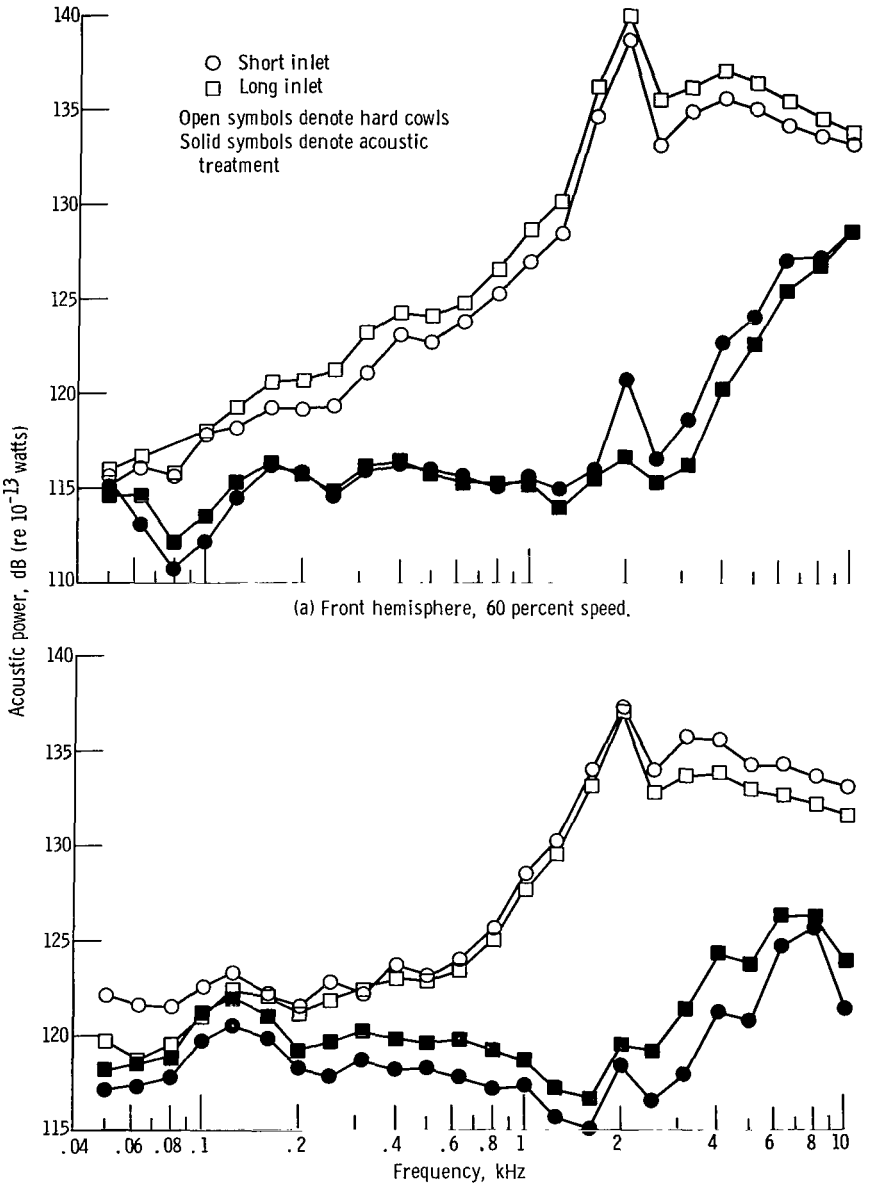

(a) Front hemisphere, 60 percent speed.

(b) Rear hemisphere, 60 percent speed.

Figure 8. - Acoustic power spectra. Standard nozzle.

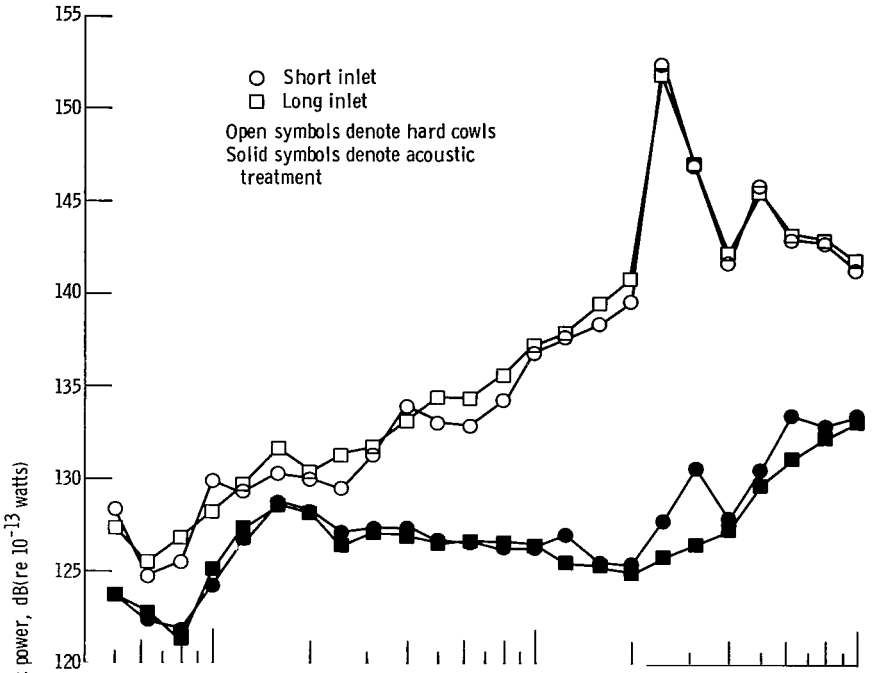

(c) Front hemisphere, 90 percent speed.

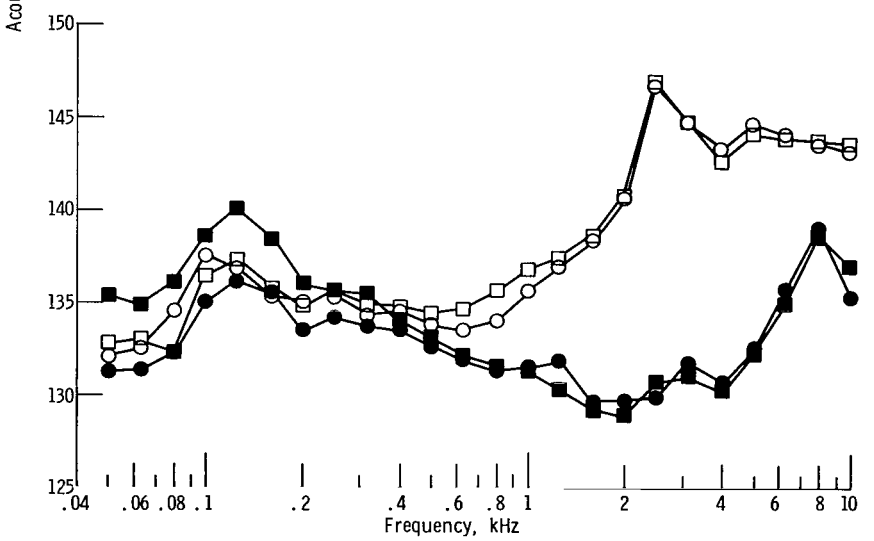

(d) Rear hemisphere, 90 percent speed.

Figure 8. - Concluded.

The inlet sound power levels at 90 percent speed are shown in figure 8(c). The situation is much like that of figure 8(a). The short suppressor greatly reduces the broad band and discrete tone noises. Additional suppressor length reduces only the discrete tones which were above the background level. With the exception of the discrete tones, a noise floor had already been reached with the short suppressor over most of the noise spectrum.

A comparison of the hard-cowl and suppressed data of figures 8(c) and (d) shows that the blade passage frequencies (fundamental and second harmonic) lie in different 1/3-octave bands. The cause of this difference was the considerably different ambient temperatures at which the data were taken and altering the rotational speed of the fan to maintain constant corrected speed.

In figure 8(d) the rear hemisphere noise at 90 percent speed can be seen. Again the longer inlet suppressor yields no additional noise reduction, which is as expected. The noise data obtained with acoustic treatment appear to identify two noise sources. The low-frequency peak (125 Hz) and a steady decrease in power with frequency (to 2000 Hz) is typical of the externally generated jet noise. Above 2000 hertz the noise is probably associated with the fan. Additional aft-end suppressors probably would not result in a gain in attenuation below 2000 hertz.

In figure 9 the curves are all for the short inlet configurations, both treated and hard. Two different exhaust nozzles are shown, however, which yield considerably different noise spectra with hard cowls. The oversized nozzle (+10 percent) configuration

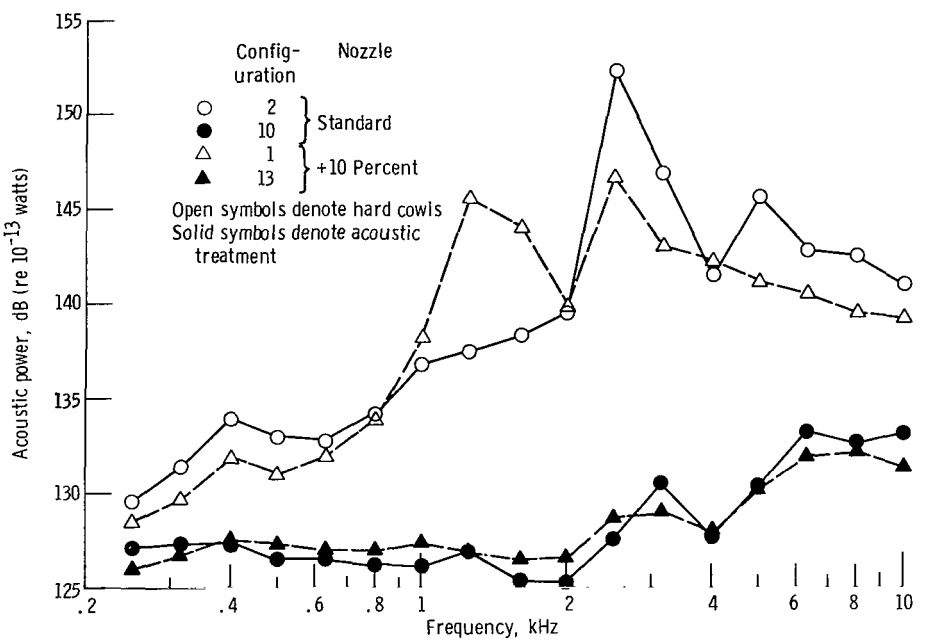

Figure 9. - Acoustic power spectra, front hemisphere, 90 percent speed, short inlet.

is rich in multiple pure tones (ref. 2) at 1250 and 1600 hertz and deficient in the blade passage frequency (and harmonics) in comparison with the standard nozzle configuration. The multiple pure tones are seen to be completely removed by the inlet suppressor.

The argument for a noise floor being reached with the short suppressor is also reinforced by the evidence in figure 9. The noise spectra after suppression are almost identical for the two nozzle configurations, although without suppression they are considerably different.

Acoustic Power Attenuations - Experimental and Theoretical

The experimental acoustic power attenuations for the exhaust and short-inlet suppressors at 60 and 90 percent speed are shown in figures 10(a) to (d). These attenuations are the differences between the hard- and soft-cowl, short-inlet curves of figure 8. As discussed previously when comparing hard- and soft-cowl data, the 90-percent-speed data show a shift in the 1/3-octave band in which the discrete tones are found. For figures 10(b) and (d) the 1/3-octave bands in which the discrete tones are found and the band above these have been reversed for the hard-cowl data.

Theoretical predictions of suppressor performance are also shown in figure 10. The attenuation theory was based upon the model of references 5 and 6, except that rectangular instead of circular geometry was used. The model assumes that a plane pressure wave enters the duct, traveling in the direction of the duct axis. A uniform, steady flow field was assumed without boundary layers or velocity gradients over the duct. The wall impedance was calculated according to equations (3) to (7). Estimates of the overall sound pressure level within the ducts were obtained from the hard-cowl, far-field data. This pressure was used in equation (5) to define the nonlinear resistance.

The calculation method based on references 5 and 6 provides attenuations for semi-infinite rectangular ducts with the same impedance on both walls. For the inlet suppressor, each passage has different materials and thus different impedances on opposing walls. To handle this situation, a result from the approximate theory of Morse (ref. 9) was used. The sound power attenuation in a duct is approximated by

$$\Delta \mathrm{dB} \approx \frac{-4.34\,\theta\,\frac{S}{A}}{\theta^2 + \chi^2} \tag{8}$$

where S/A is the ratio of treated surface area to duct cross-sectional area. When put in terms of S/A, equation (8) provides an approximation for either circular or rectangu-

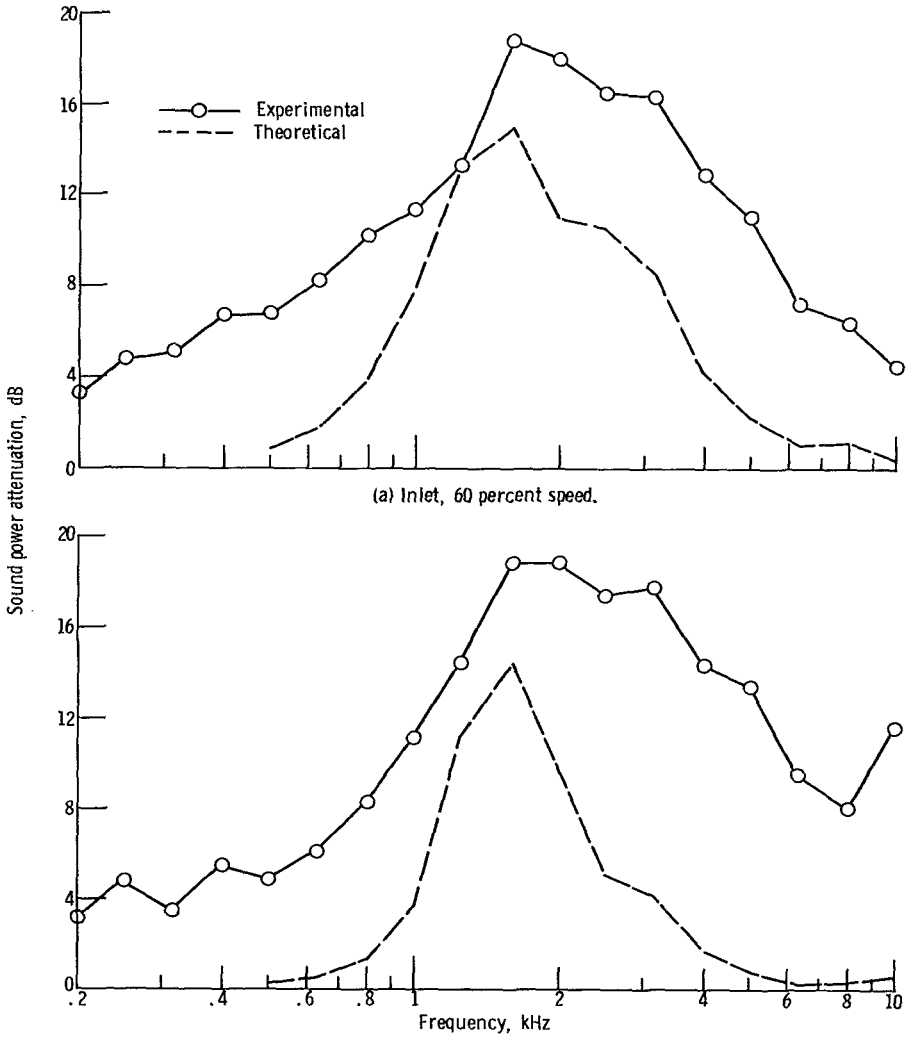

(a) Inlet, 60 percent speed.

(b) Exhaust duct, 60 percent speed.

Figure 10. - Comparison of theoretical and experimental sound power attenuation.

lar ducts. For the case of walls of different impedance on two sides of a duct, the following procedure was used: The attenuation calculations were performed as if just one of the materials was present on both walls of the duct. The calculations were repeated with the second material. According to equation (8) the attenuation is approximately proportional to the area of acoustic treatment. The attenuation for each material was thus weighted by its proportion of the total area of acoustic treatment. The total attenuation was then the sum of these weighted attenuations.

When several lined passages are involved, such as in the fan inlet suppressor, a uniform sound power flux was assumed at the duct inlets. In cases where a radial sound

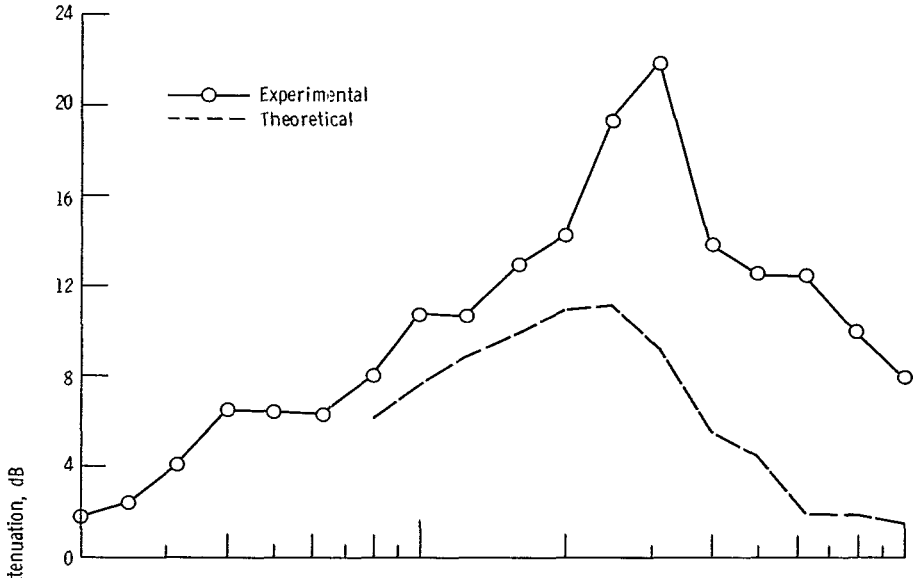

(c) Inlet, 90 percent speed.

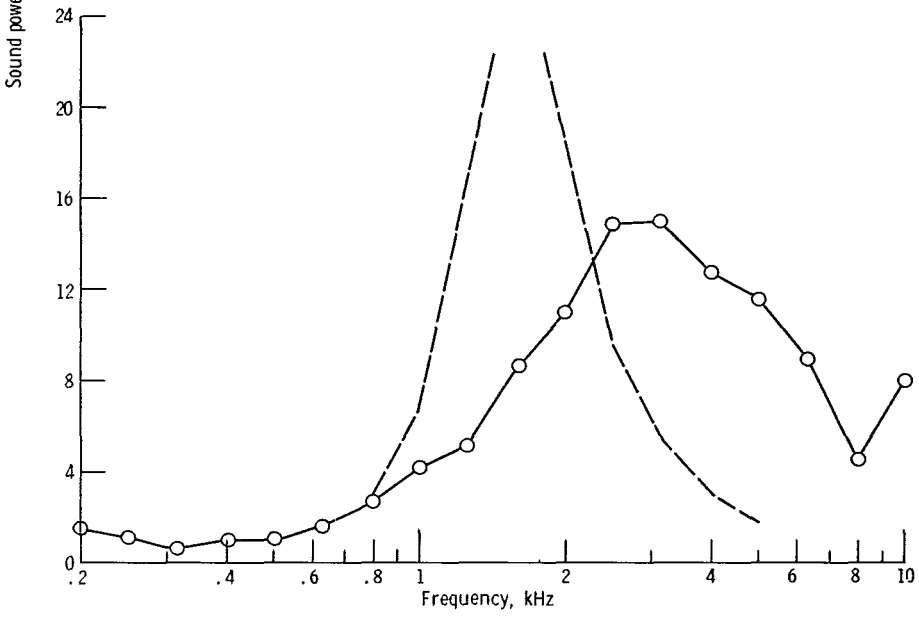

(d) Exhaust, 90 percent speed.

Figure 10. - Concluded.

intensity profile is known to exist, this assumption should be changed.

Figures 10(a) to (c) have several characteristics in common. For frequencies both high and low, in comparison to the frequency of maximum attenuation, the experimental sound power attenuation is considerably higher than that predicted by theory. This difference is probably greater than is indicated; it was pointed out in the previous section that noise floors may have been reached except at the blade passage frequency and its harmonics. Shorter liners might have yielded essentially the same experimental results, but then the associated theoretical curves would have been reduced.

Another common characteristic of the three figures is that the frequency for maximum sound power attenuation has been fairly well predicted. At approach speed (60 percent), the magnitude is also fairly well predicted.

The differences between theory and experiment at high and low frequencies are not easy to explain. For the low frequencies a different dependence of wall impedance on frequency than that of equations (3) to (7) may provide better agreement between theory and experiment. However, for the high frequencies the sound power attenuations are near the theoretical maximums over a considerable frequency range. No real wall material could have the impedance characteristics which are necessary for this behavior (ref. 7). This would require a resistance which increases and a reactance which becomes more negative (stiffness controlled) with increasing frequency (see fig. 6).

A possible explanation, especially for the high frequencies, for the behavior of the experimental data is as follows. The present theory assumes an axially propagating sound wave (at the lined duct entrance) with no transverse wave motion. This is the most conservative estimate available. Most of the acoustic power is directed axially, while only transversely directed power can be absorbed at the lined wall. The turning of the axial power into the walls must be accomplished by the proper impedance match between the duct and the wall. However, if some other mechanism exists which can redirect the acoustic power into the walls, the attenuation might be greatly increased. Such a mechanism exists in the form of gradients in the steady flow velocity. Propagation of sound in a duct with sheared flow has been investigated in references 10 to 13. When the ratio of sound wavelength to boundary layer thickness is less than or nearly equal to 1, the acoustic energy can be drastically redistributed. The presence of the boundary layers alone in the exit duct may not be sufficient to account for the large high-frequency attenuation. Some radial velocity gradients over the exit duct were observed downstream from the stators. Application of the theory of reference 13 with these velocity gradients may be sufficient to account for the larger attenuations.

For the inlet duct, refraction of sound in the boundary layers in the lined passages will direct the acoustic energy toward the center of the passage and therefore, reduce attenuation. However, the sound waves may be refracted in velocity gradients across the duct, in the axial space between the rotor blades and the trailing edges of the inlet

splitter rings. The sound waves will then enter the lined splitter ring sections at an angle rather than purely axially. This will result in increased higher-order transverse mode content with resulting increased acoustic power attenuation.

The comparison of theory and experiment in figure 10(d) yields the same results as the previous three parts only at high frequencies. At low frequencies there is virtually no experimental sound power attenuation. At intermediate frequencies (centered around 1600 Hz) the theory greatly overpredicts the attenuation. Both these effects are probably caused by the emergence of the fan jet noise as the dominant source at low and intermediate frequencies. The rear-end power spectra for the treated ducts in figure 8(d) support this contention. The jet noise is seen to peak at about 125 hertz and then steadily decrease to 2000 hertz, beyond which another noise source dominates. Once the suppressor has reduced the internal intermediate frequency noise to the level of jet noise which is produced externally, further reduction will not produce observable differences. At low frequencies, where internal jet noise already dominates over internally generated noise, the suppressor can produce no observable effect in the far field.

There is a strong temptation to consider the sound power attenuations at low frequencies as systematic errors in the data in figures 10(a) to (c). One might be justified in shifting the attenuation curves downward by 3 to 5 decibels. This, however, raises some very difficult questions. Why would the hard-cowl power spectra generally be measured too high or else the soft-cowl data be measured too low? Why do these errors generally disappear at high engine speeds in the rear hemisphere when jet noise dominates? At present then, it must be assumed that the measurements are not in error and that the noise suppressors are working over an extremely wide frequency range.

One further possibility for the difference in predicted and observed sound power attenuations should be considered. Inlet splitters may have an effect on the rotor which reduces noise production. This reduced noise should not be credited to the suppressor as a simple noise absorption.

Perceived Noise Levels

The perceived noise levels for simulated approach and takeoff conditions were calculated according to reference 14 and are shown in figures 11(a) and (b). These figures are for a single fan.

The single-fan approach condition can be seen in figure 11(a). The perceived noise levels are given for 60 percent speed on a 375-foot (114.3-m) sideline. Two data points (120° and 130°) appear to be in error for the standard nozzle condition with a short acoustically treated inlet. The 10-percent-oversized-nozzle data are thus presented to obtain the noise levels at these angles. The acoustic treatment reduces the maximum

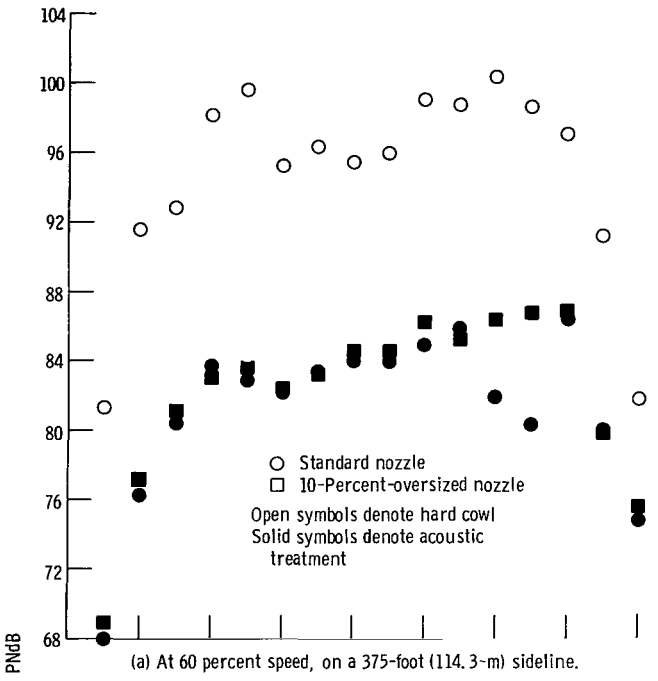

(a) At 60 percent speed, on a 375-foot (114.3-m) sideline.

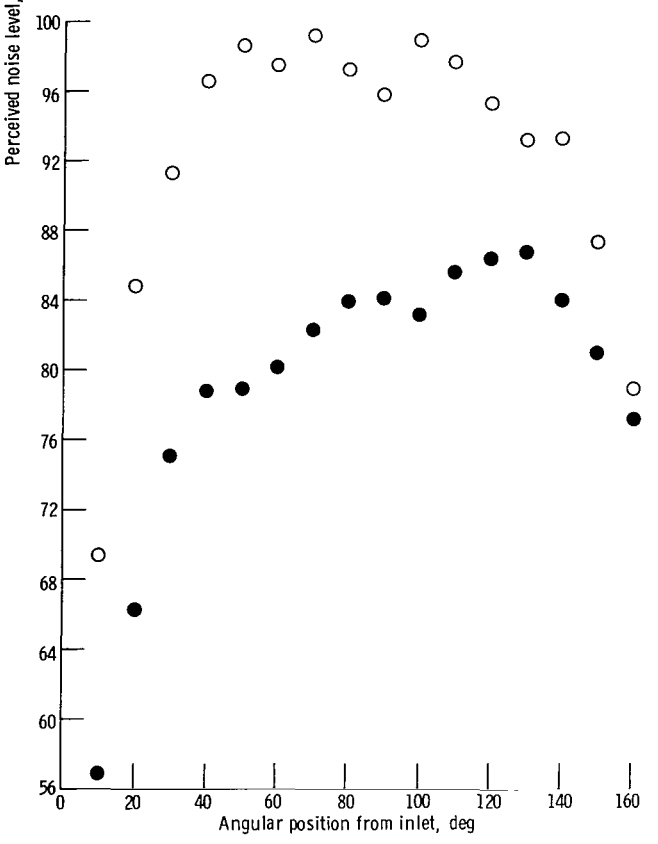

(b) At 90 percent speed, on a 1000-foot (304.8-m) sideline.

Figure 11. - Effect of acoustic treatment on perceived noise level. Short-inlet design nozzle.

perceived noise level of the fan at approach by 13 PNdB (from 100 to 87 PNdB).

The single-fan takeoff condition is given in figure 11(b). The perceived noise levels are for 90 percent speed on a 1000-foot (304.8-m) sideline. The reduction in maximum perceived noise level due to the noise suppressors is 12 PNdB (from 99 to 87 PNdB) at takeoff.

An estimate of the perceived noise levels for an aircraft with four fans can be made by adding 6 decibels to the maximum values in figure 11. Four fans with acoustically treated inlet and exhaust ducts would thus produce 93 PNdB at both takeoff and approach. The current DC-8 figures given by Pendley and Marsh (ref. 15) are 117 PNdB at takeoff (1000 ft, 304.8 m) and 120 PNdB at approach (370 ft, 112.8 m). The reductions in perceived noise level are thus 24 PNdB at takeoff and 27 PNdB at approach. These noise reductions are obtained by considering the fan noise only, and will be realized only if the core jet and turbine noise can be kept below the fan noise in an actual engine.

Estimates of the effective perceived noise levels have been calculated for an aircraft with four turbofan engines. Again it is emphasized that these noise levels are valid only if the core engine noise is less than the suppressed fan noise. Both tone and time duration corrections are considered by use of the calculation procedure of reference 16. The effective perceived noise level calculations are made using the noise spectra from the standard nozzle, short inlet configurations. The following comparisons are made between the hard-cowl and acoustically treated versions. For simulated takeoff conditions, the effective perceived noise level was reduced by 17 EPNdB (102.7 to 85.7 EPNdB) and, for approach, by 14.3 EPNdB (102.5 to 88.2 EPNdB). The effective perceived noise level calculations were made using a relative humidity of 70 percent and a temperature of 77° F (298.2 K). For takeoff, the climbout angle was 5.6°, the velocity along the flight path was 292 feet per second (89 m/sec), and the engine centerline was 9.1° from horizontal. For approach, the glide angle was -3°, the velocity along the flight path was 241 feet per second (73.5 m/sec), and the engine centerline was 0.5° from horizontal.

Aerodynamic Performance with Acoustic Treatment

The internal flow losses of the nacelle cowling were not measured directly, but the installed fan performance was obtained with both hard and acoustic surfaces lining the cowling. These data are presented in the following table for 60 and 90 percent fan speeds, which represent the landing and takeoff operating conditions. Fan pressure ratios shown include the inlet cowling losses because the pressure rise was measured from ambient to the fan stator discharge. Thrust includes all the cowl losses because it is the momentum measured at the nacelle exhaust. The data indicate that the acoustic

Percent speed	Inlet	Wall material	Airflow		Pressure ratio	Thrust	
			lbm/sec	kg/sec		lbf	N
60	Short	Hard	505	229	1.14	7 200	32 000
		Lined	493	224	1.14	7 400	32 900
	Long	Hard	484	220	1.15	7 200	32 000
		Lined	486	220	1.14	7 200	32 000
90	Short	Hard	741	336	1.36	16 700	74 300
		Lined	749	340	1.36	16 800	74 700
	Long	Hard	736	334	1.36	16 400	73 000
		Lined	739	335	1.35	16 400	73 000

liner did not degrade the fan performance as much as did the long inlet cowling.

The differences shown are all within the experimental measurement error, which was estimated to be about 2 percent of the full-speed values. These errors are 16 pounds per second (7.3 kg/sec) on airflow, 0.01 on pressure ratio, and 400 pounds force (1780 N) on thrust.

SUMMARY OF RESULTS

The inlet and exhaust noise suppressors for a 6-foot- (183-m-) diameter fan have been tested. Some of the more important results were as follows.

1. The suppressors provided more peak noise attenuation and much broader band attenuation than was predicted.

2. The duct sound transmission theory predicted the frequency of peak attenuation fairly well. The exception occurred when a fairly obvious jet noise floor dominated at the frequency of predicted peak attenuation.

3. Some noise floors of unknown origin were apparently reached even with the short treated inlet.

4. The noise suppressors provided a noise reduction of 13 PNdB at simulated approach conditions and 12 PNdB at takeoff, compared to the fan noise produced with hard passages.

5. The suppressor and fan combination achieved significant noise reductions when compared to the current DC-8 aircraft. The simulated approach and takeoff noise reductions were 27 and 24 PNdB, respectively. These results are obtained under the assumption that the core engine noise is insignificant.

6. Degradations of the aerodynamic performance due to the noise suppressors were within the experimental error of measurement.

Lewis Research Center,
National Aeronautics and Space Administration,
Cleveland, Ohio, September 14, 1970,
126-61.

APPENDIX - ACOUSTIC DATA

The acoustic data in the form of 1/3-octave-band sound-pressure-level frequency spectra (in dB referenced to 2×10^{-4} microbar) are presented here. All data are for nacelle configurations with acoustic treatment. The sound pressure levels have been corrected to a 100-foot (30.48-m) radius and to standard-day conditions (70 percent relative humidity; 59^{o} F, 288.2 K).

Four configurations are referred to in figures 12 to 75. These result from using two inlet lengths and two nozzles. The short inlet is as shown in figure 2. The long inlet is obtained by adding a 41-inch (1.04-m) cylindrical section. The standard nozzle area is 1895 square inches (1.223 m^2). The 10-percent-oversized nozzle has an area of 2150 square inches (1.387 m^2).

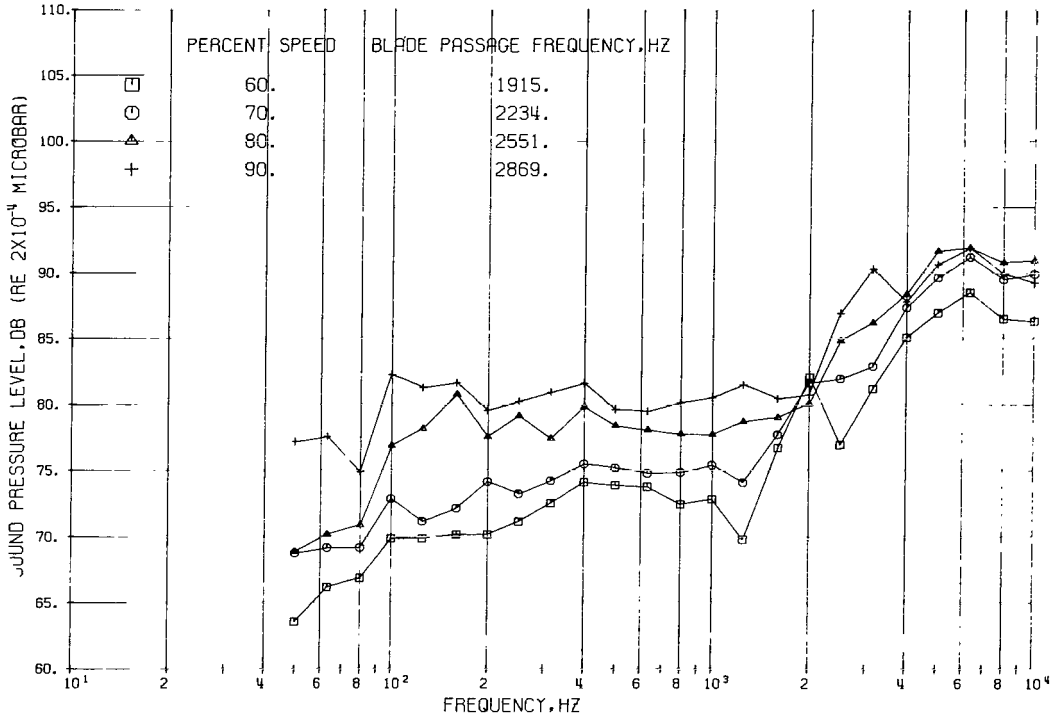

FIGURE 12. -SOUND PRESSURE LEVEL ON 100-FOOT RADIUS. CONFIGURATION 10. 10-DEGREE ANGLE. SHORT INLET; STANDARD NOZZLE; ACOUSTICALLY TREATED.

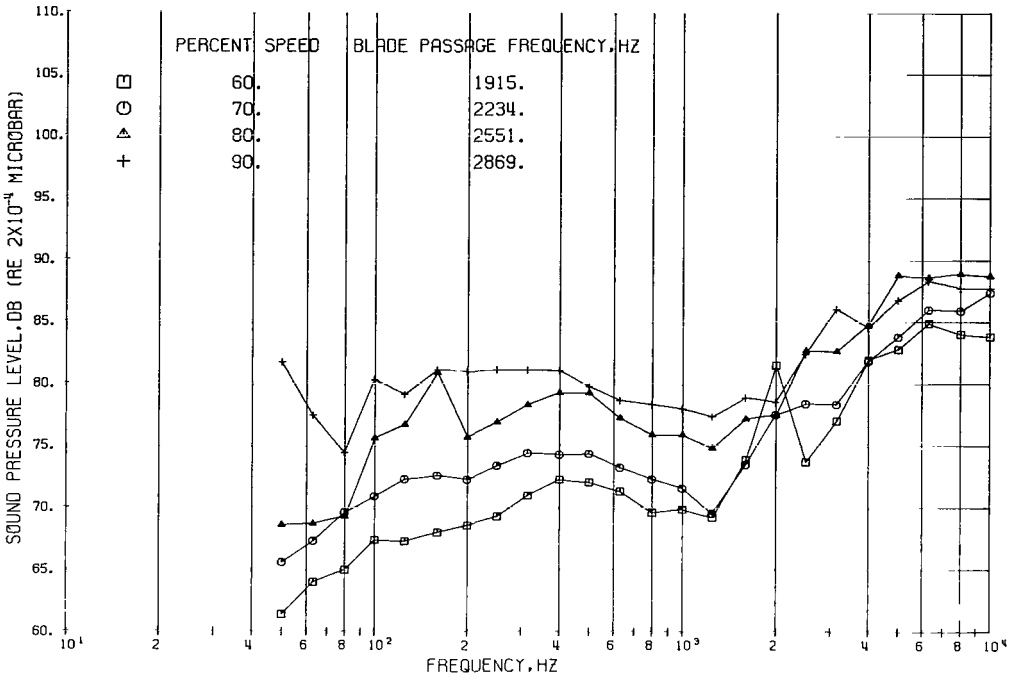

FIGURE 13. -SOUND PRESSURE LEVEL ON 100-FOOT RADIUS. CONFIGURATION 10, 20-DEGREE ANGLE. SHORT INLET; STANDARD NOZZLE; ACOUSTICALLY TREATED.

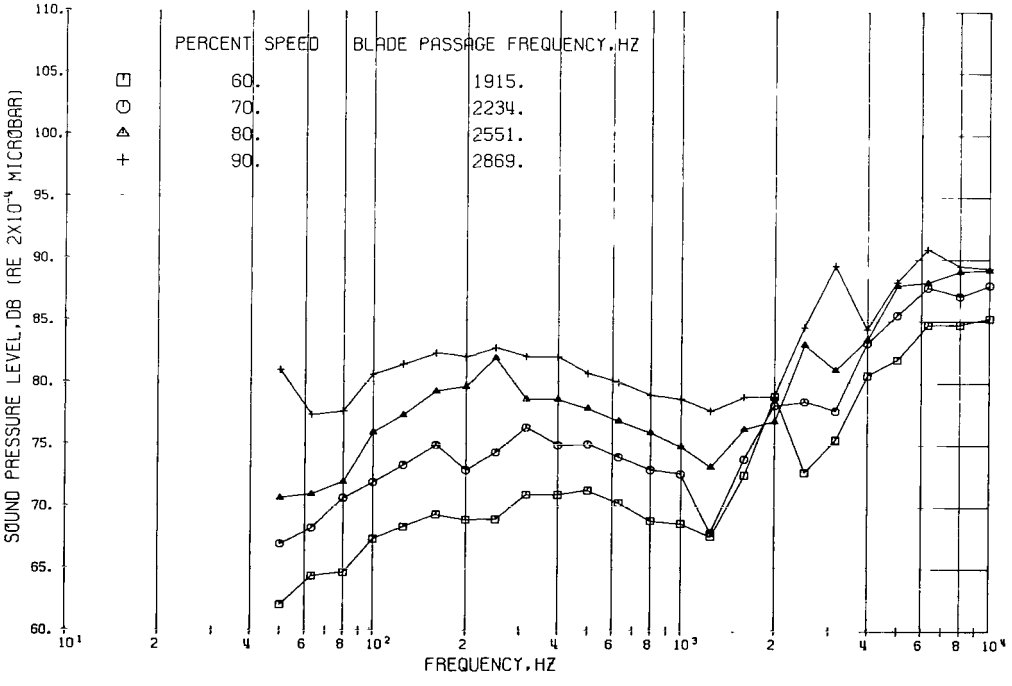

FIGURE 14. -SOUND PRESSURE LEVEL ON 100-FOOT RADIUS. CONFIGURATION 10, 30-DEGREE ANGLE. SHORT INLET; STANDARD NOZZLE; ACOUSTICALLY TREATED.

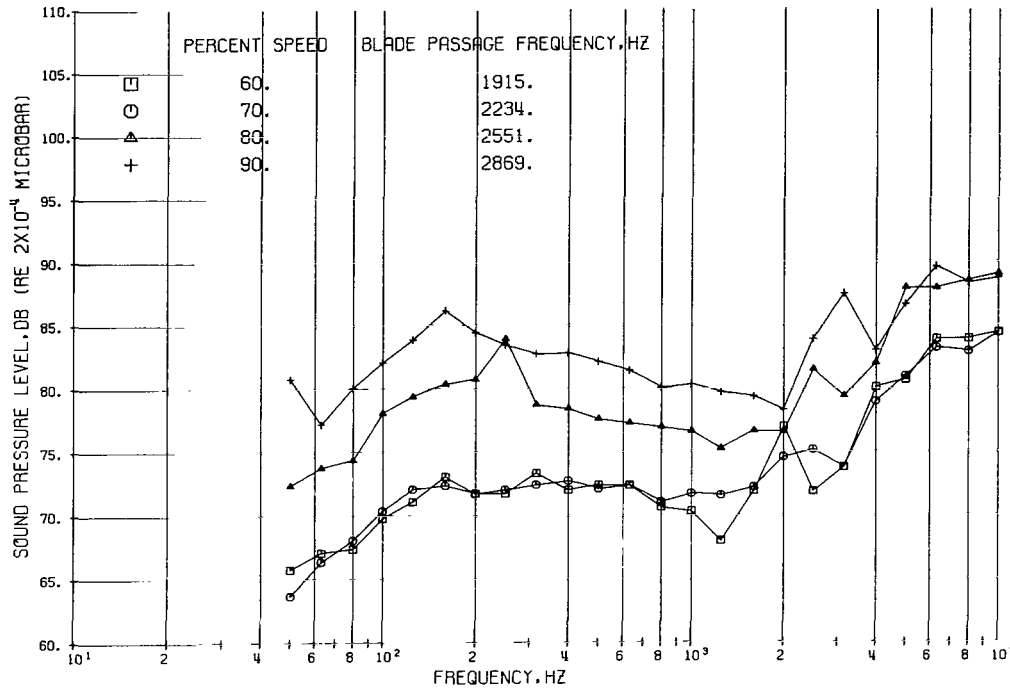

FIGURE 15. -SOUND PRESSURE LEVEL ON 100-FOOT RADIUS. CONFIGURATION 10, 40-DEGREE ANGLE. SHORT INLET; STANDARD NOZZLE; ACOUSTICALLY TREATED.

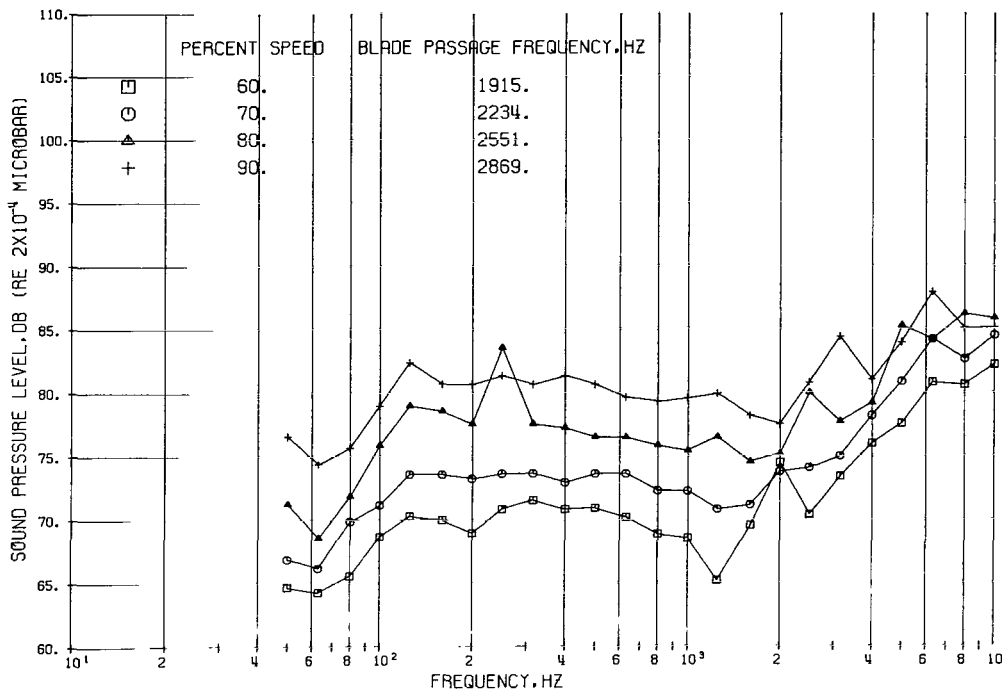

FIGURE 16. -SOUND PRESSURE LEVEL ON 100-FOOT RADIUS. CONFIGURATION 10, 50-DEGREE ANGLE. SHORT INLET; STANDARD NOZZLE; ACOUSTICALLY TREATED.

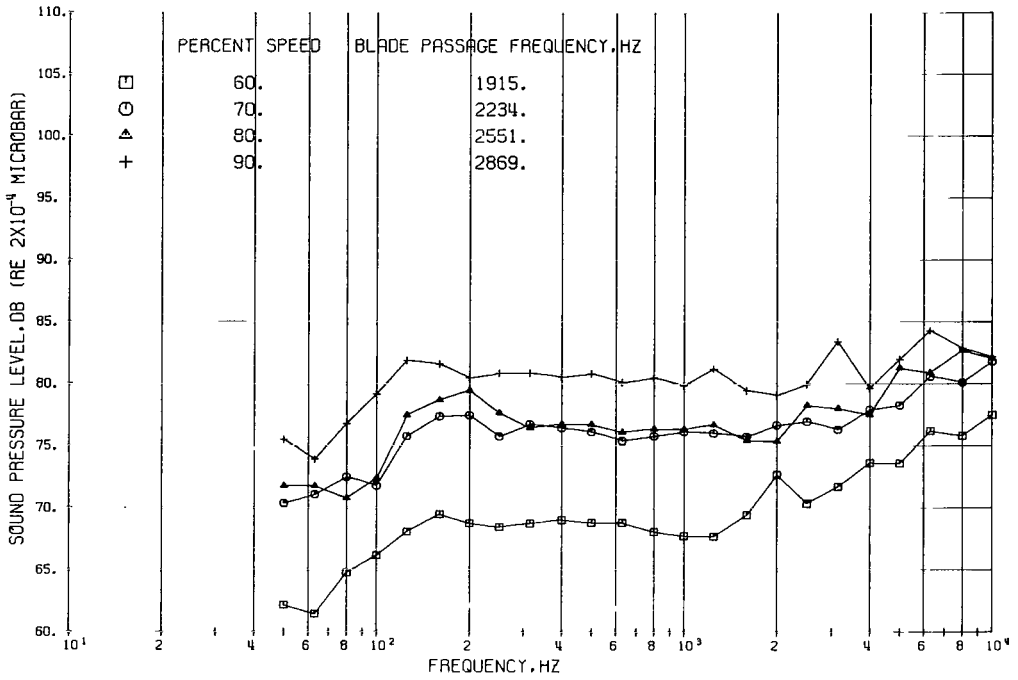

FIGURE 17 . -SOUND PRESSURE LEVEL ON 100-FOOT RADIUS. CONFIGURATION 10, 60-DEGREE ANGLE. SHORT INLET; STANDARD NOZZLE; ACOUSTICALLY TREATED.

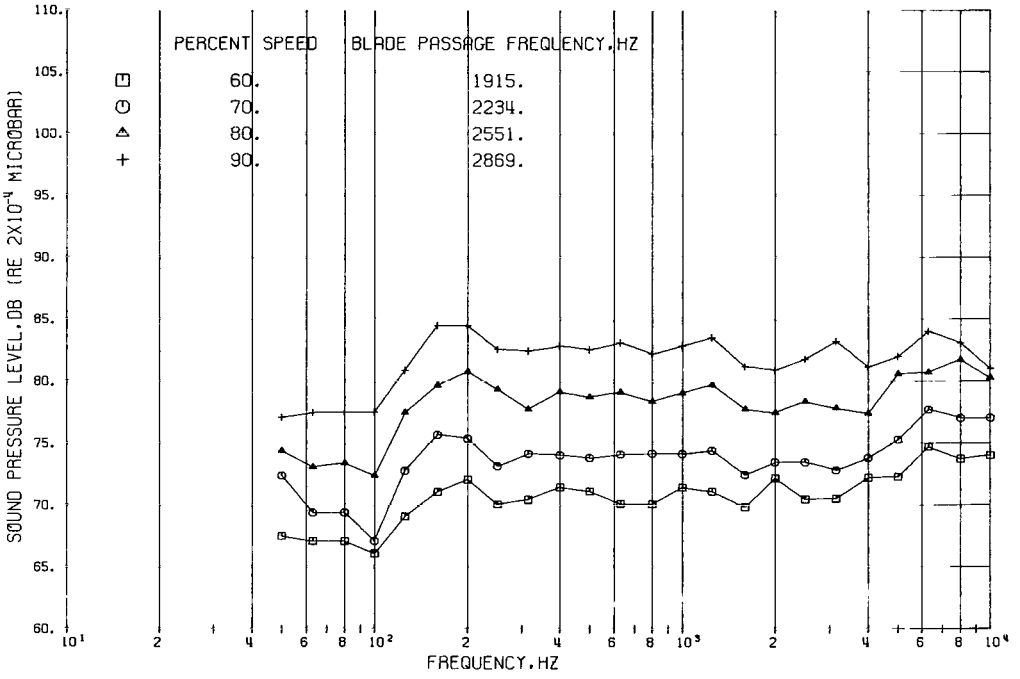

FIGURE 18. -SOUND PRESSURE LEVEL ON 100-FOOT RADIUS. CONFIGURATION 10, 70-DEGREE ANGLE. SHORT INLET; STANDARD NOZZLE; ACOUSTICALLY TREATED.

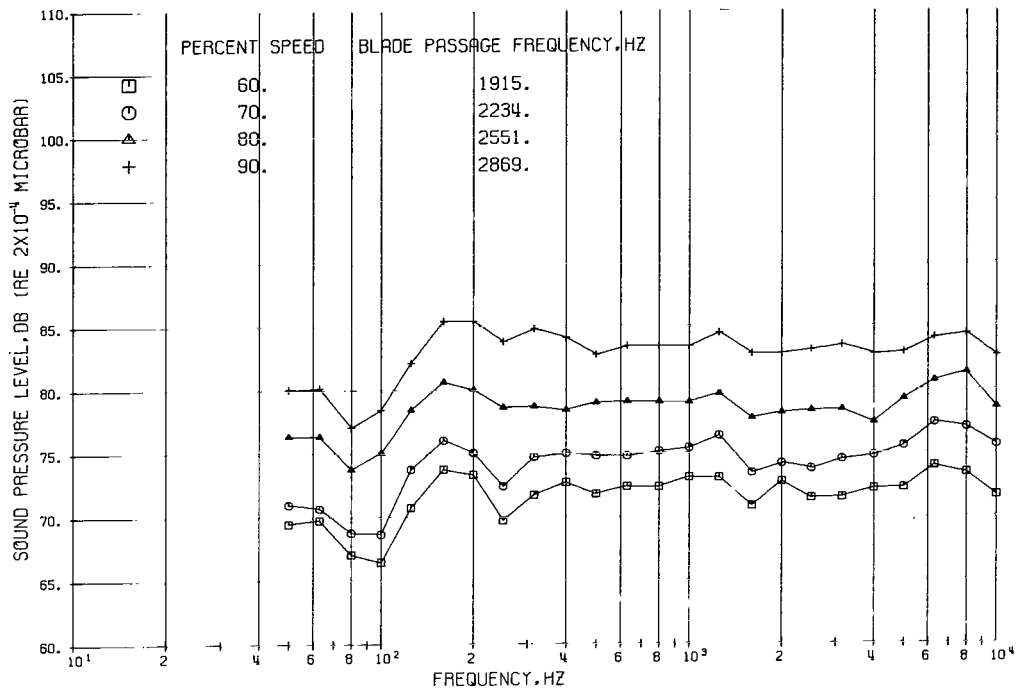

FIGURE 19. -SOUND PRESSURE LEVEL ON 100-FOOT RADIUS. CONFIGURATION 10, 80-DEGREE ANGLE. SHORT INLET; STANDARD NOZZLE; ACOUSTICALLY TREATED.

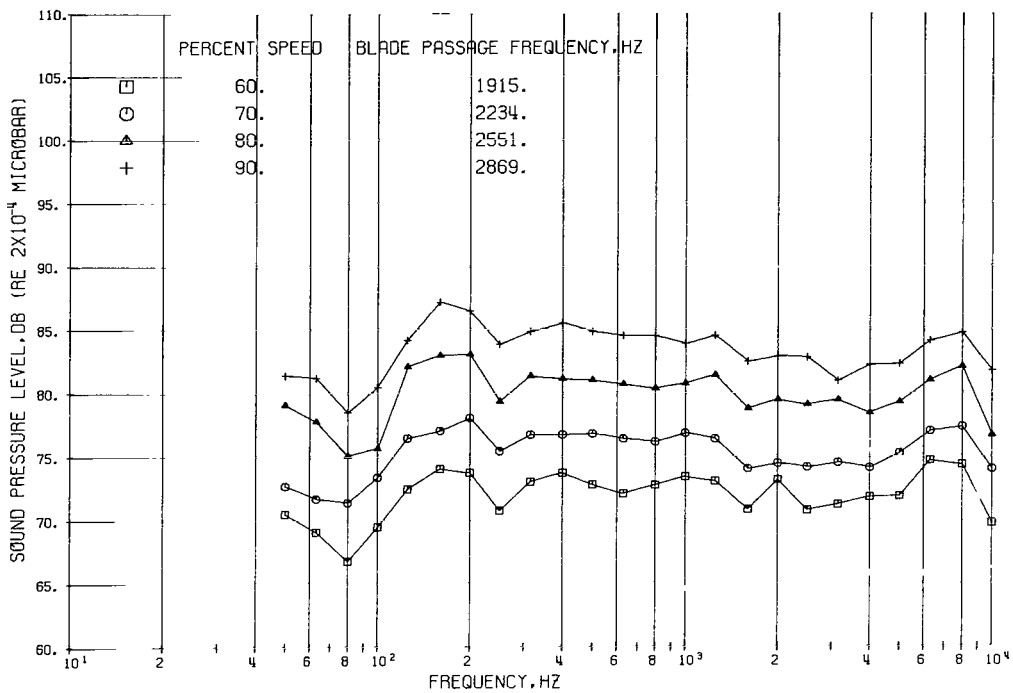

FIGURE 20. -SOUND PRESSURE LEVEL ON 100-FOOT RADIUS. CONFIGURATION 10, 90-DEGREE ANGLE. SHORT INLET; STANDARD NOZZLE; ACOUSTICALLY TREATED.

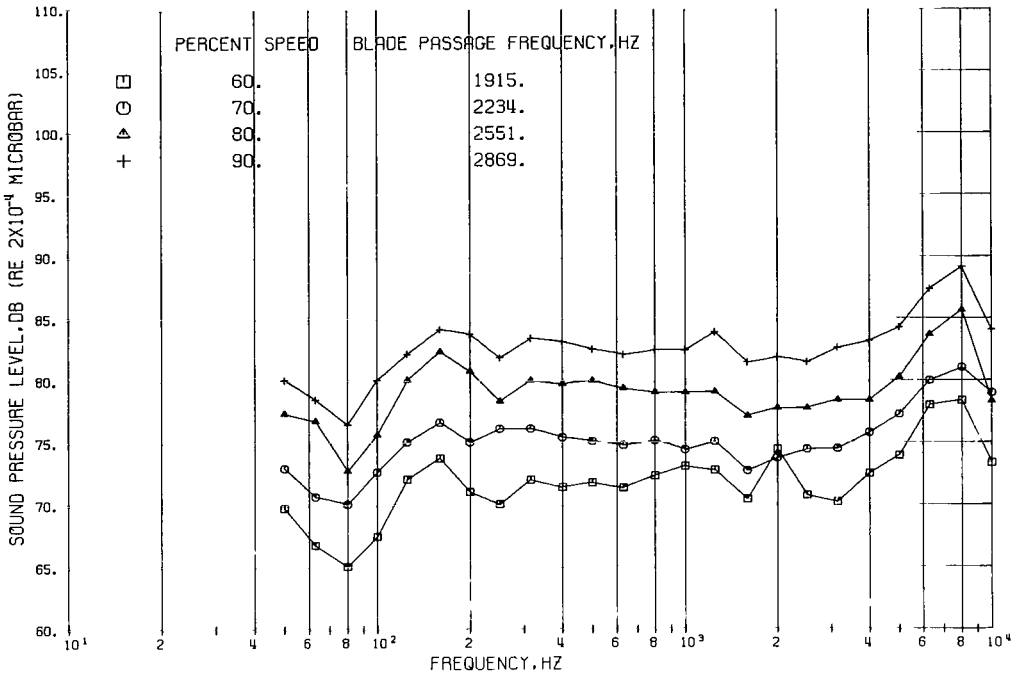

FIGURE 21. -SOUND PRESSURE LEVEL ON 100-FOOT RADIUS. CONFIGURATION 10, 100-DEGREE ANGLE. SHORT INLET; STANDARD NOZZLE; ACOUSTICALLY TREATED.

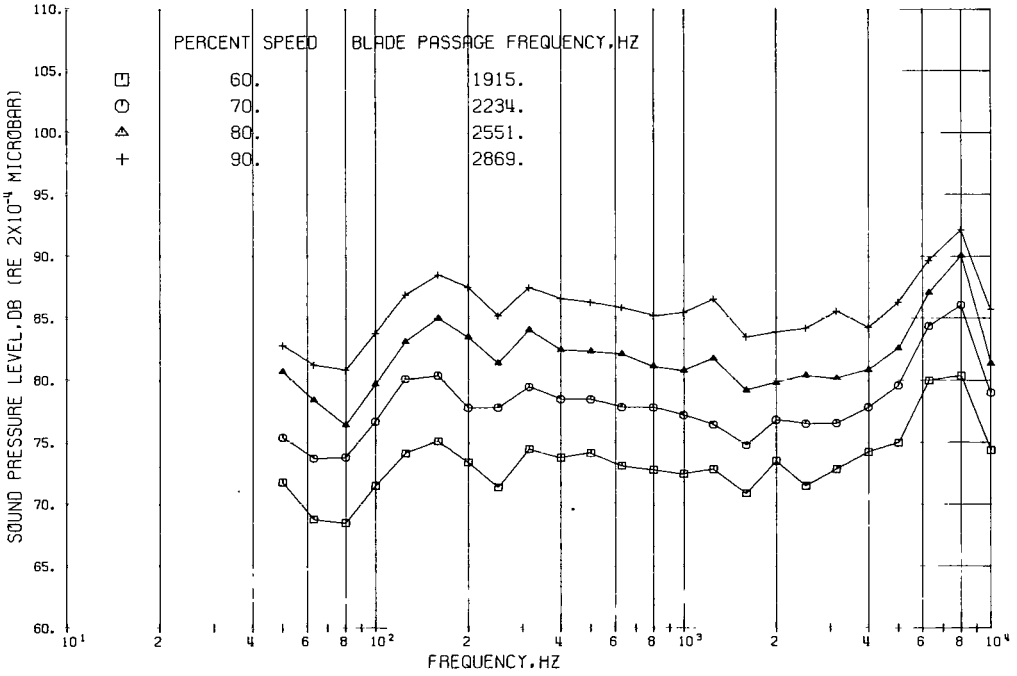

FIGURE 22. -SOUND PRESSURE LEVEL ON 100-FOOT RADIUS. CONFIGURATION 10, 110-DEGREE ANGLE. SHORT INLET; STANDARD NOZZLE; ACOUSTICALLY TREATED.

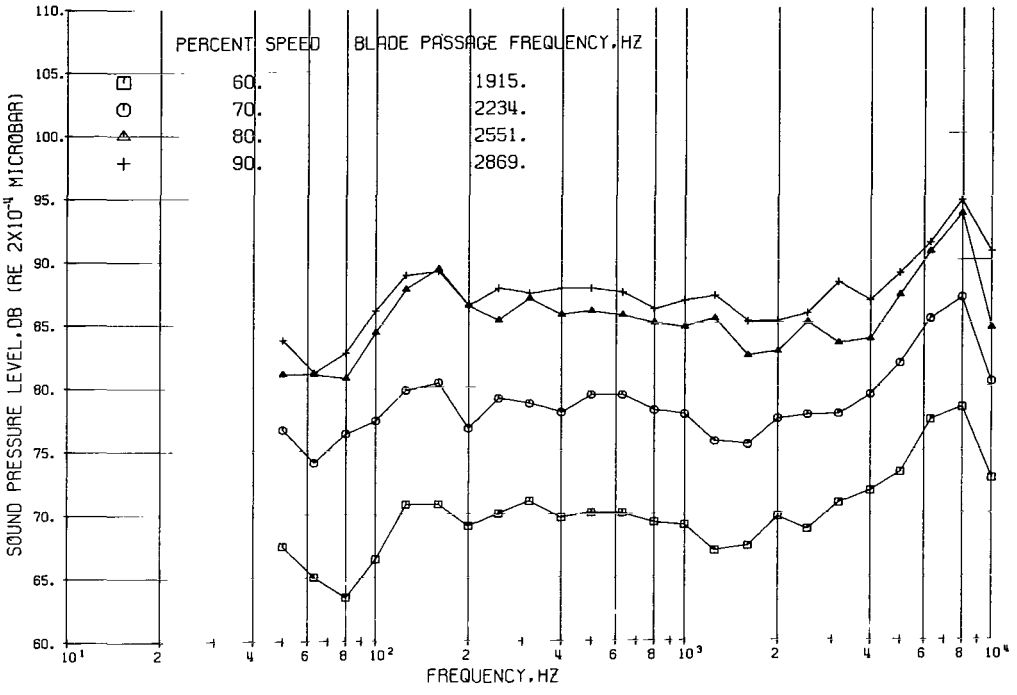

FIGURE 23. -SOUND PRESSURE LEVEL ON 100-FOOT RADIUS. CONFIGURATION 10, 120-DEGREE ANGLE. SHORT INLET; STANDARD NOZZLE; ACOUSTICALLY TREATED.

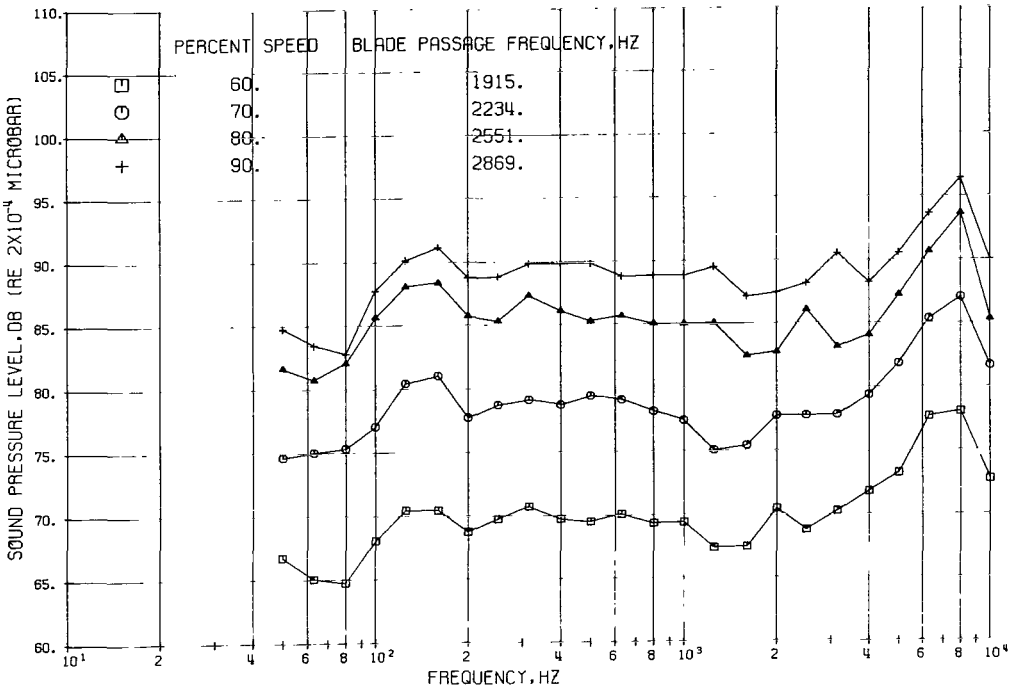

FIGURE 24. -SOUND PRESSURE LEVEL ON 100-FOOT RADIUS. CONFIGURATION 10, 130-DEGREE ANGLE. SHORT INLET; STANDARD NOZZLE; ACOUSTICALLY TREATED.

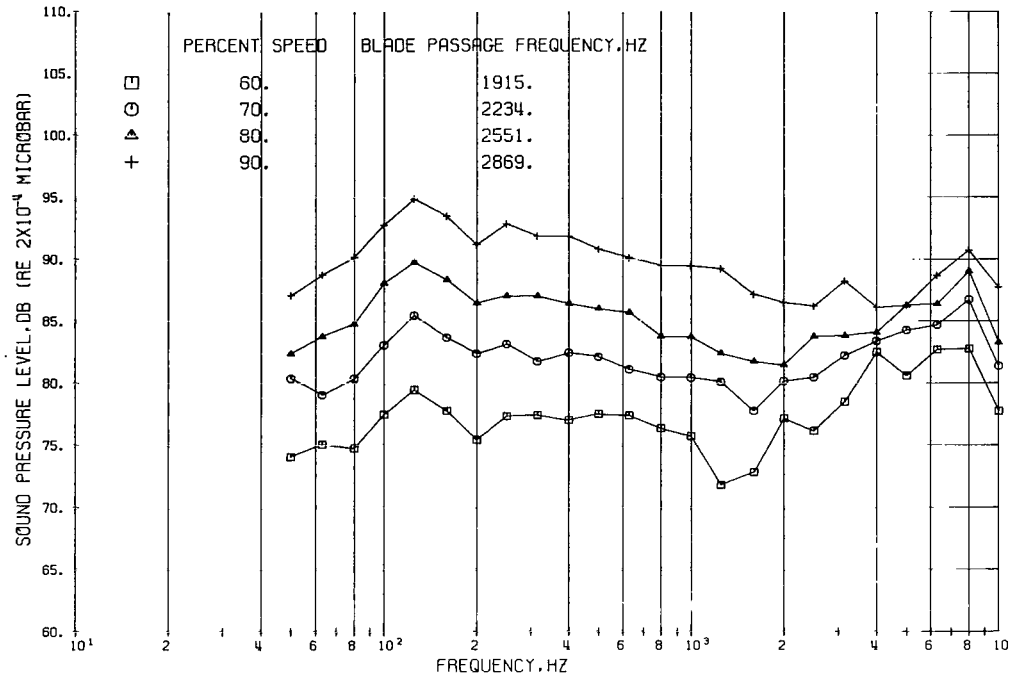

FIGURE 25. -SOUND PRESSURE LEVEL ON 100-FOOT RADIUS. CONFIGURATION 10, 140-DEGREE ANGLE. SHORT INLET; STANDARD NOZZLE; ACOUSTICALLY TREATED.

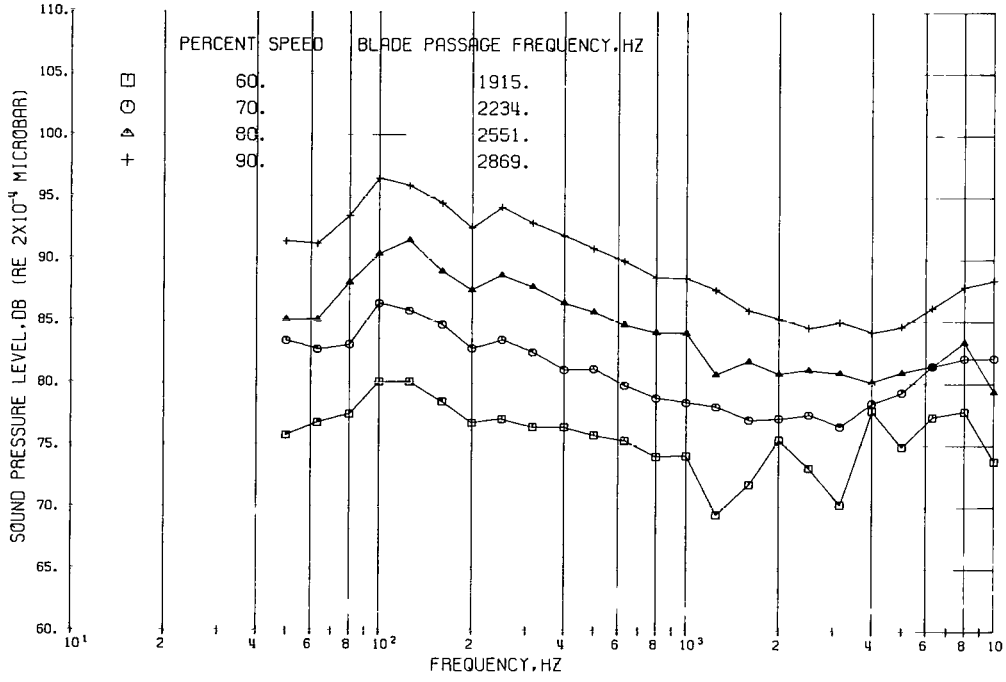

FIGURE 26. -SOUND PRESSURE LEVEL ON 100-FOOT RADIUS. CONFIGURATION 10, 150-DEGREE ANGLE. SHORT INLET; STANDARD NOZZLE; ACOUSTICALLY TREATED.

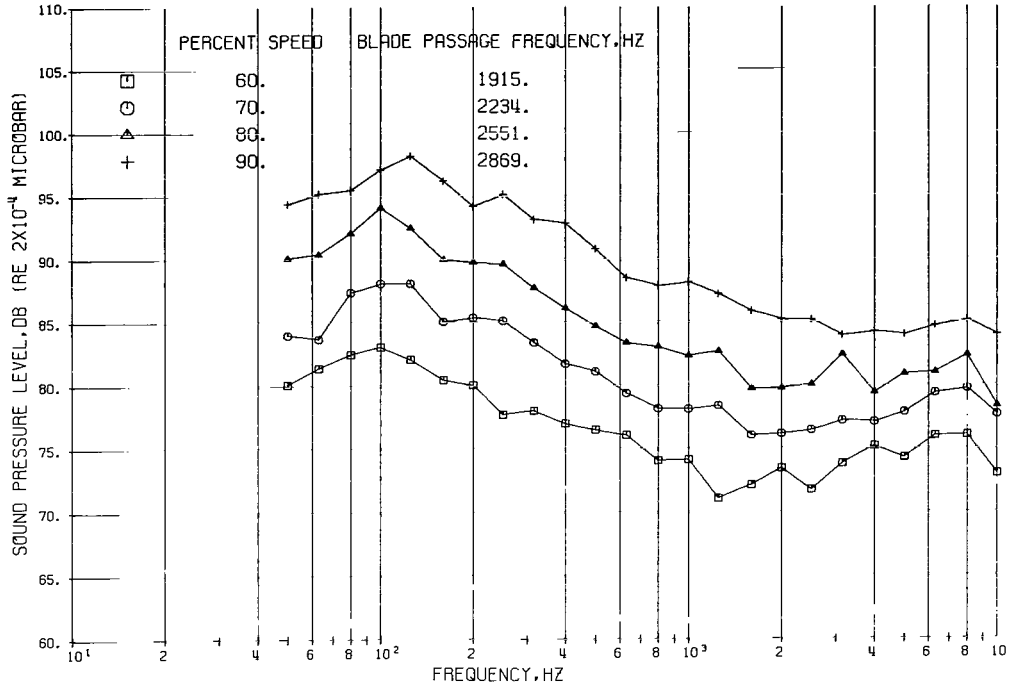

FIGURE 27. -SOUND PRESSURE LEVEL ON 100-FOOT RADIUS. CONFIGURATION 10, 160-DEGREE ANGLE. SHORT INLET; STANDARD NOZZLE; ACOUSTICALLY TREATED.

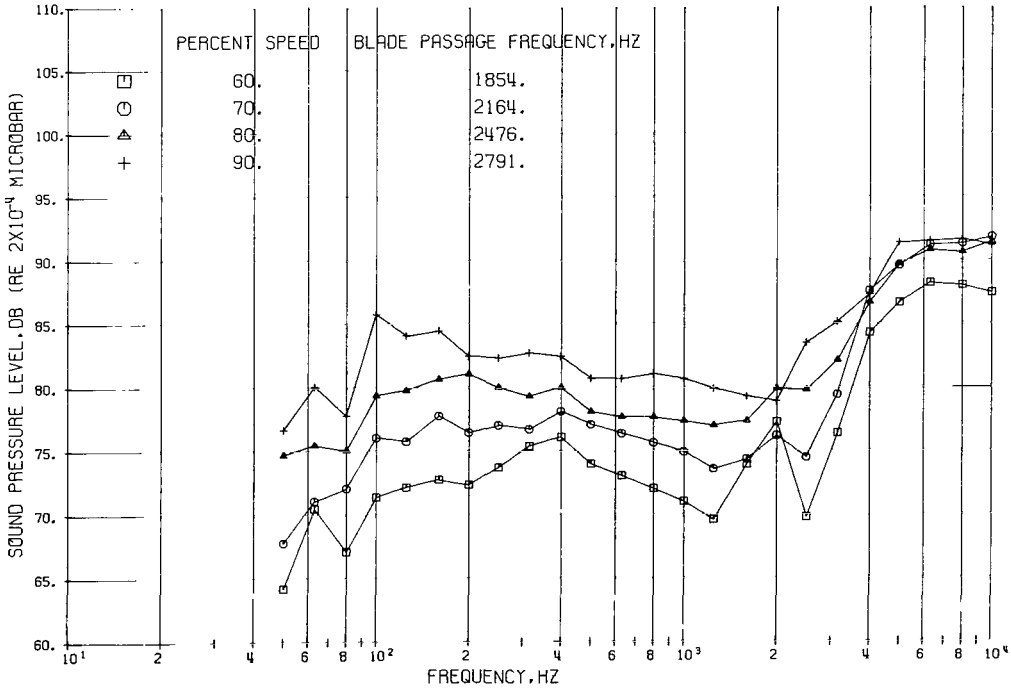

FIGURE 28. -SOUND PRESSURE LEVEL ON 100-FOOT RADIUS. CONFIGURATION 11, 10-DEGREE ANGLE. LONG INLET; STANDARD NOZZLE; ACOUSTICALLY TREATED.

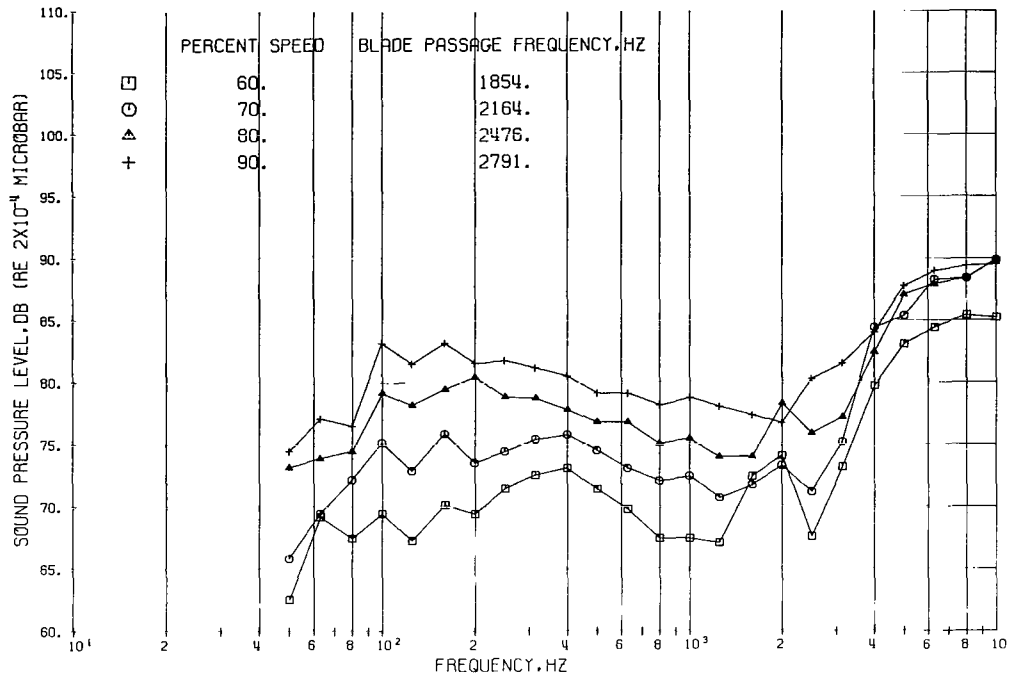

FIGURE 29. -SOUND PRESSURE LEVEL ON 100-FOOT RADIUS. CONFIGURATION 11, 20-DEGREE ANGLE. LONG INLET; STANDARD NOZZLE; ACOUSTICALLY TREATED.

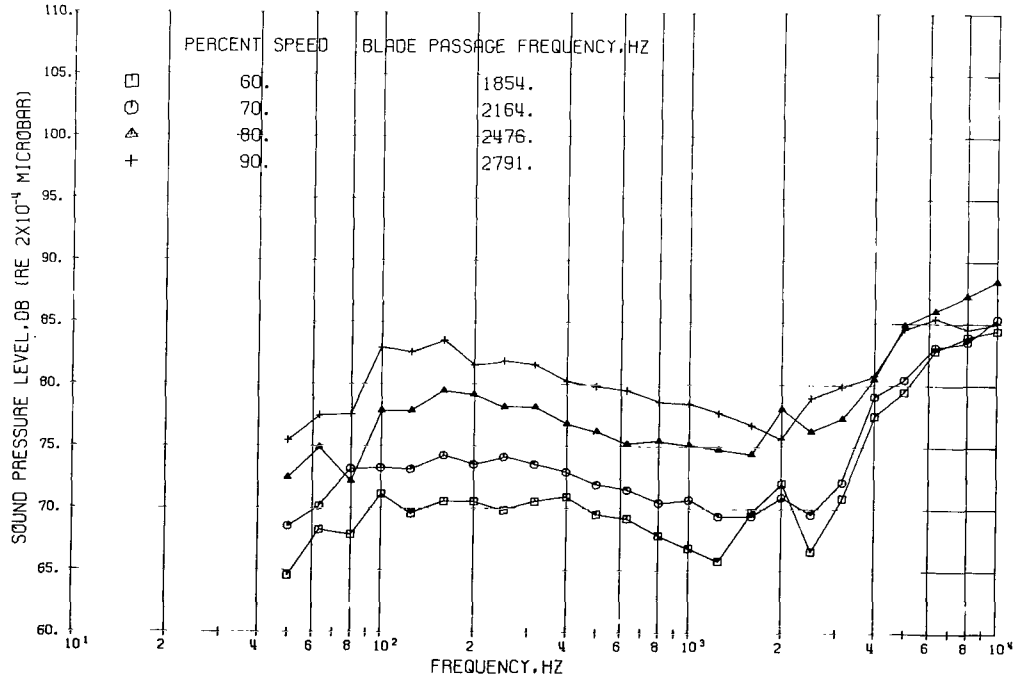

FIGURE 30. -SOUND PRESSURE LEVEL ON 100-FOOT RADIUS. CONFIGURATION 11, 30-DEGREE ANGLE. LONG INLET; STANDARD NOZZLE; ACOUSTICALLY TREATED.

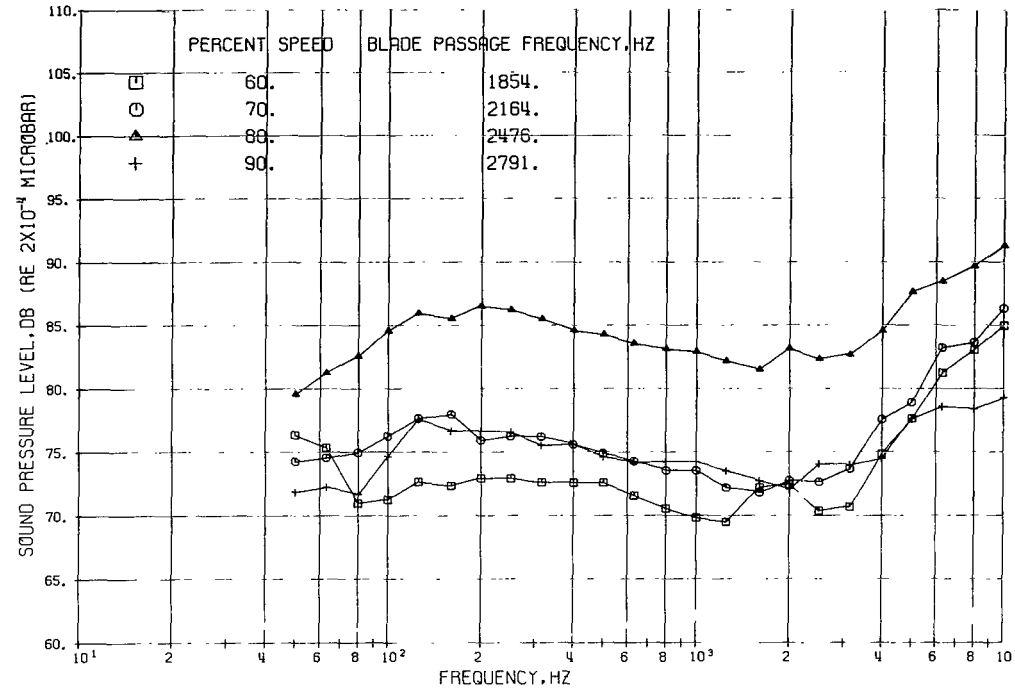

FIGURE 31. -SOUND PRESSURE LEVEL ON 100-FOOT RADIUS. CONFIGURATION 11, 40-DEGREE ANGLE. LONG INLET; STANDARD NOZZLE; ACOUSTICALLY TREATED.

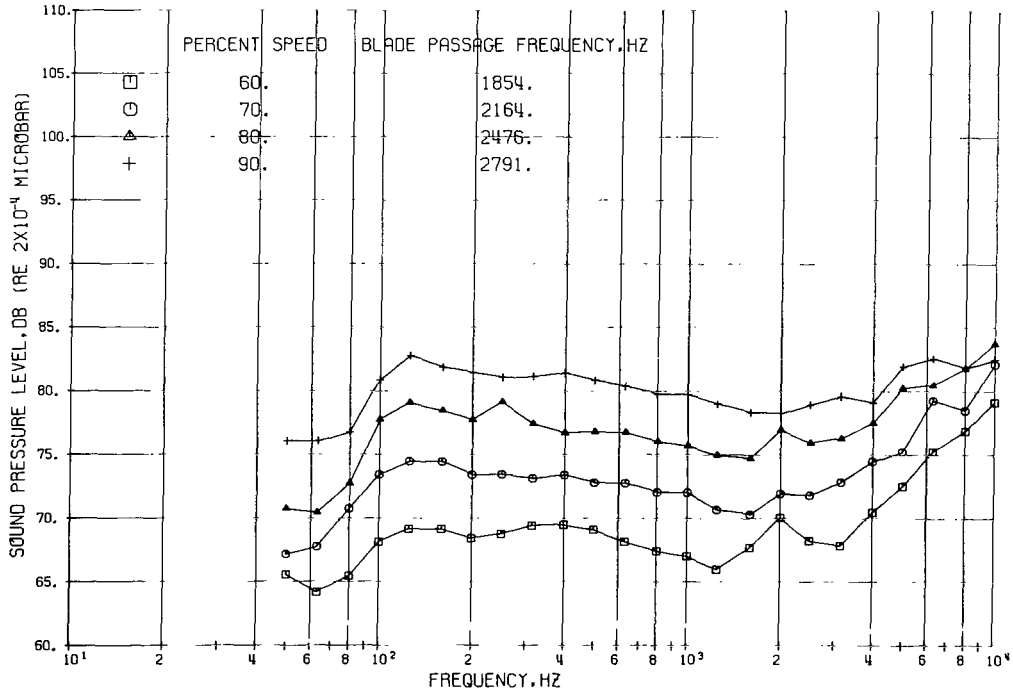

FIGURE 32. -SOUND PRESSURE LEVEL ON 100-FOOT RADIUS. CONFIGURATION 11. 50-DEGREE ANGLE. LONG INLET; STANDARD NOZZLE; ACOUSTICALLY TREATED.

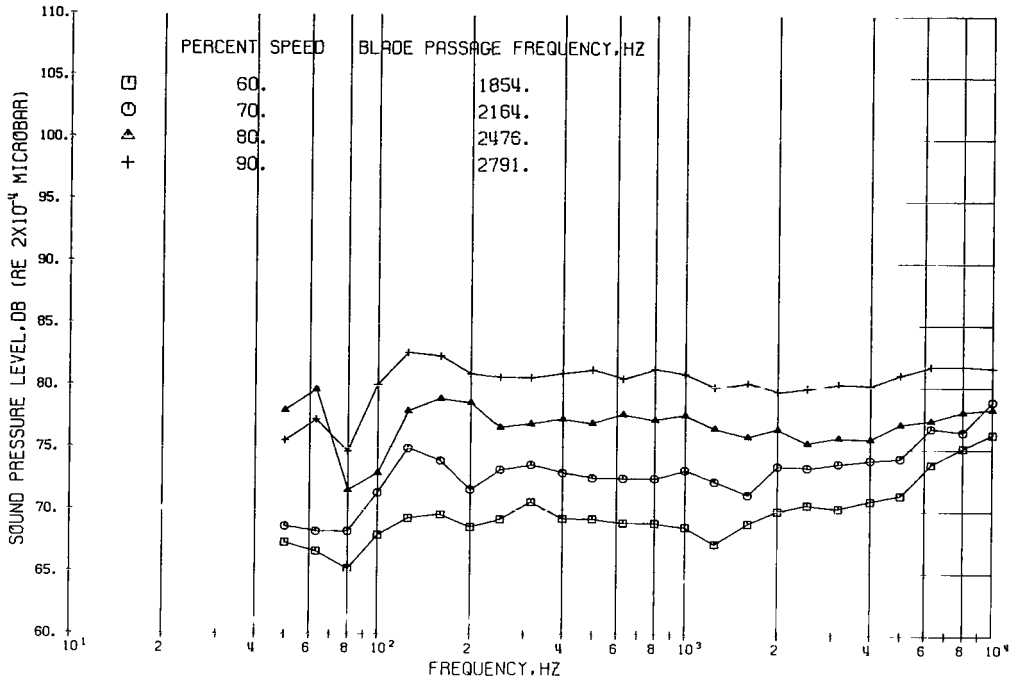

FIGURE 33. -SOUND PRESSURE LEVEL ON 100-FOOT RADIUS. CONFIGURATION 11. 60-DEGREE ANGLE. LONG INLET; STANDARD NOZZLE; ACOUSTICALLY TREATED.

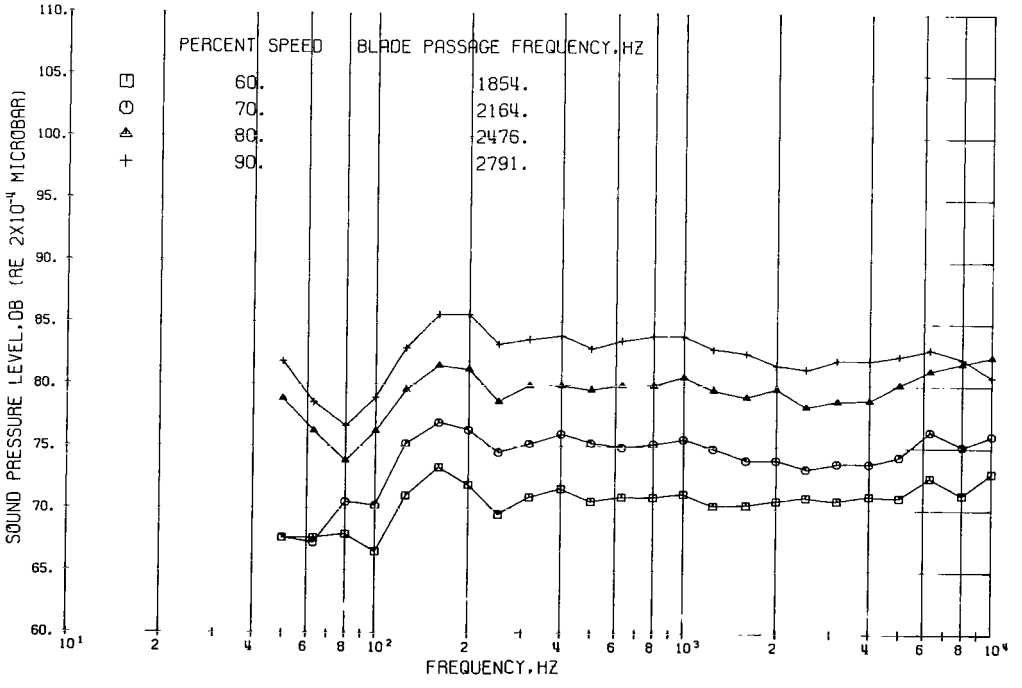

FIGURE 34. -SOUND PRESSURE LEVEL ON 100-FOOT RADIUS. CONFIGURATION 11. 70-DEGREE ANGLE. LONG INLET; STANDARD NOZZLE; ACOUSTICALLY TREATED.

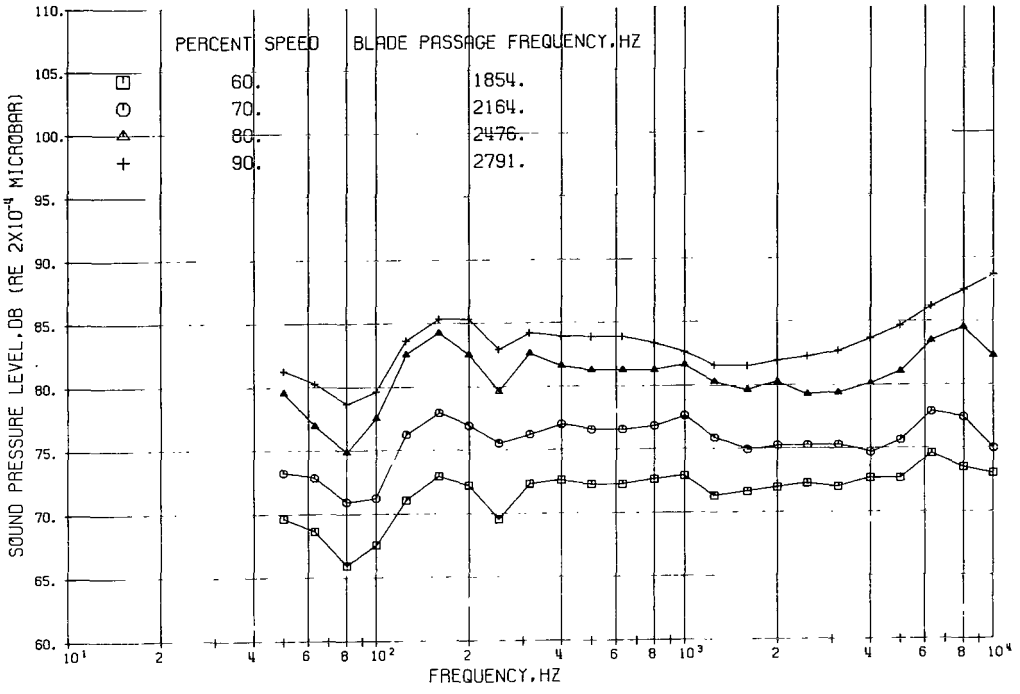

FIGURE 35. -SOUND PRESSURE LEVEL ON 100-FOOT RADIUS. CONFIGURATION 11, 80-DEGREE ANGLE. LONG INLET; STANDARD NOZZLE; ACOUSTICALLY TREATED.

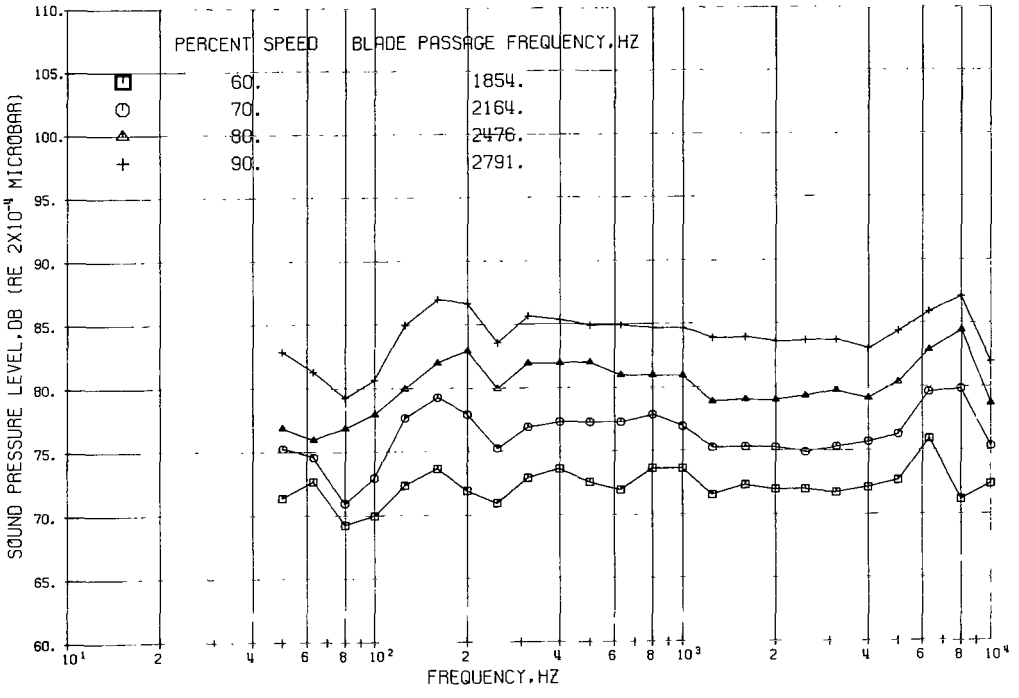

FIGURE 36. -SOUND PRESSURE LEVEL ON 100-FOOT RADIUS. CONFIGURATION 11, 90-DEGREE ANGLE. LONG INLET; STANDARD NOZZLE; ACOUSTICALLY TREATED.

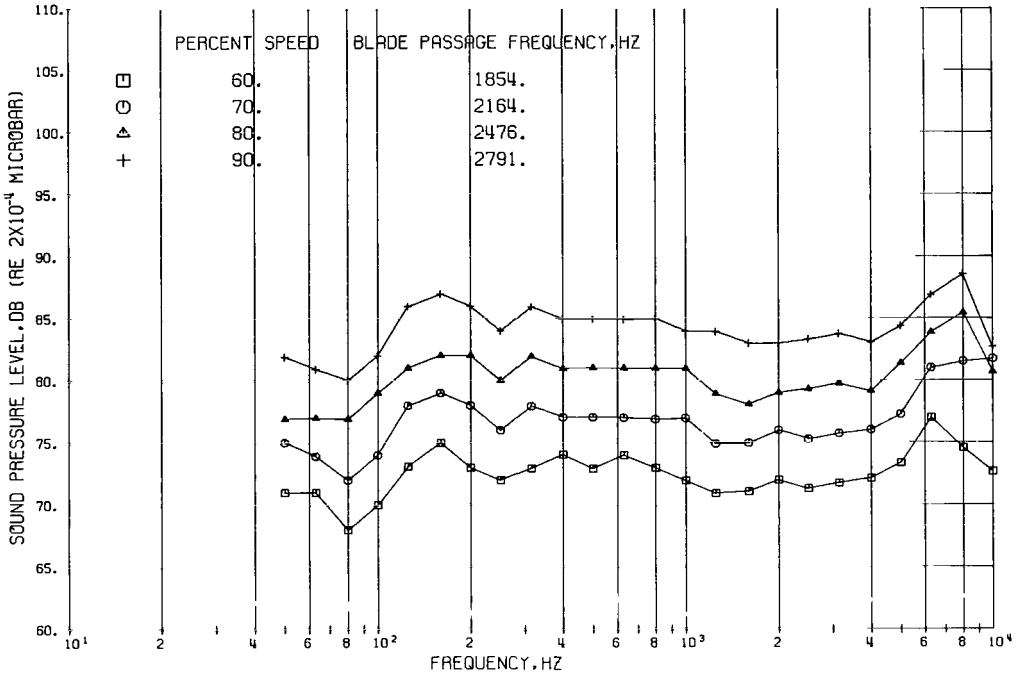

FIGURE 37 . -SOUND PRESSURE LEVEL ON 100-FOOT RADIUS. CONFIGURATION 11, 100-DEGREE ANGLE. LONG INLET; STANDARD NOZZLE; ACOUSTICALLY TREATED.

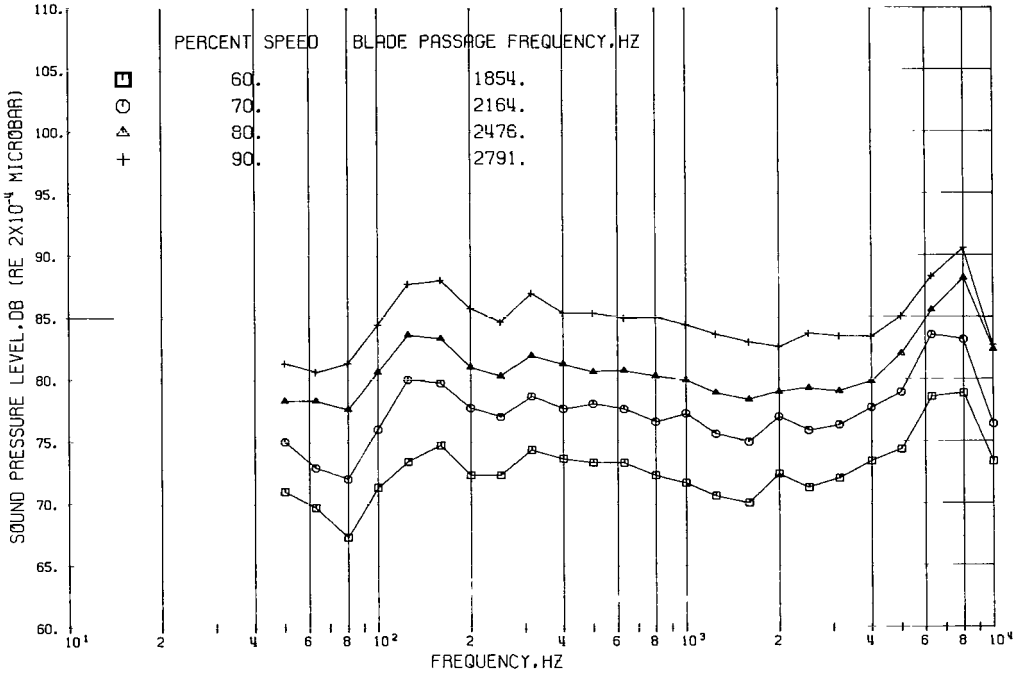

FIGURE 38 . -SOUND PRESSURE LEVEL ON 100-FOOT RADIUS. CONFIGURATION 11, 110-DEGREE ANGLE. LONG INLET; STANDARD NOZZLE; ACOUSTICALLY TREATED.

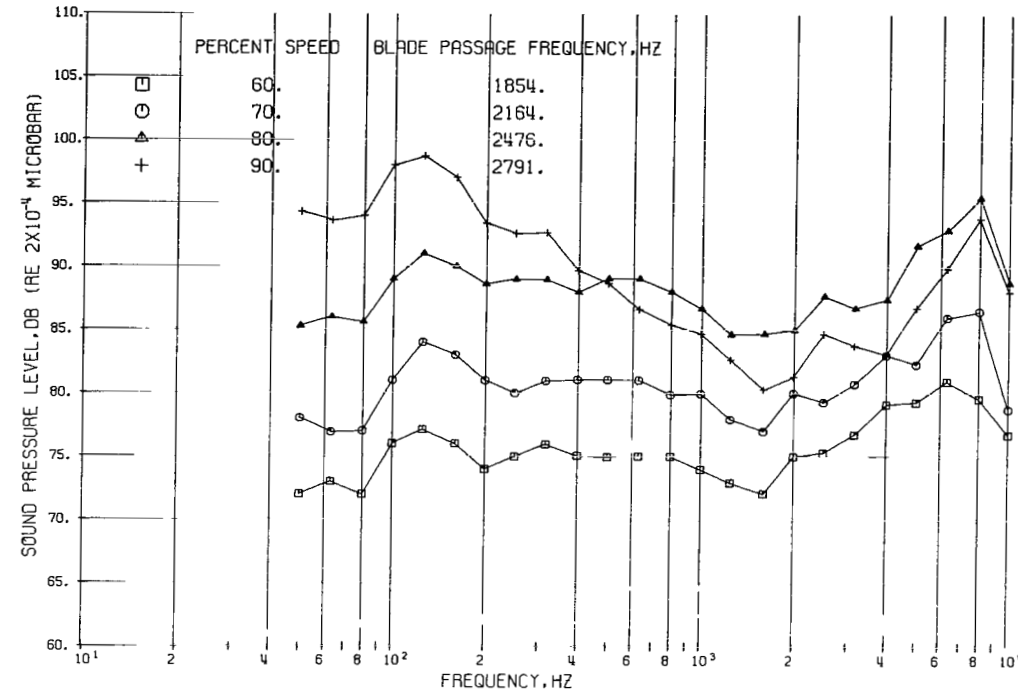

FIGURE 39. -SOUND PRESSURE LEVEL ON 100-FOOT RADIUS. CONFIGURATION 11, 120-DEGREE ANGLE. LONG INLET; STANDARD NOZZLE; ACOUSTICALLY TREATED.

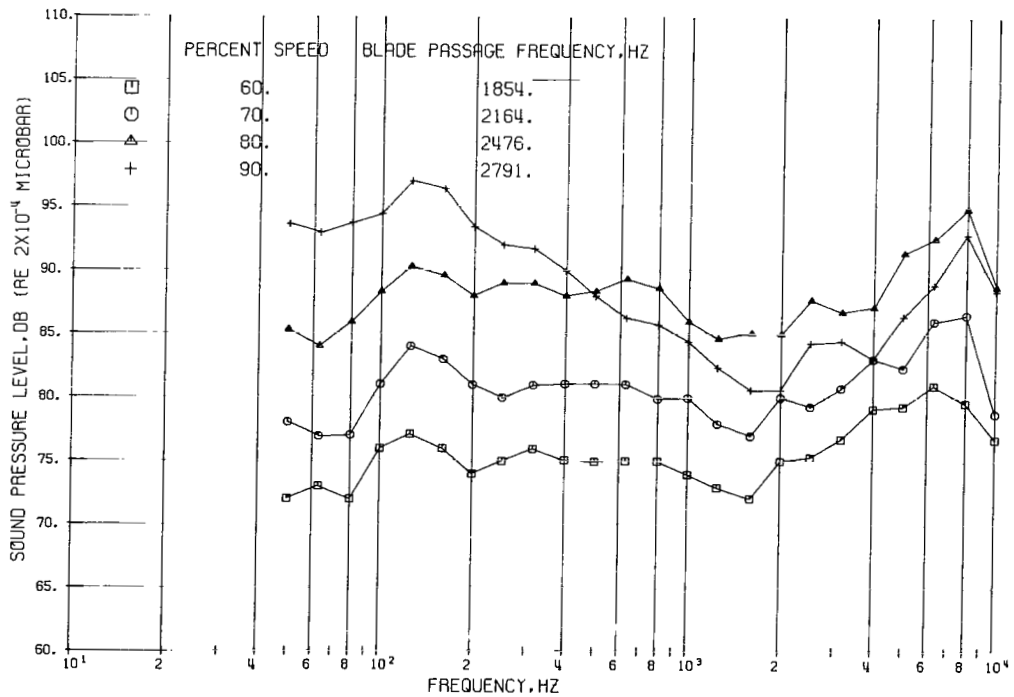

FIGURE 40. -SOUND PRESSURE LEVEL ON 100-FOOT RADIUS. CONFIGURATION 11, 130-DEGREE ANGLE. LONG INLET; STANDARD NOZZLE; ACOUSTICALLY TREATED.

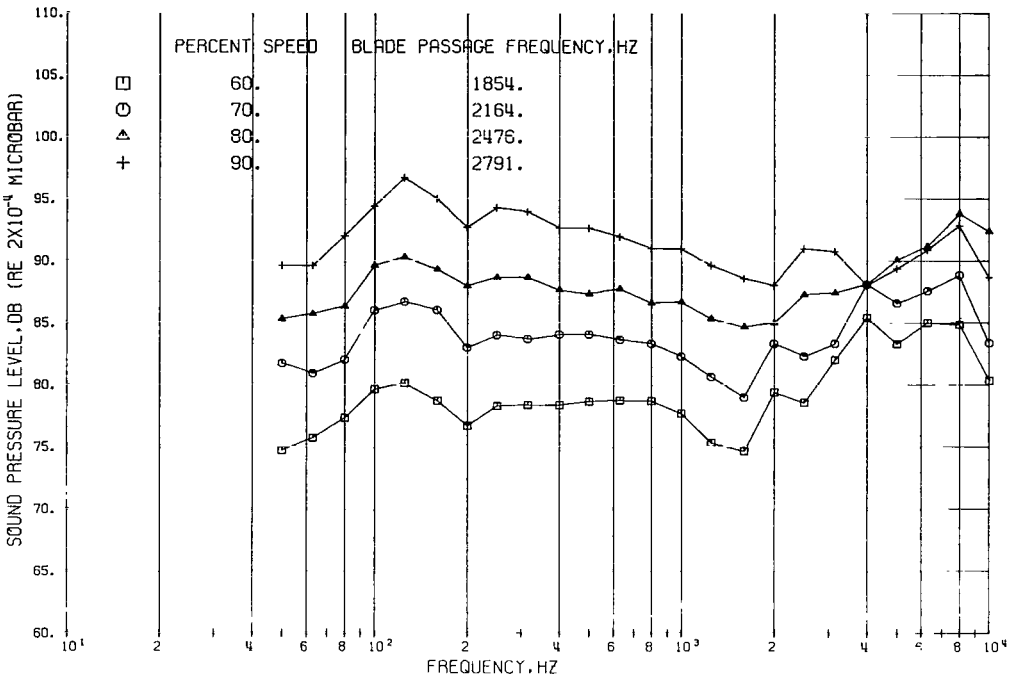

FIGURE 41. -SOUND PRESSURE LEVEL ON 100-FOOT RADIUS. CONFIGURATION 11, 140-DEGREE ANGLE. LONG INLET; STANDARD NOZZLE; ACOUSTICALLY TREATED.

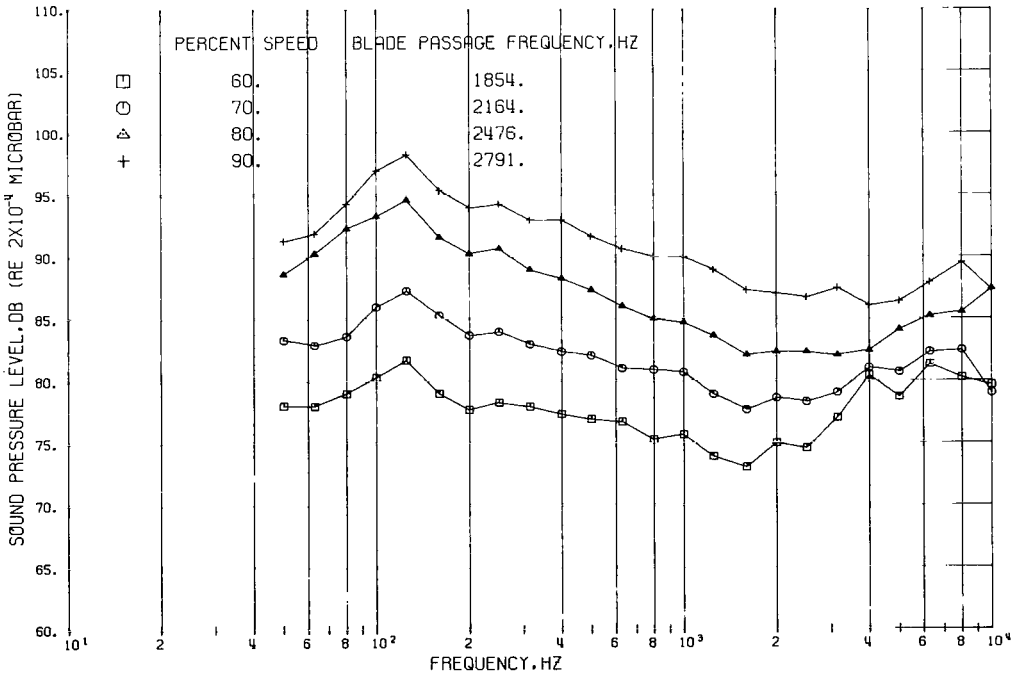

FIGURE 42. -SOUND PRESSURE LEVEL ON 100-FOOT RADIUS. CONFIGURATION 11, 150-DEGREE ANGLE. LONG INLET; STANDARD NOZZLE; ACOUSTICALLY TREATED.

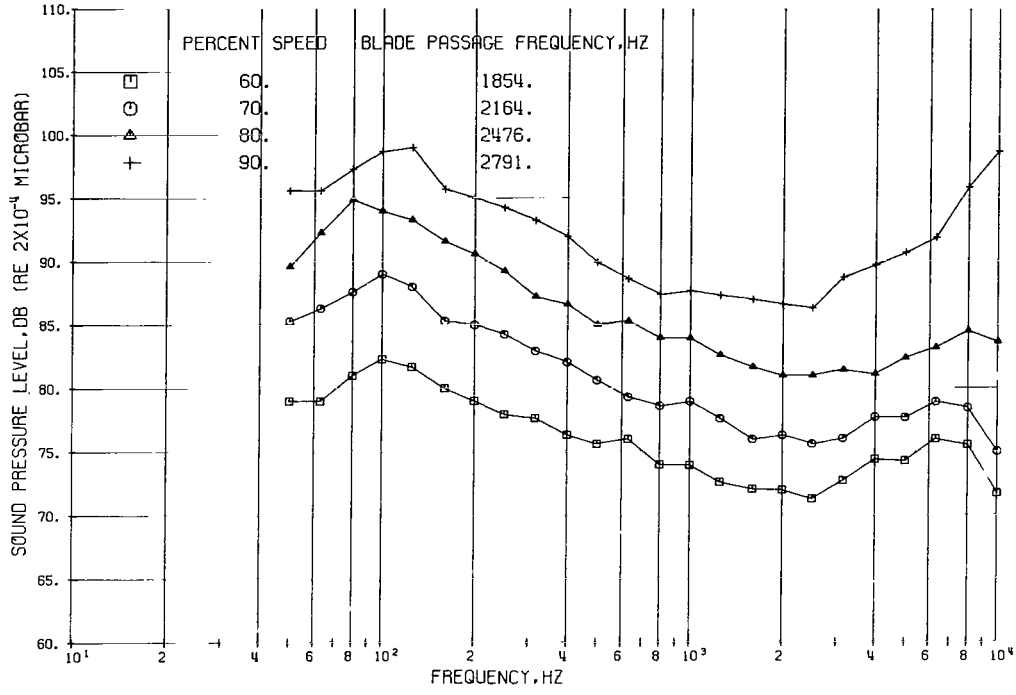

FIGURE 43 . -SOUND PRESSURE LEVEL ON 100-FOOT RADIUS. CONFIGURATION 11, 160-DEGREE ANGLE. LONG INLET; STANDARD NOZZLE; ACOUSTICALLY TREATED.

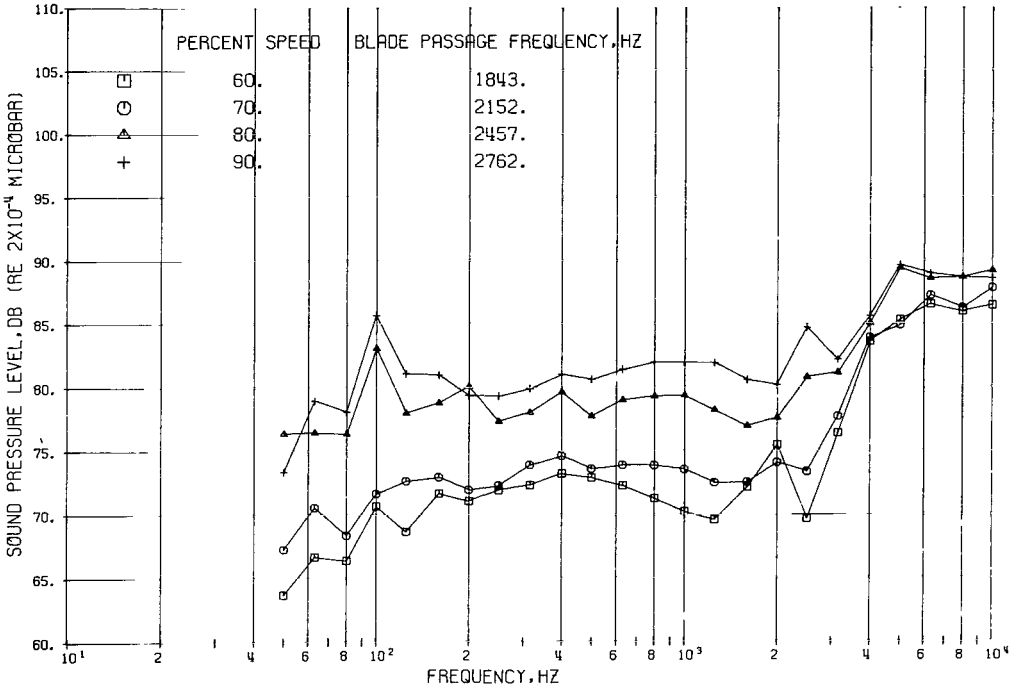

FIGURE 44 . -SOUND PRESSURE LEVEL ON 100-FOOT RADIUS. CONFIGURATION 12, 10-DEGREE ANGLE. LONG INLET; 10-PERCENT OVERSIZE NOZZLE; ACOUSTICALLY TREATED.

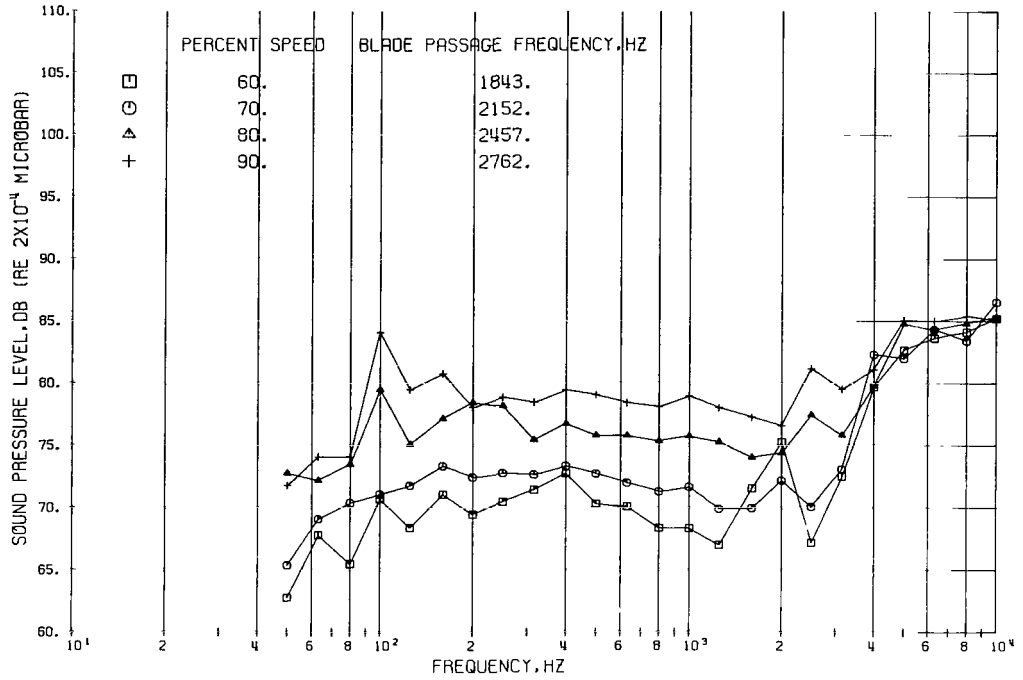

FIGURE 45. -SOUND PRESSURE LEVEL ON 100-FOOT RADIUS. CONFIGURATION 12, 20-DEGREE ANGLE. LONG INLET; 10-PERCENT OVERSIZE NOZZLE; ACOUSTICALLY TREATED.

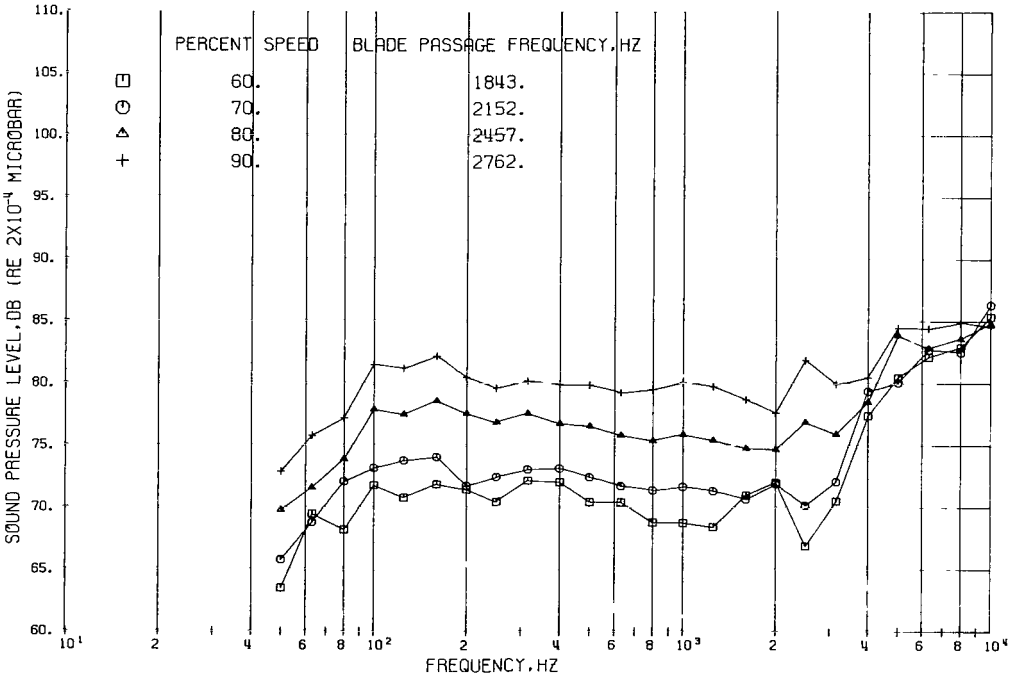

FIGURE 46. -SOUND PRESSURE LEVEL ON 100-FOOT RADIUS. CONFIGURATION 12, 30-DEGREE ANGLE. LONG INLET; 10-PERCENT OVERSIZE NOZZLE; ACOUSTICALLY TREATED.

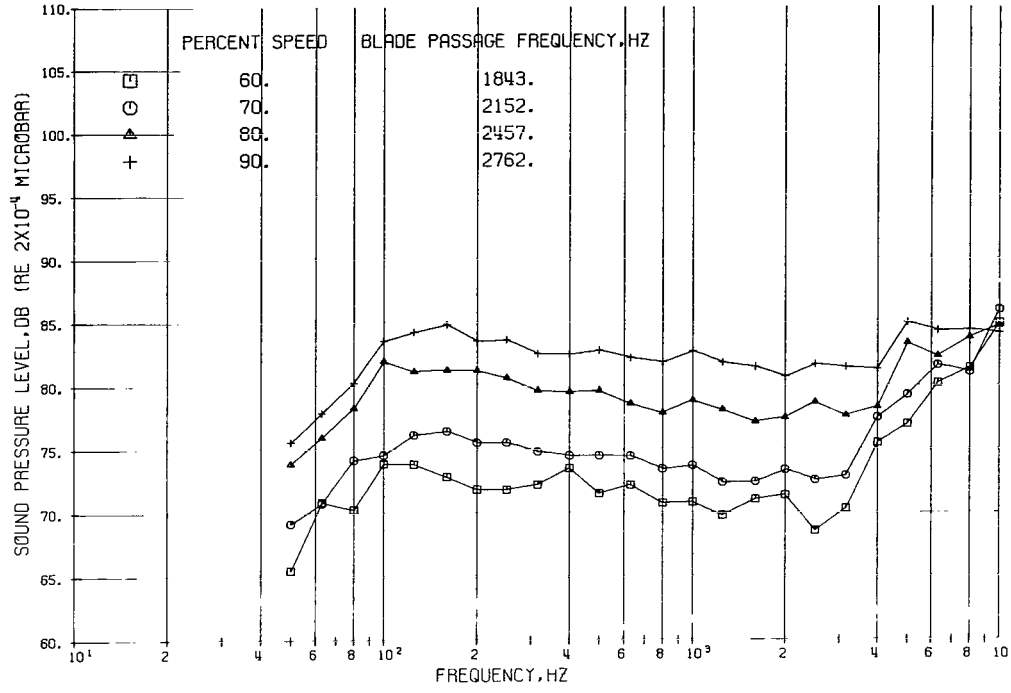

FIGURE 47 . -SOUND PRESSURE LEVEL ON 100-FOOT RADIUS. CONFIGURATION 12, 40-DEGREE ANGLE. LONG INLET; 10-PERCENT OVERSIZE NOZZLE; ACOUSTICALLY TREATED.

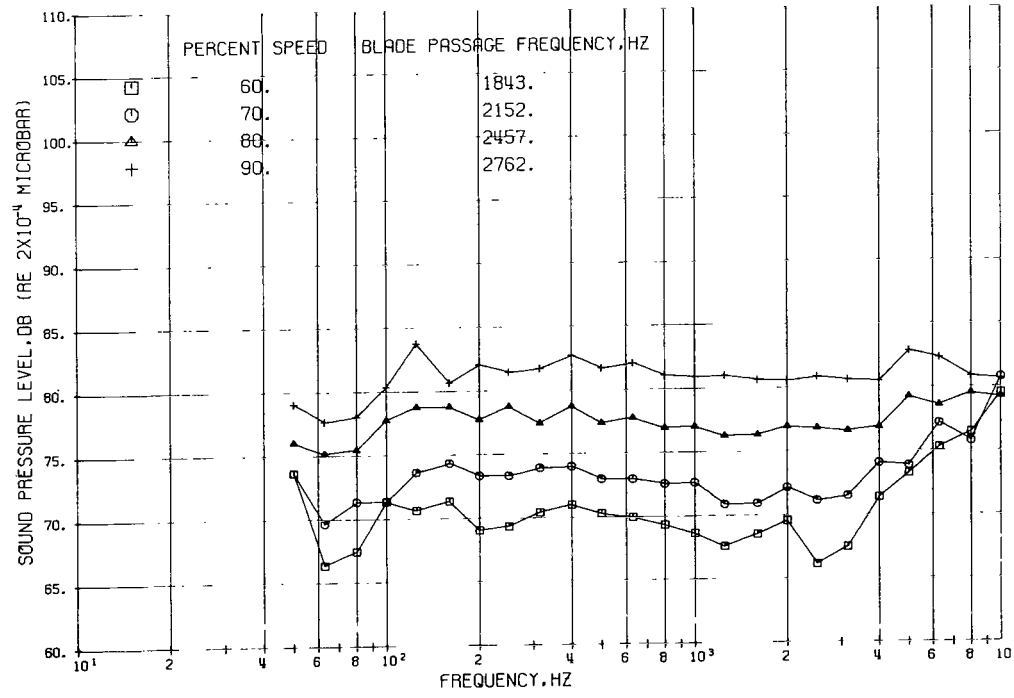

FIGURE 48 . -SOUND PRESSURE LEVEL ON 100-FOOT RADIUS. CONFIGURATION 12, 50-DEGREE ANGLE. LONG INLET; 10-PERCENT OVERSIZE NOZZLE; ACOUSTICALLY TREATED.

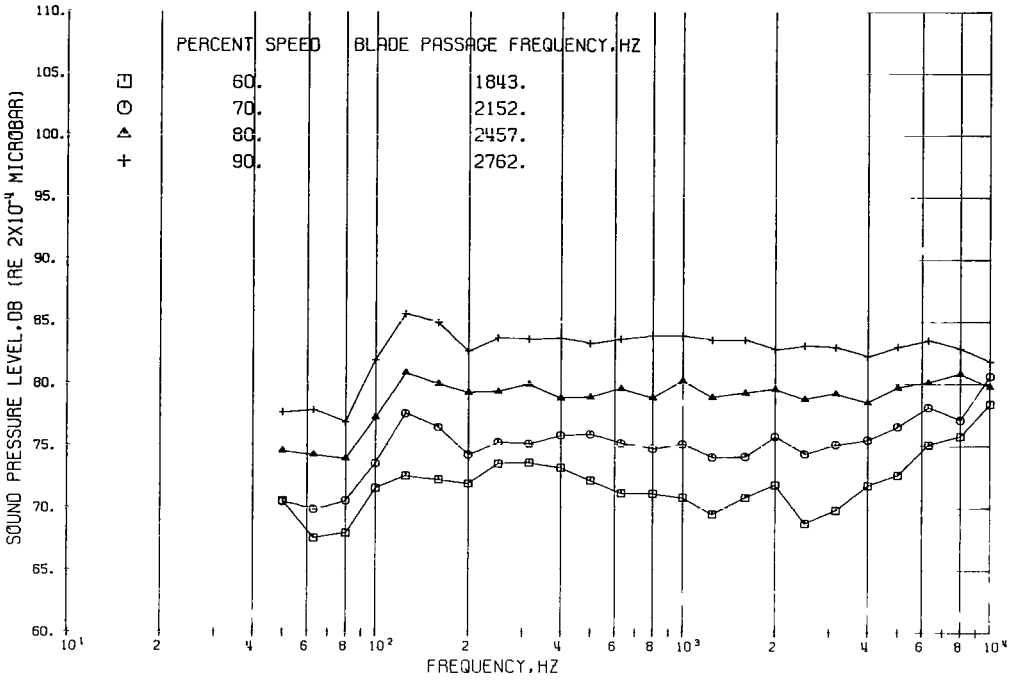

FIGURE 49 . -SOUND PRESSURE LEVEL ON 100-FOOT RADIUS. CONFIGURATION 12, 60-DEGREE ANGLE. LONG INLET; 10-PERCENT OVERSIZE NOZZLE; ACOUSTICALLY TREATED.

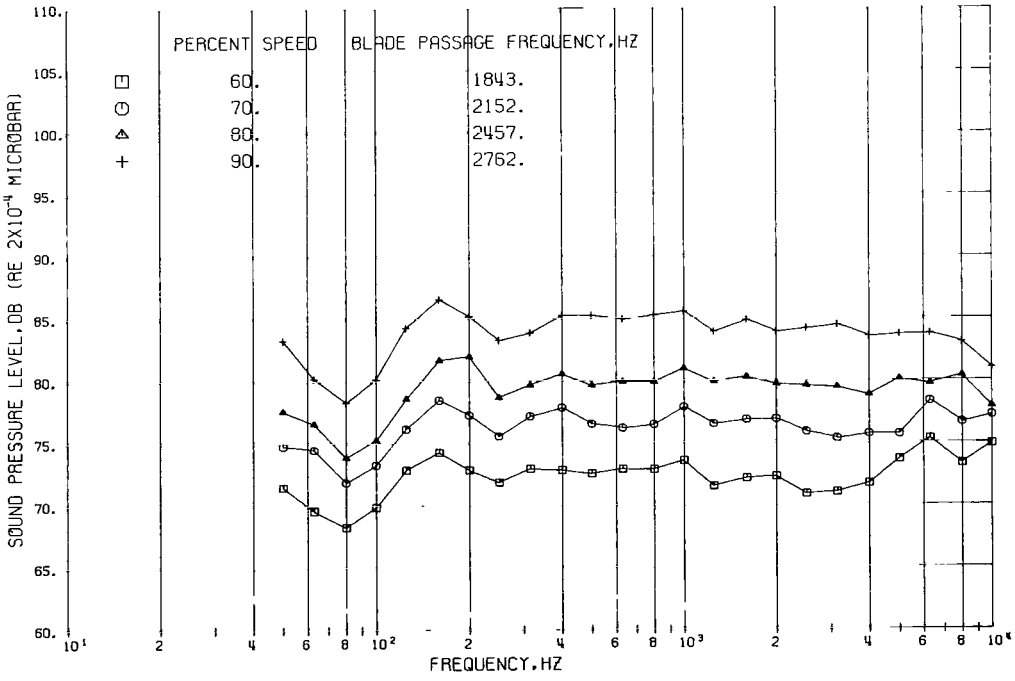

FIGURE 50 . -SOUND PRESSURE LEVEL ON 100-FOOT RADIUS. CONFIGURATION 12, 70-DEGREE ANGLE. LONG INLET; 10-PERCENT OVERSIZE NOZZLE; ACOUSTICALLY TREATED.

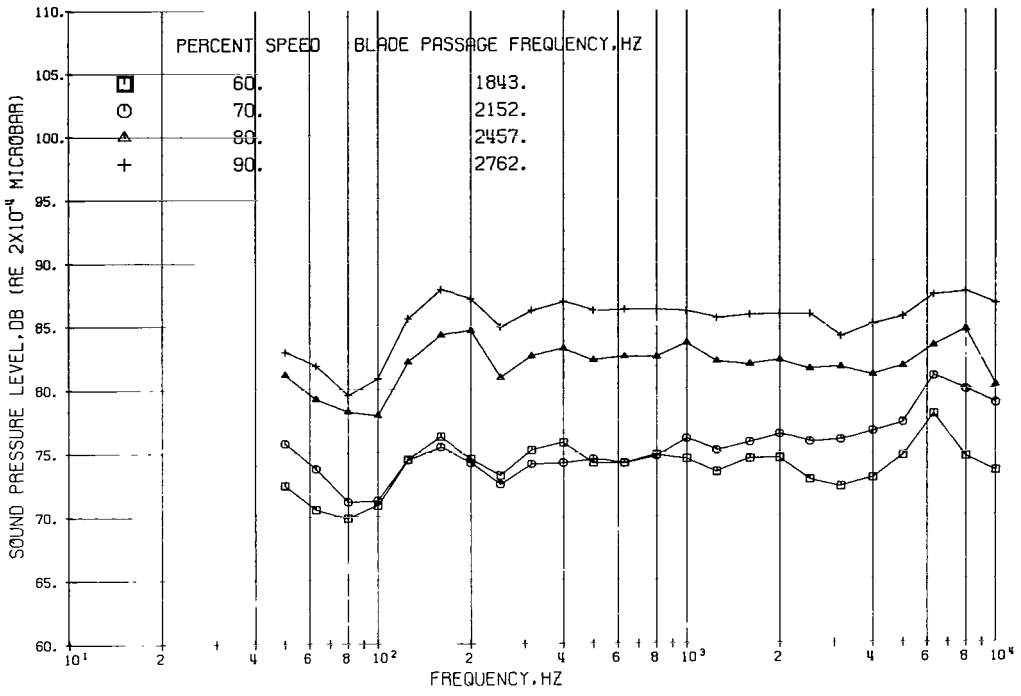

FIGURE 51. -SOUND PRESSURE LEVEL ON 100-FOOT RADIUS. CONFIGURATION 12, 80-DEGREE ANGLE. LONG INLET; 10-PERCENT OVERSIZE NOZZLE; ACOUSTICALLY TREATED.

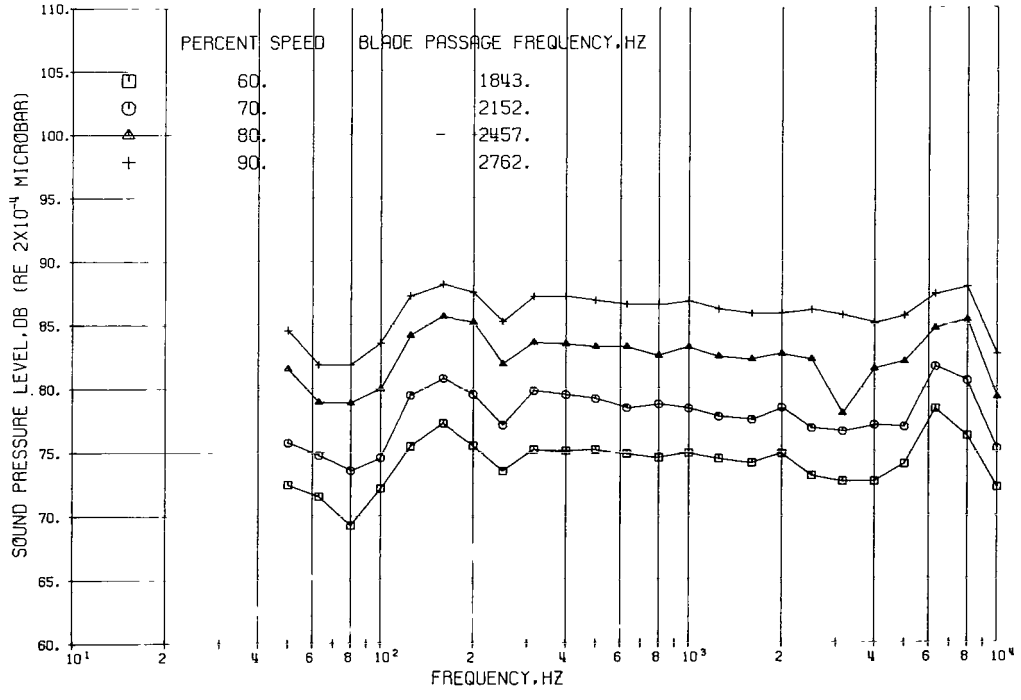

FIGURE 52. -SOUND PRESSURE LEVEL ON 100-FOOT RADIUS. CONFIGURATION 12, 90-DEGREE ANGLE. LONG INLET; 10-PERCENT OVERSIZE NOZZLE; ACOUSTICALLY TREATED.

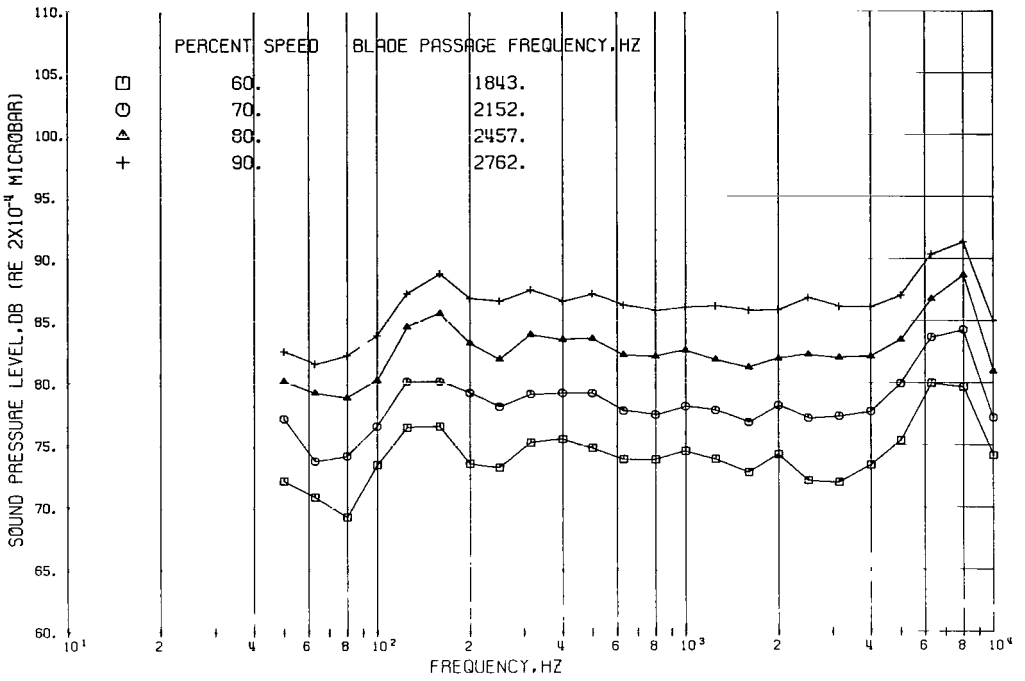

FIGURE 53. -SOUND PRESSURE LEVEL ON 100-FOOT RADIUS. CONFIGURATION 12, 100-DEGREE ANGLE. LONG INLET; 10-PERCENT OVERSIZE NOZZLE; ACOUSTICALLY TREATED.

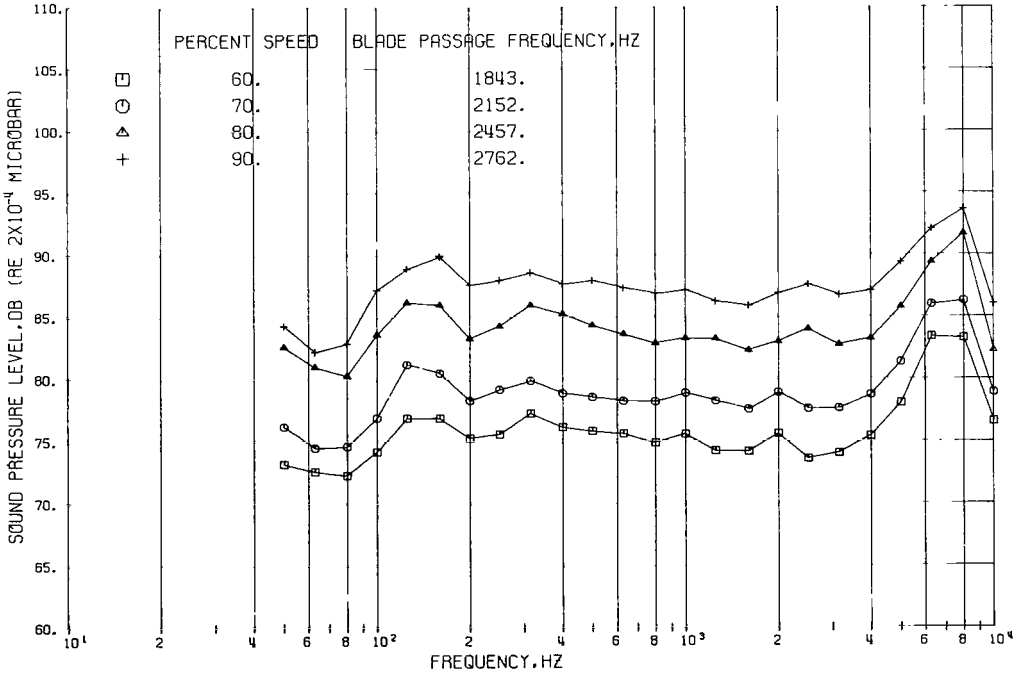

FIGURE 54. -SOUND PRESSURE LEVEL ON 100-FOOT RADIUS. CONFIGURATION 12, 110-DEGREE ANGLE. LONG INLET; 10-PERCENT OVERSIZE NOZZLE; ACOUSTICALLY TREATED.

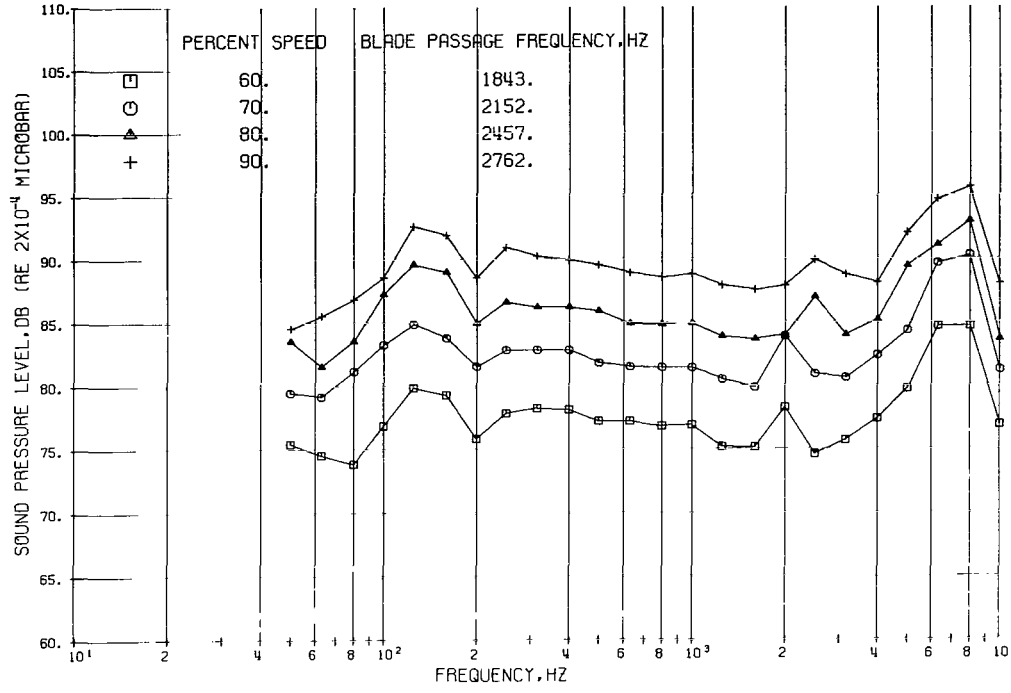

FIGURE 55 . -SOUND PRESSURE LEVEL ON 100-FOOT RADIUS. CONFIGURATION 12, 120-DEGREE ANGLE. LONG INLET; 10-PERCENT OVERSIZE NOZZLE; ACOUSTICALLY TREATED.

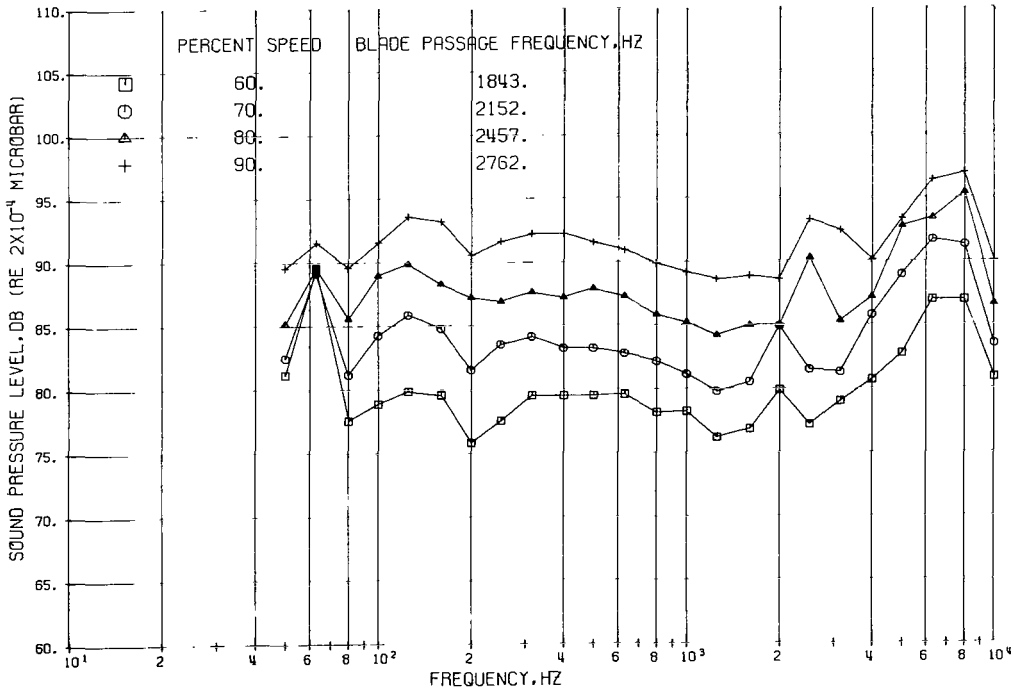

FIGURE 56. -SOUND PRESSURE LEVEL ON 100-FOOT RADIUS. CONFIGURATION 12, 130-DEGREE ANGLE. LONG INLET; 10-PERCENT OVERSIZE NOZZLE; ACOUSTICALLY TREATED.

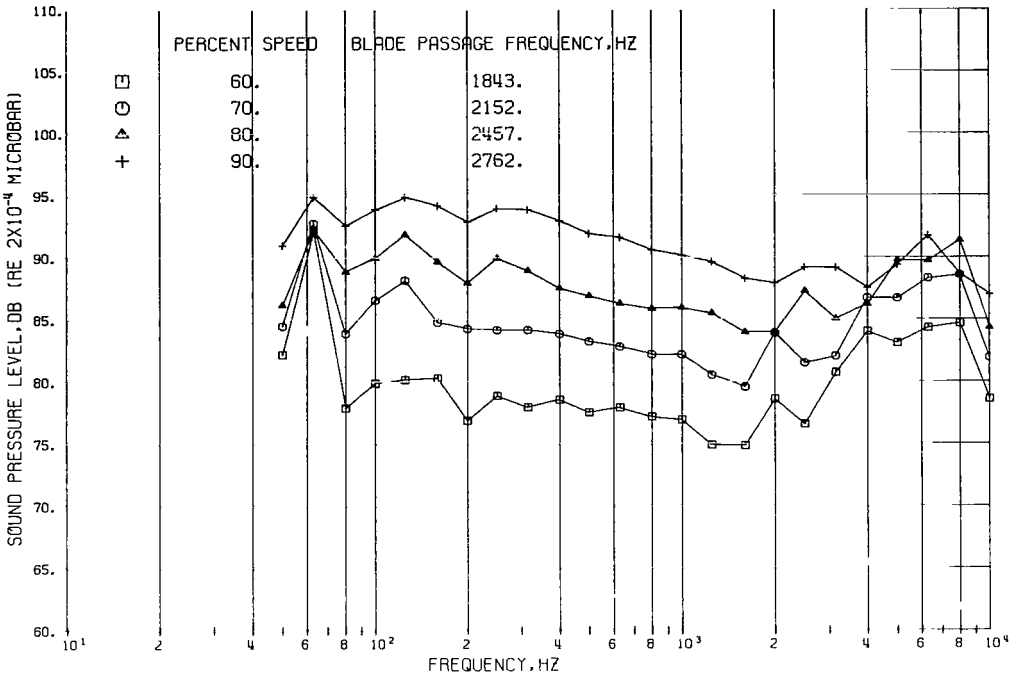

FIGURE 57 . -SOUND PRESSURE LEVEL ON 100-FOOT RADIUS. CONFIGURATION 12, 140-DEGREE ANGLE. LONG INLET; 10-PERCENT OVERSIZE NOZZLE; ACOUSTICALLY TREATED.

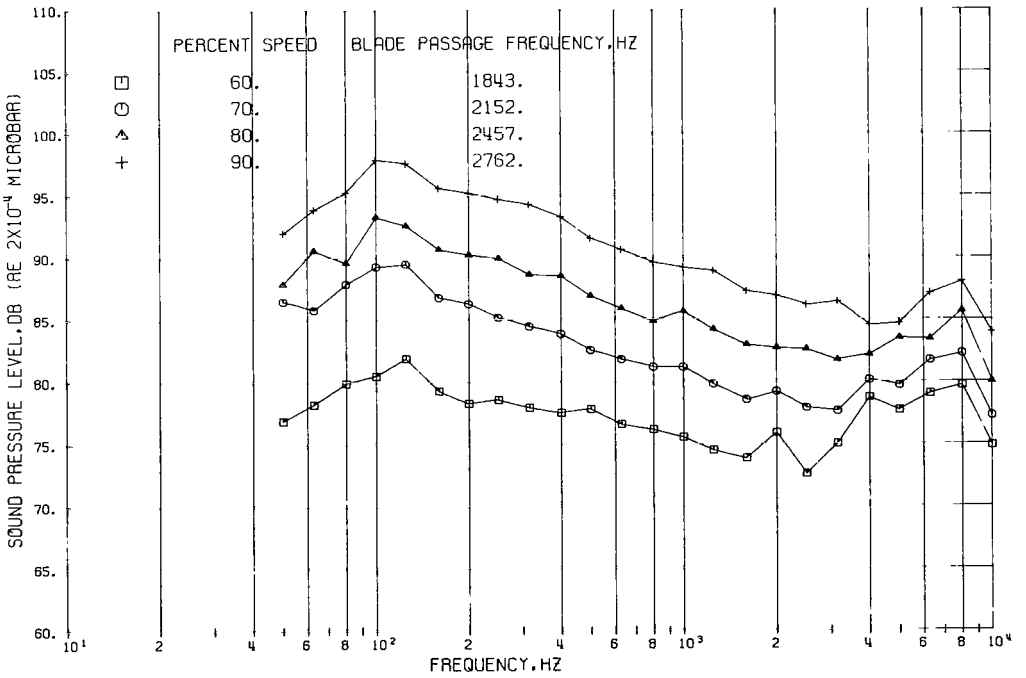

FIGURE 58. -SOUND PRESSURE LEVEL ON 100-FOOT RADIUS. CONFIGURATION 12, 150-DEGREE ANGLE. LONG INLET; 10-PERCENT OVERSIZE NOZZLE; ACOUSTICALLY TREATED.

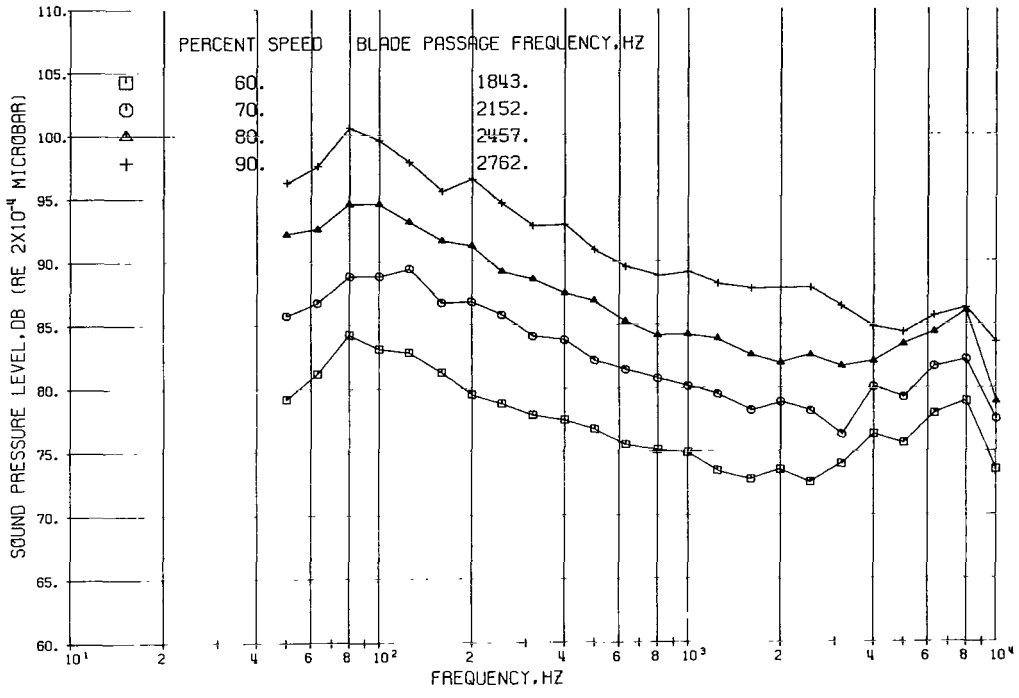

FIGURE 59. -SOUND PRESSURE LEVEL ON 100-FOOT RADIUS. CONFIGURATION 12, 160-DEGREE ANGLE. LONG INLET; 10-PERCENT OVERSIZE NOZZLE; ACOUSTICALLY TREATED.

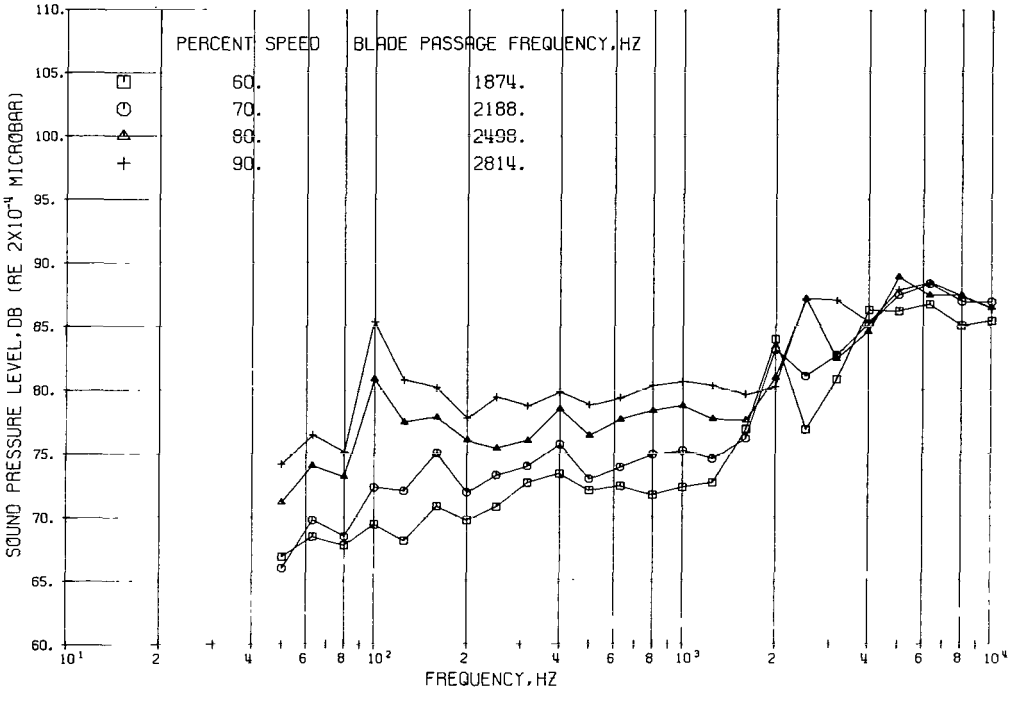

FIGURE 60. -SOUND PRESSURE LEVEL ON 100-FOOT RADIUS. CONFIGURATION 13, 10-DEGREE ANGLE. SHORT INLET; 10-PERCENT OVERSIZE NOZZLE; ACOUSTICALLY TREATED.

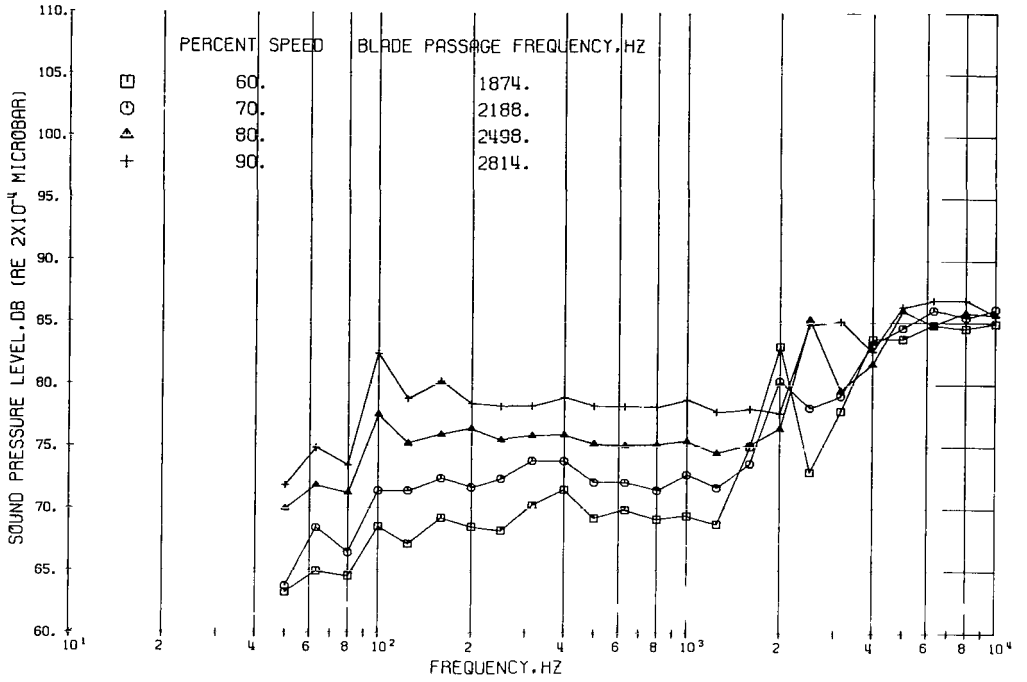

FIGURE 61. -SOUND PRESSURE LEVEL ON 100-FOOT RADIUS. CONFIGURATION 13, 20-DEGREE ANGLE. SHORT INLET; 10-PERCENT OVERSIZE NOZZLE; ACOUSTICALLY TREATED.

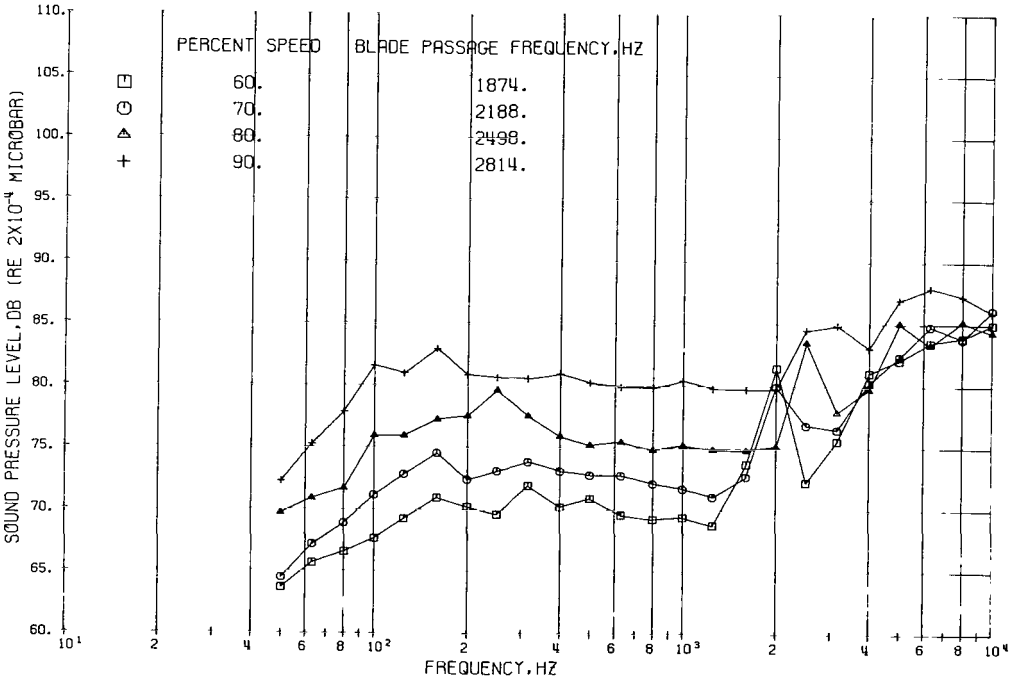

FIGURE 62. -SOUND PRESSURE LEVEL ON 100-FOOT RADIUS. CONFIGURATION 13, 30-DEGREE ANGLE. SHORT INLET; 10-PERCENT OVERSIZE NOZZLE; ACOUSTICALLY TREATED.

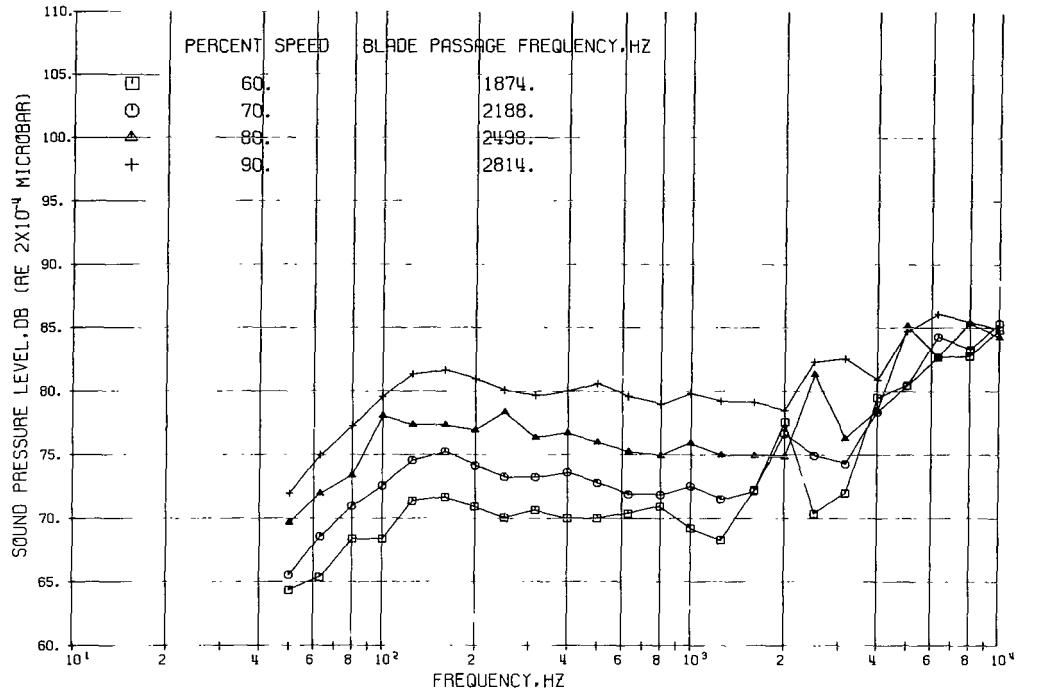

FIGURE 63. -SOUND PRESSURE LEVEL ON 100-FOOT RADIUS. CONFIGURATION 13, 40-DEGREE ANGLE. SHORT INLET; 10-PERCENT OVERSIZE NOZZLE; ACOUSTICALLY TREATED.

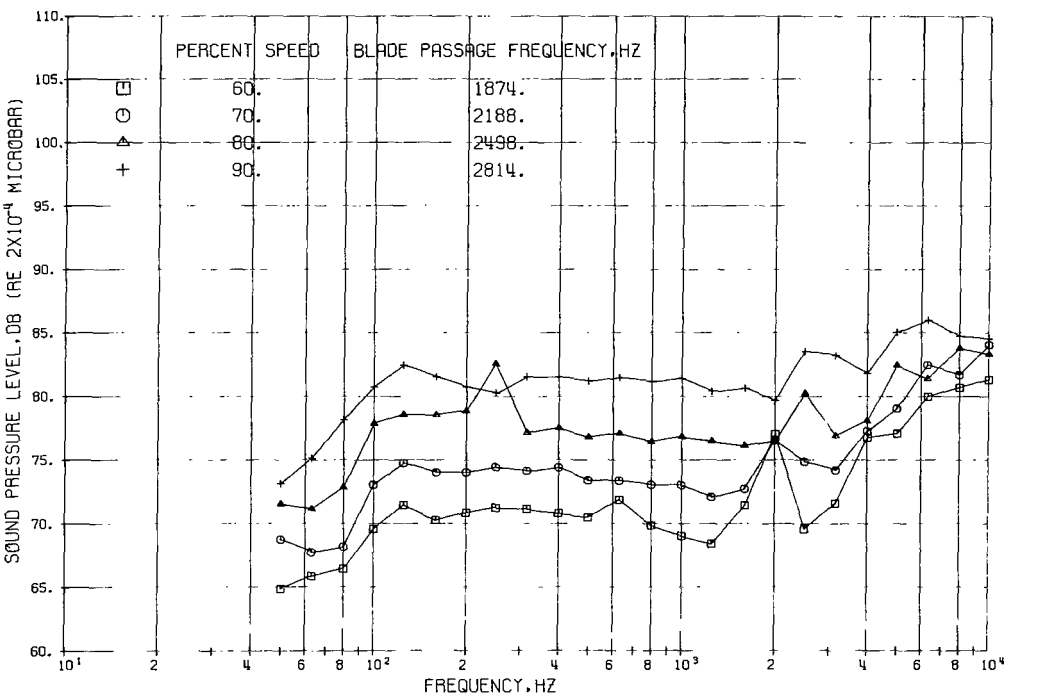

FIGURE 64. -SOUND PRESSURE LEVEL ON 100-FOOT RADIUS. CONFIGURATION 13, 50-DEGREE ANGLE. SHORT INLET; 10-PERCENT OVERSIZE NOZZLE; ACOUSTICALLY TREATED.

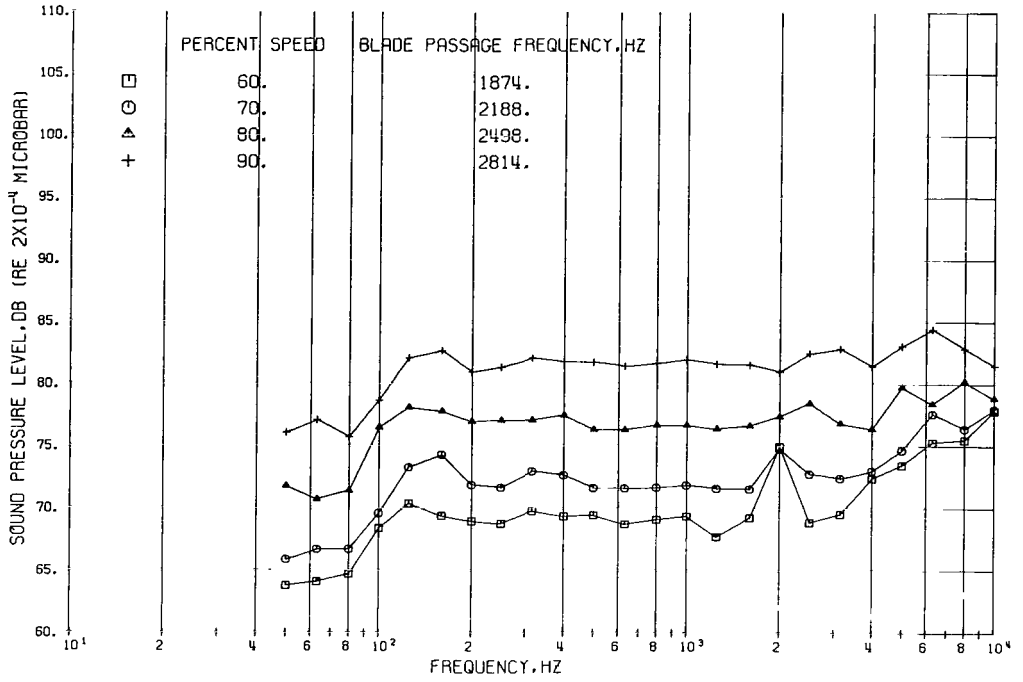

FIGURE 65 . -SOUND PRESSURE LEVEL ON 100-FOOT RADIUS. CONFIGURATION 13, 60-DEGREE ANGLE. SHORT INLET; 10-PERCENT OVERSIZE NOZZLE; ACOUSTICALLY TREATED.

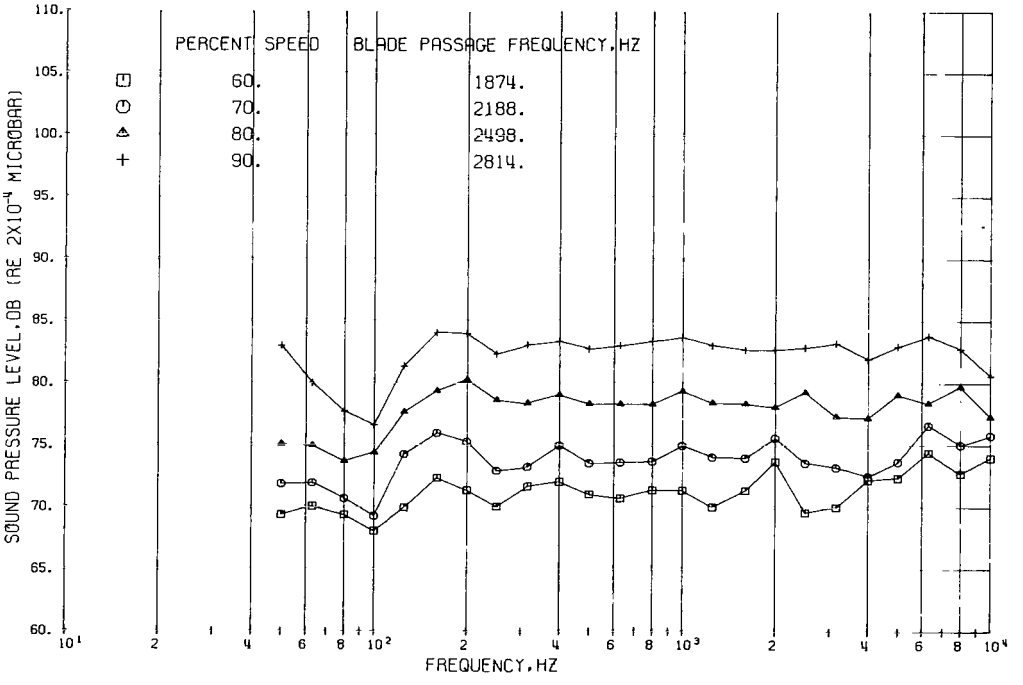

FIGURE 66 . -SOUND PRESSURE LEVEL ON 100-FOOT RADIUS. CONFIGURATION 13, 70-DEGREE ANGLE. SHORT INLET; 10-PERCENT OVERSIZE NOZZLE; ACOUSTICALLY TREATED.

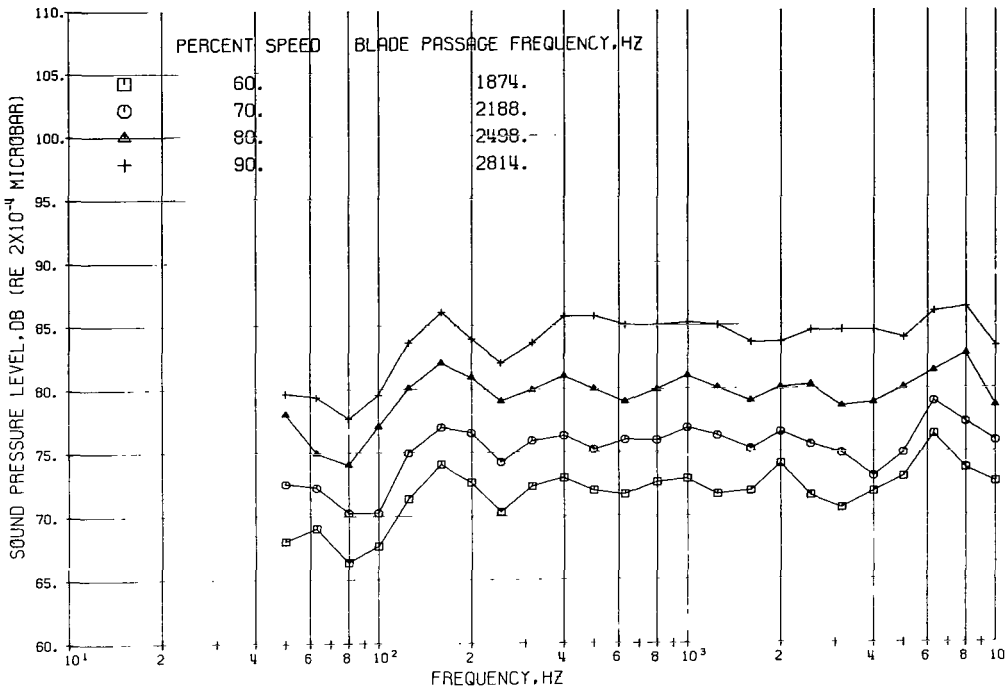

FIGURE 67 . -SOUND PRESSURE LEVEL ON 100-FOOT RADIUS. CONFIGURATION 13, 80-DEGREE ANGLE. SHORT INLET; 10-PERCENT OVERSIZE NOZZLE; ACOUSTICALLY TREATED.

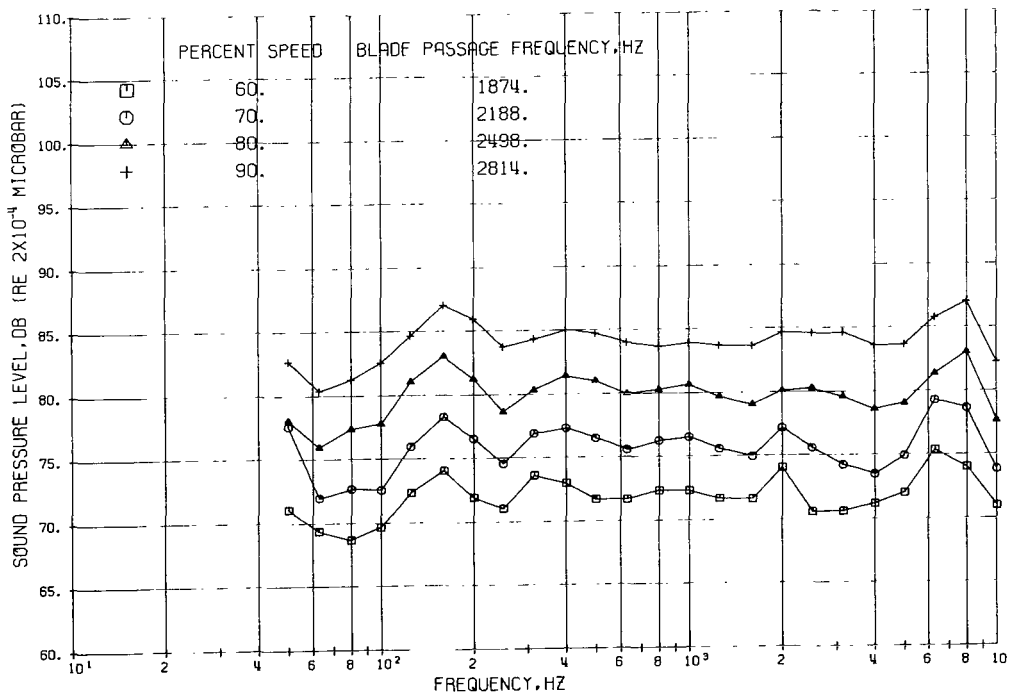

FIGURE 68 . -SOUND PRESSURE LEVEL ON 100-FOOT RADIUS. CONFIGURATION 13, 90-DEGREE ANGLE. SHORT INLET; 10-PERCENT OVERSIZE NOZZLE; ACOUSTICALLY TREATED.

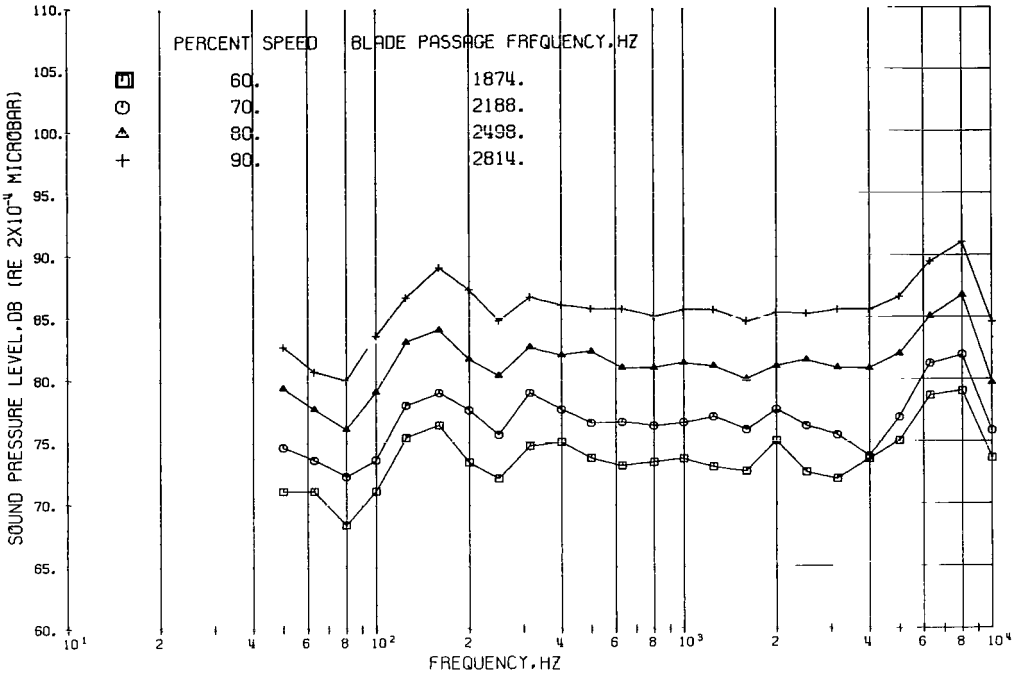

FIGURE 69. -SOUND PRESSURE LEVEL ON 100-FOOT RADIUS. CONFIGURATION 13, 100-DEGREE ANGLE. SHORT INLET; 10-PERCENT OVERSIZE NOZZLE; ACOUSTICALLY TREATED.

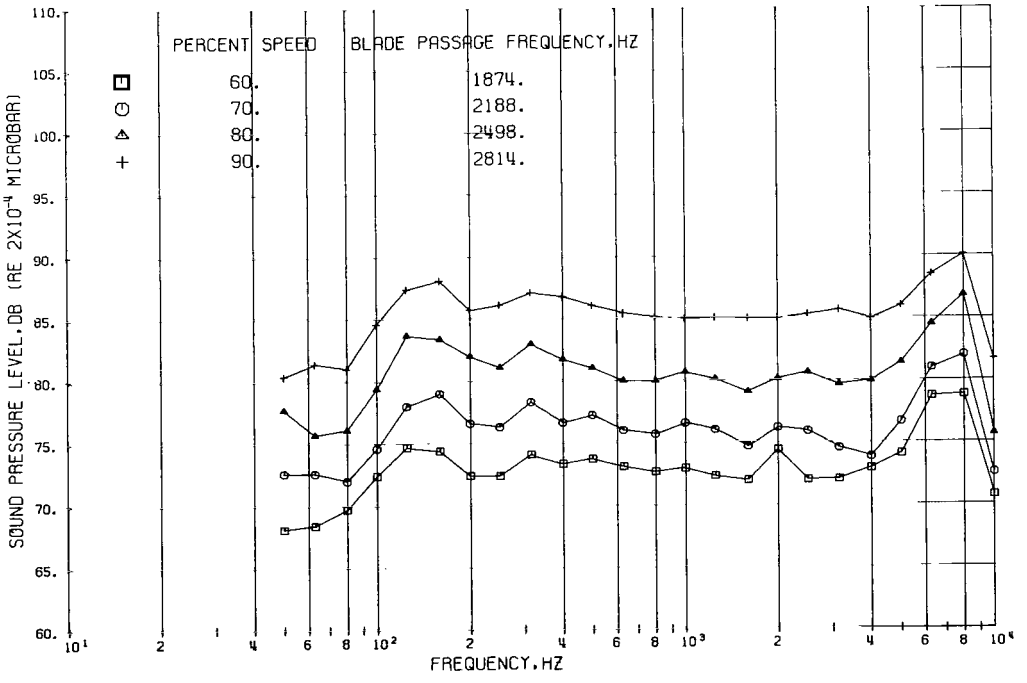

FIGURE 70. -SOUND PRESSURE LEVEL ON 100-FOOT RADIUS. CONFIGURATION 13, 110-DEGREE ANGLE. SHORT INLET; 10-PERCENT OVERSIZE NOZZLE; ACOUSTICALLY TREATED.

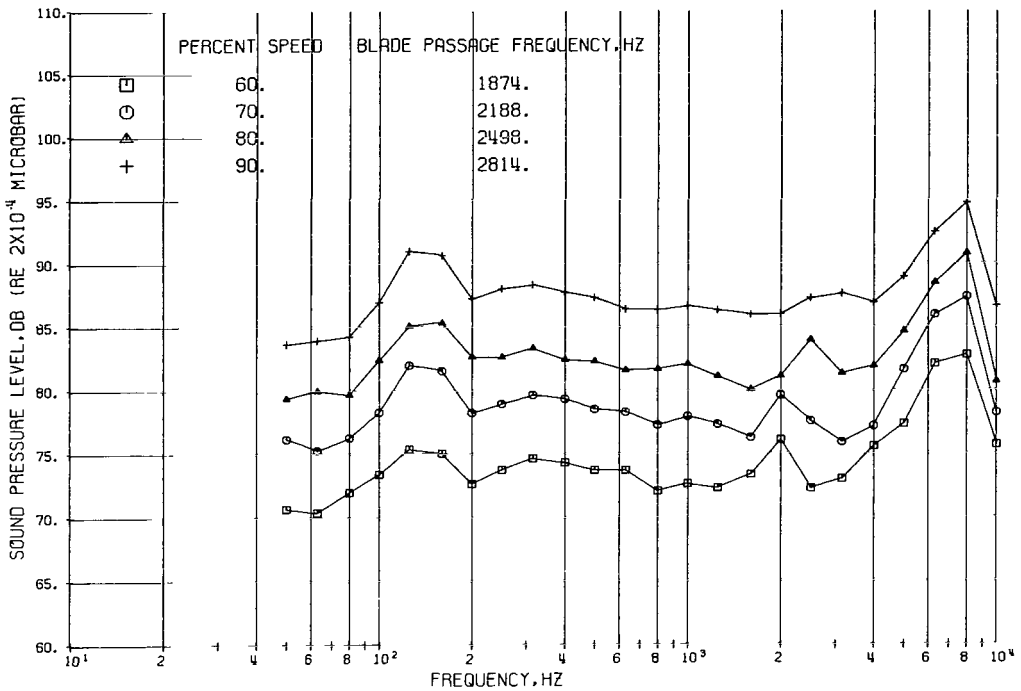

FIGURE 71. -SOUND PRESSURE LEVEL ON 100-FOOT RADIUS. CONFIGURATION 13, 120-DEGREE ANGLE. SHORT INLET, 10-PERCENT OVERSIZE NOZZLE; ACOUSTICALLY TREATED.

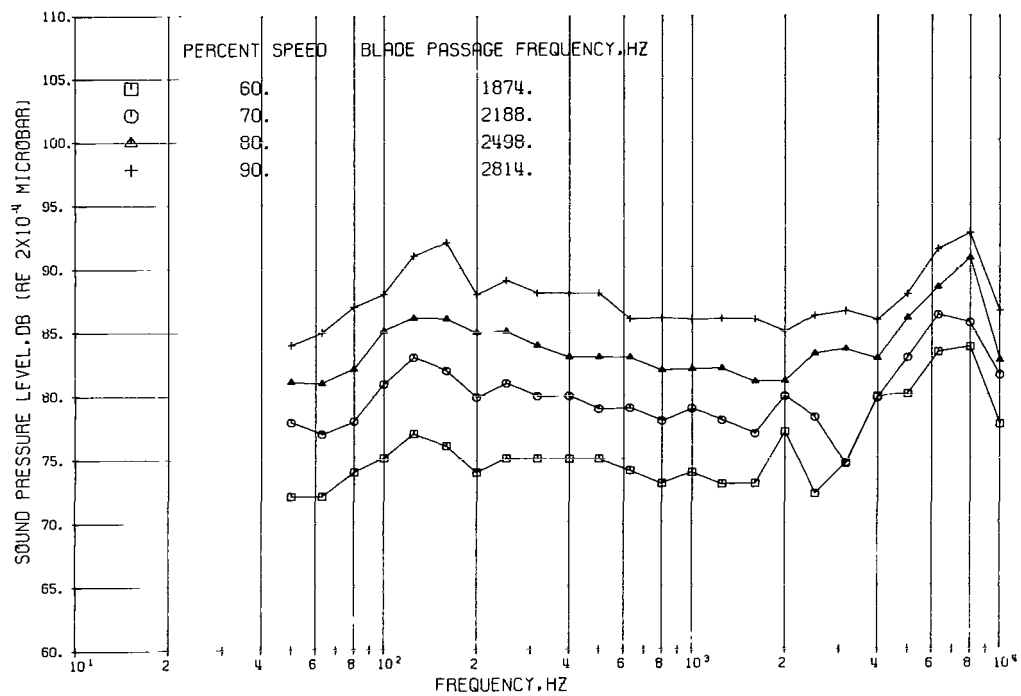

FIGURE 72. SOUND PRESSURE LEVEL ON 100-FOOT RADIUS. CONFIGURATION 13, 130-DEGREE ANGLE. SHORT INLET; 10-PERCENT OVERSIZE NOZZLE; ACOUSTICALLY TREATED.

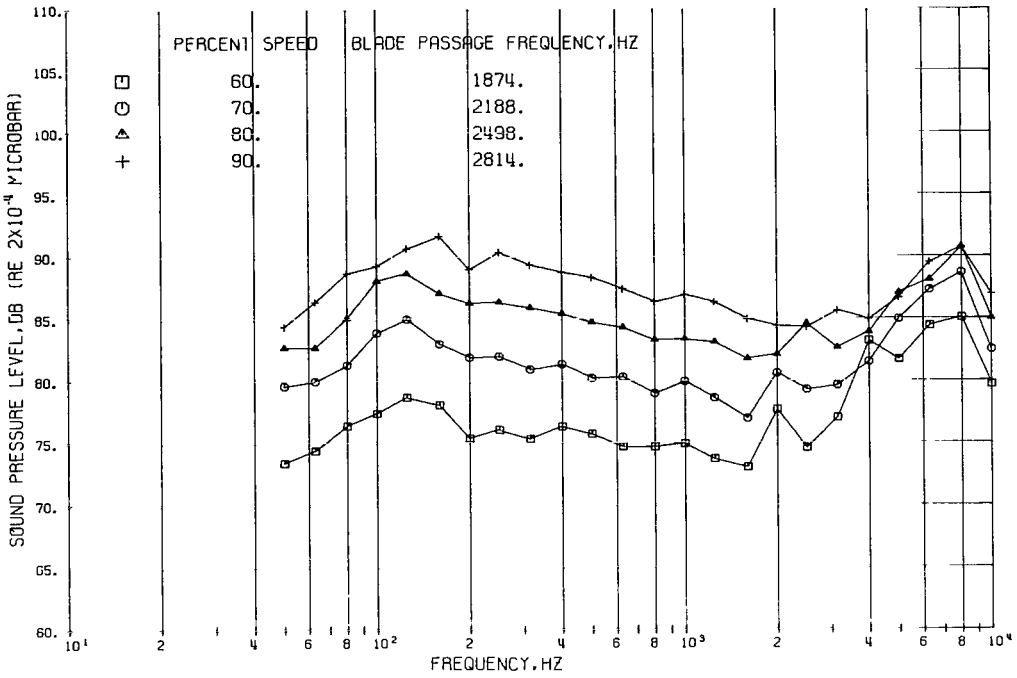

FIGURE 73 . -SOUND PRESSURE LEVEL ON 100-FOOT RADIUS. CONFIGURATION 13, 140-DEGREE ANGLE. SHORT INLET; 10-PERCENT OVERSIZE NOZZLE, ACOUSTICALLY TREATED.

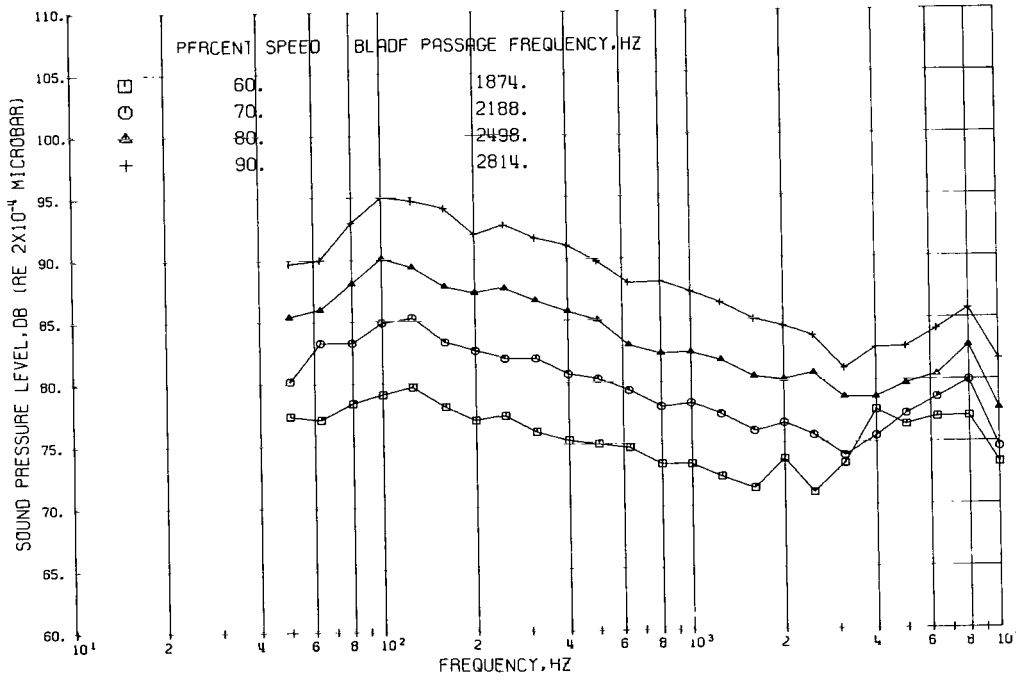

FIGURE 74 . -SOUND PRESSURE LEVEL ON 100-FOOT RADIUS. CONFIGURATION 13, 150-DEGREE ANGLE. SHORT INLET; 10-PERCENT OVERSIZE NOZZLE; ACOUSTICALLY TREATED.

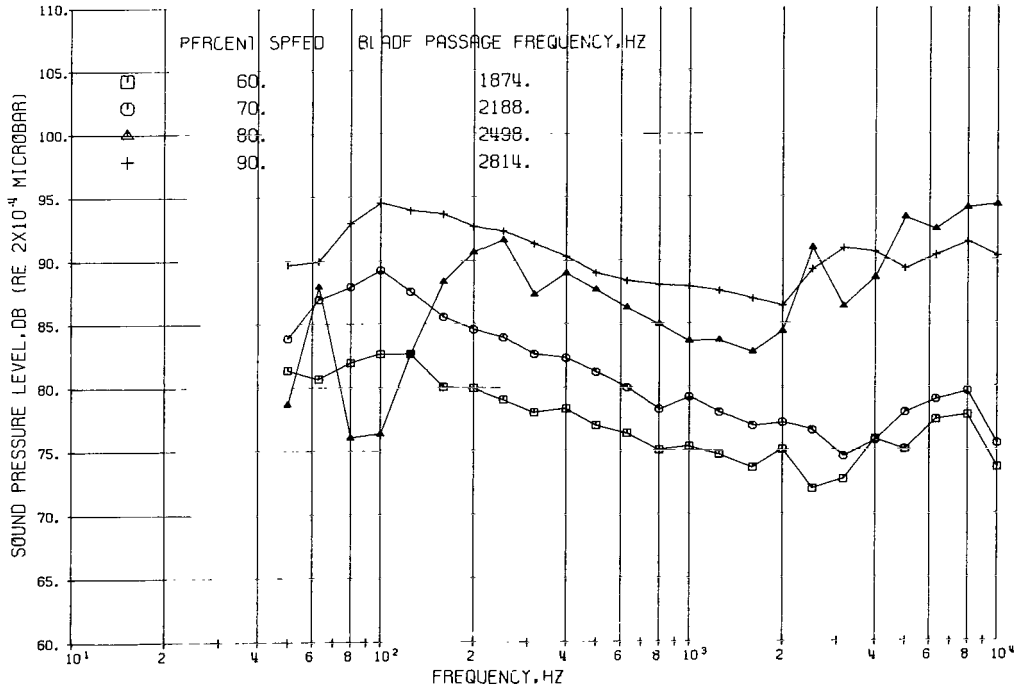

FIGURE 75. -SOUND PRESSURE LEVEL ON 100-FOOT RADIUS. CONFIGURATION 13, 160-DEGREE ANGLE. SHORT INLET; 10-PERCENT OVERSIZE NOZZLE; ACOUSTICALLY TREATED.

REFERENCES

1. Leonard, Bruce R.; Schmiedlin, Ralph F.; Stakolich, Edward G.; and Neumann, Harvey E.: Acoustic and Aerodynamic Performance of a 6-Foot-Diameter Fan for Turbofan Engines. I - Design of Facility and QF-1 Fan. NASA TN D-5877, 1970.

2. Goldstein, Arthur W.; Lucas, James G.; and Balombin, Joseph R.: Acoustic and Aerodynamic Performance of a 6-Foot-Diameter Fan for Turbofan Engines. II - Performance of QF-1 Fan in Nacelle Without Acoustic Suppression. NASA TN D-6080, 1970.

3. Progress of NASA Research Relating to Noise Alleviation of Large Subsonic Jet Aircraft. NASA SP-189, 1968.

4. NASA Acoustically Treated Nacelle Program. NASA SP-220, 1969.

5. Rice, Edward J.: Attenuation of Sound in Soft-Walled Circular Ducts. Aerodynamic Noise. H. S. Ribner, ed., Univ. Toronto Press, 1969, pp. 229-249.

6. Rice, Edward J.: Propagation of Waves in an Acoustically Lined Duct with a Mean Flow. Basic Aerodynamic Noise Research. NASA SP-207, 1969, pp. 345-355.

7. Groenweg, John F.: Current Understanding of Helmholtz Resonator Arrays as Duct Boundary Conditions. Basic Aerodynamic Noise Research. NASA SP-207, 1969, pp. 357-368.

8. Anon.: Standard Values of Atmospheric Absorption as a Function of Temperature and Humidity for Use in Evaluating Aircraft Fly-Over Noise. Aerospace Recommended Practice 866, SAE, 1964.

9. Morse, Philip M.: Vibration and Sound. Second ed., McGraw-Hill Book Co., Inc., 1948.

10. Pridmore-Brown, D. C.: Sound Propagation in a Fluid Flowing Through an Attenuating Duct. J. Fluid Mech., vol. 4, pt. 4, Aug. 1958, pp. 393-406.

11. Tack, D. H.; and Lambert, R. F.: Influence of Shear Flow on Sound Attenuation in a Lined Duct. J. Acoust. Soc. Am., vol. 38, no. 4, Oct. 1965, pp. 655-666.

12. Mungur, P.; and Gladwell, G. M. L.: Acoustic Wave Propagation in a Sheared Fluid Contained in a Duct. J. Sound Vib., vol. 9, 1969, pp. 28-48.

13. Mungur, P.; and Plumblee, H. E.: Propagation and Attenuation of Sound in a Soft-Walled Annular Duct Containing a Sheared Flow. Basic Aerodynamic Noise Research. NASA SP-207, 1969, pp. 305-327.

14. Anon.: Definitions and Procedures for Computing the Perceived Noise Level of Aircraft Noise. Aerospace Recommended Procedure 865A, SAE, Aug. 1969.

15. Pendley, Robert E.; and Marsh, Alan H.: Noise Prodictions and Economic Effects of Nacelle Modifications to McDonnell Douglas DC-8 Airplanes. Progress of NASA Research Relating to Noise Alleviation of Large Subsonic Jet Aircraft. NASA SP-189, 1968, pp. 173-195.

16. Anon.: Noise Standards: Aircraft Type Certification. Vol. III, Part 36 of Federal Aviation Regulations.

NASA-Langley, 1971 —— 28 E-5878

"The aeronautical and space activities of the United States shall be conducted so as to contribute . . . to the expansion of human knowledge of phenomena in the atmosphere and space. The Administration shall provide for the widest practicable and appropriate dissemination of information concerning its activities and the results thereof."

— NATIONAL AERONAUTICS AND SPACE ACT OF 1958

NASA SCIENTIFIC AND TECHNICAL PUBLICATIONS

TECHNICAL REPORTS: Scientific and technical information considered important, complete, and a lasting contribution to existing knowledge.

TECHNICAL NOTES: Information less broad in scope but nevertheless of importance as a contribution to existing knowledge.

TECHNICAL MEMORANDUMS: Information receiving limited distribution because of preliminary data, security classification, or other reasons.

CONTRACTOR REPORTS: Scientific and technical information generated under a NASA contract or grant and considered an important contribution to existing knowledge.

TECHNICAL TRANSLATIONS: Information published in a foreign language considered to merit NASA distribution in English.

SPECIAL PUBLICATIONS: Information derived from or of value to NASA activities. Publications include conference proceedings, monographs, data compilations, handbooks, sourcebooks, and special bibliographies.

TECHNOLOGY UTILIZATION PUBLICATIONS: Information on technology used by NASA that may be of particular interest in commercial and other non-aerospace applications. Publications include Tech Briefs, Technology Utilization Reports and Technology Surveys.

Details on the availability of these publications may be obtained from:

SCIENTIFIC AND TECHNICAL INFORMATION OFFICE

NATIONAL AERONAUTICS AND SPACE ADMINISTRATION

Washington, D.C. 20546